ABSTRACT

Title of Document:	IMPROVED PROBABILISTIC LIFE ESTIMATION IN ENGINEERING STRUCTURES: MODELING MULTI-SITE FATIGUE CRACKING
	Abdallah (Moh'd AR.) (Sh. M.) Al Tamimi, PhD, 2014
Directed By:	Minta Martin Professor of Engineering, Mohammad Modarres, Reliability engineering

The purpose of this paper is to investigate the effect of fatigue, in the presence of neighboring cracks, and to integrate that into a probabilistic physics of failure based model that could be used to predict crack growth. A total of 20 fatigue experiments were performed at different loading conditions using dog-bone samples of API-5L grade B carbon steel containing neighboring cracks. The fatigue testing was conducted to generate the data needed for the probabilistic fatigue life prediction model development. Moreover, these experiments have investigated the impact of both neighboring cracks dimensional variability and the loading conditions on cracks interaction, coalescence and growth. The experiment layout was designed to improve some of the existing experimental layouts presented in the literature. Moreover, a new approach for measuring the neighboring cracks depth and the associated number of

cycles in dog-bone shaped samples using different microscopy tools and image-processing techniques was proposed. On the other hand, simulation efforts were also performed to assess the Stress Intensity Factor (SIF) around neighboring cracks. Models discussing how the SIF of single semi-elliptical crack could be corrected to account for the neighboring cracks interaction were discussed in order to better understand the fatigue behavior. A combination of these models was integrated to compute the SIF values necessary for the probabilistic life prediction modeling purposes. Also, a new strategy for investigating ligament failure by detecting when it occurs rather than how it occurs was developed in this work. A demonstration of an improved understanding of the impact of different loading conditions on the ligament failure phenomena both using experiments and simulation was also discussed. Finally, a multi-site fatigue crack growth rate model was developed and its parameters including their uncertainties were estimated. A Bayesian approach was adopted to perform uncertainty characterization and model validation.

IMPROVED PROBABILISTIC REMAINING USEFUL LIFE ESTIMATION IN
ENGINEERING STRUCTURES: MODELING MULTI-SITE FATIGUE
CRACKING

By

Abdallah (Moh'd AR.) (Sh. M.) Al Tamimi

Advisory Committee:
Professor Mohammad Modarres, Chair and Advisor
Professor Mohamad Al-Sheikhly, Dean's Representative
Professor Ali Mosleh
Professor Balakumar Balachandran
Associate Professor Enrique Lopez Droguett

Dedication

I dedicate my dissertation work to my parents.

A special feeling of gratitude to my loving parents, their words of encouragement and push for tenacity ring in my ears. They made my journey meaningful.

Thank you,

Acknowledgements

Table of Contents

List of Tables

List of Figures

List of Nomenclature

PPoF	Probabilistic Physics of Failure
MSD	Multi-Site Damage
LEFM	Linear Elastic Fracture Mechanics
EPFM	Elastic Plastic Fracture Mechanics
ASME	American Society of Mechanical Engineers
BSI	British Standard Institute
ADNOC	Abu Dhabi National Oil Company
SCC	Stress Corrosion Cracking
EDM	Electric Discharge Machining
CIF	Cracks Interaction Factor
PHM	Prognostic health management
WinBUGS	Window based computer software for MCMC
MCMC	Markov chain Monte Carlo
BIC	Bayesian Information Criterion
AIC	Akaike Information criterion
SIF	Stress Intensity Factor
K	Stress Intensity Factor
K_{SC}	Stress Intensity Factor of a single crack
K_{NC}	Stress Intensity Factor of neighboring cracks
pdf	Probability density function
a	Crack depth
r	Surface crack length, crack radius
r_y	Plastic distance ahead of the crack tip
b	Half of the sample width
S	Separation distance between the inner tips of the two cracks
d	Separation distance between the two cracks centers
$\emptyset$	Crack growth angle
σ_s	Stress
σ_t	Uniform tension stress
σ_b	Uniform bending stress

H	Bending multiplier for surface crack in a plate
F	Boundary correction factor
Q	Shape factor for an ellipse
t	Sample thickness
E	Distance between the crack tip and the sample edge
M_i	Curve-fitting functions; boundary correction factor for the crack front
g	Fine tuning equation
f_w	Finite width correction factor
$f_\emptyset$	Angular function derived from embedded elliptical crack solution
F'	Geometry factor
C	Paris law empirical constant
C_a	Paris law empirical constant for the crack front growth
C_c	Paris law empirical constant for the surface crack growth
n	Paris law empirical constant
LR	Loading ratio
λ	Empirical constant that indicates the influence of the loading ratio on the fatigue crack growth in different materials (Walker Model)
m	Empirical constant that indicates the influence of the loading ratio on the fatigue crack growth in different materials (Modified Paris law model)
α	Numerical constant in crack growth equation
B	Geometry correction factor
γ	Cracks interaction factor
K_I'	Stress intensity factor including the influence of interaction
K_I	Stress intensity factor without the influence of interaction
V_i	Empirical constants for the interaction factor empirical model
N	Number of cycles
N_f	Number of cycles to failure
F	Frequency
$a_{(\mu/\mu)}$	Two identical neighboring cracks notch geometry; reference geometry
$a_{(\mu-2\sigma/\mu-2\sigma)}$	Two identical neighboring cracks notch geometry; depth reduced by

	two standard deviations
a_(μ-2σ/μ)	Two non-identical neighboring cracks; left crack depth reduced by two standard deviations
a_(μ-σ/μ)	Two non-identical neighboring cracks; left crack depth reduced by one standard deviation
a_(μ/μ+σ)	Two non-identical neighboring cracks; right crack depth increased by one standard deviation
a_(μ/μ+2σ)	Two non-identical neighboring cracks; right crack depth increased by two standard deviations
r_(μ-σ/μ)	Two non-identical neighboring cracks; left crack radius reduced by one standard deviation
r_(μ-2σ/μ)	Two non-identical neighboring cracks; left crack radius reduced by two standard deviations
S_(μ-σ)	Two identical neighboring cracks notch geometry; spacing reduced by one standard deviation
S_(μ-2σ)	Two identical neighboring cracks notch geometry; spacing reduced by two standard deviations
S_(μ+2σ)	Two identical neighboring cracks notch geometry; spacing increased by two standard deviations
θi	Uncertain parameter
σ	Standard deviation
$\sigma_{standard}$	Standard uncertainty
$\sigma_{combined}$	Combined standard uncertainty
Δ_{ε}	Random variable of the naked eye measurement error
P_{avg}	Average crack depth value of the repeated measurements in pixels
m_{ε}	Sizing error model parameter representing the correlation between the repeated crack measurements difference and the average value
b_{ε}	Sizing error model parameter
da/dN_i	Crack growth rate true value
$da/dN_{e,i}$	Crack growth rate value obtained experimentally
$da/dN_{m,i}$	Crack growth rate value obtained from the model developed

F_e The multiplicative error of the experimental crack growth value with respect to the true value

F_m The multiplicative error of the model crack growth prediction with respect to the true value

b_e The experimental mean multiplicative error

s_e The Standard deviation of the experimental multiplicative error

b_m The model mean multiplicative error

s_m The standard deviation of the model multiplicative error

F_t The multiplicative error of experiment with respect to model prediction

n   Sample size

k   Number of uncertain parameters

1. Chapter One: Introduction

1.1 Dissertation Overview

Many engineering structures are susceptible to various degradation mechanisms and flaws. A good example for such structures is the oil and gas transport pipelines which operate under severe conditions: internal pressure, cyclic load, internal and external environments. As a result, the combination of these different factors can lead to a potential increase in the risk of damage and unexpected fracture.

The continuously rising cost of service structures replacement, maintenance and inspection means that there are now aging systems whose continued operation requires special analysis and improved crack detection techniques. This demands continuous safety and performance improvement so that there can be increased service life of pipeline networks, maintenance, and cost control. Additionally, this necessitates stronger prevention and control measures to avoid the likelihood of structural failures.

One of the critical failure mechanisms in structures is fatigue. According to Bayley [1], fatigue is a stable crack growth process that occurs under cyclic loading over the life of most engineering structures. This degradation process occurs at stresses less than the yield strength of the material until either the critical stress intensity factor is reached, leading to fracture, or until net section yielding takes place. As crack initiation occurs in localized areas of stress concentrations, or due to environmental conditions, multiple pits and/or initial cracks are present in many structures. As these cracks interact and affect each other, the stress intensity factor around the cracks increases leading to faster crack growth rate and shorter component life. Bayley [1] defined crack coalescence as several small adjacent cracks increasing in size and eventually growing together

forming a single larger crack. Many crack configurations and shapes have been investigated using simulations and experiments in the literature (e.g., Leek and Howard [2], [3] and Murakami [4], [5]) to define the impact of neighboring cracks on each other's stress intensity factor and crack propagation.

In Figure 1.1, a breakdown of possible causes of failure in oil and gas service structures and the associated failure events and consequences is illustrated. Many of the failure causes illustrated lead to formation of neighboring cracks which might impose higher risks by growing and forming larger cracks when coupled with external stresses. Other factors like the loading conditions, material properties, temperature, and the corrosive environment could also accelerate the manifestation of such failure events.

Causes
- Accidental denting
- Manufacturing flaws
- Material imperfections

- Pitting Corrosion
- SCC
- Corrosion-Fatigue

- Human error
- Aging
- Sabotage

Events
- Degradation of structures
- Leaks and ruptures
- Failures

Consequences
- Inspection and repair cost
- Loss of production cost
- Safety hazard
- Environmental damage
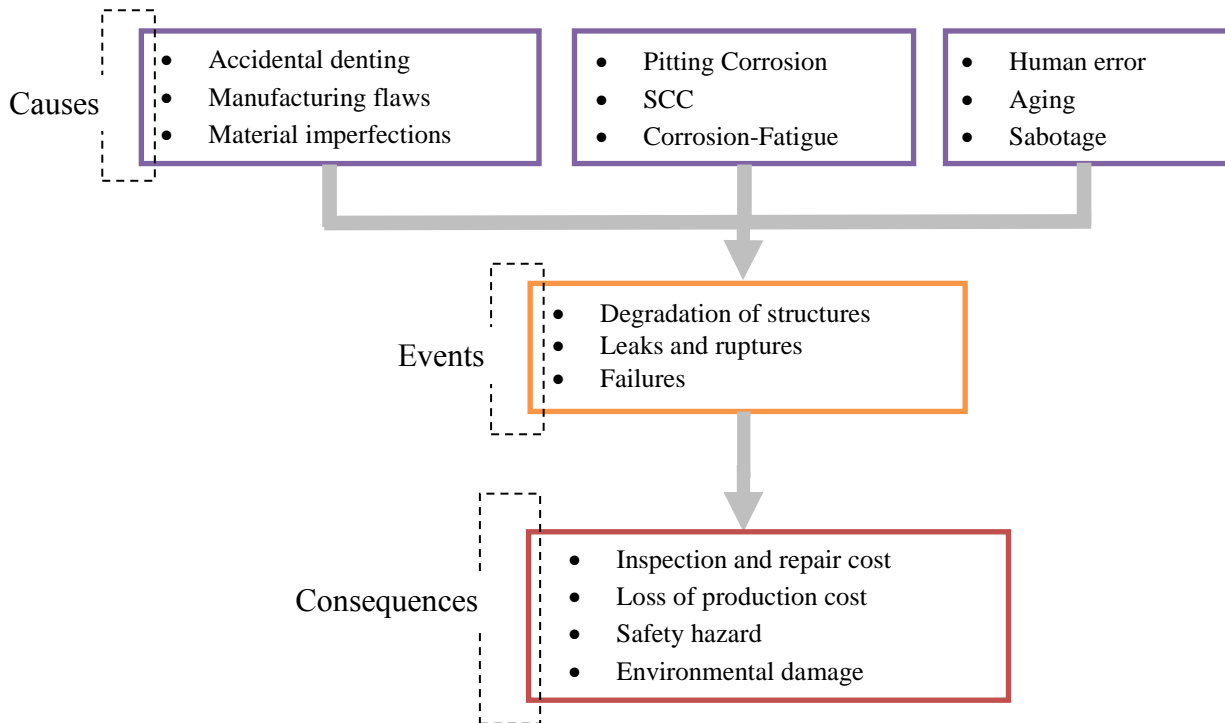
Figure 1.1: Causes of failures and their relative consequences. Adapted from "Structuring a Probabilistic Model for Reliability Evaluation of Piping Subject to Corrosion-fatigue Degradation, PhD dissertation" by M. Al Alseyabi, 2009 [6]

In this dissertation, a literature review summarizing some of crack coalescence models was used side by side with a set of experiments to build a model that can predict the life of carbon steel specimens subject to fatigue of neighboring cracks.

1.2 Dissertation Objective

The purpose of this study is to investigate and model the interaction, coalescence and growth of neighboring cracks under fatigue loading and integrate that into a life prediction model that could be used to estimate the life of engineering structures. As such, the development of a method that accounts for applicable and realistic cracks interaction, validated with acceptable modeling error, is the main objective of the study.

Based on the literature review performed in this research, a large portion of the work done in crack propagation modeling has been directed towards investigation of single crack growth. It was apparent that there is a need to acquire more information about neighboring cracks growth. Hence, the prime objective of this research is to develop further understanding of modeling fatigue of neighboring cracks through the following steps:

- Adopt a degradation model for fatigue crack growth by investigating the most relevant mechanistic physics based models available in the literature

- Identify the associated model variables and uncertain parameters in the adopted model

- Gather information about the prior data/information of the adopted model uncertain parameters

- Develop an experimental test method to provide the scatter of data required for both updating the uncertain parameters and validating the final model proposed

3

- Develop a simulation technique that can be used to compute a crack's front stress intensity factor and accounts for the neighboring cracks interactions

- Identify a Bayesian updating approach to updated posterior distributions of the model parameters based on the experimental and simulation evidence data gathered

- Quantify the model uncertainties and validate it

1.3 Approach

The approach to develop the probabilistic life prediction model consists of three main steps:

1. Data generation
   a. Experimental data collection
   b. Stress intensity factor simulation
2. Model development
3. Model uncertainty characterization and validation

The first step includes performing experiments in order to collect data about the failure mechanism investigated. Fatigue tests were performed under different loading conditions for diverse neighboring crack geometries. Moreover, simulations were performed in order to quantify the Stress Intensity Factor (SIF) at the crack front in order to explain the effect of cracks interaction on SIF and complete the data scatter required for the model development.

The second step was to perform the necessary probabilistic statistical analysis in order to develop the structural life prediction model. Bayesian analyses will be the core of the model development.

Finally, uncertainty characterization and model validation will be performed to account for the model errors and confirm its outputs. This kind of analysis provides a more realistic characterization of the failure mechanism. Moreover, the model will be tested for validity under different loading and crack geometrical conditions.

1.4 Contributions

The main contributions of this dissertation are as follows:

- Developed an improved experimental layout and procedure to investigate cracks interaction, coalescence and growth in carbon steel materials

- Gained a better understanding of the effect of neighboring cracks dimensional variability on their interaction, coalescence and growth process

- Broadened the state of the art on the effect of different loading conditions on crack interaction, coalescence and growth process

- Characterized the SIF behavior at the crack front during different crack development stages

- Identified a new strategy for investigating ligament failure by detecting when it occurs rather than how it occur

- Developed and demonstrated an improved understanding of the impact of different loading conditions on the ligament failure phenomena both using experiments and simulation

- Developed a new PPOF model of crack growth that accounts for neighboring cracks interaction and coalescence along with proper identification of its' parameters and uncertainties

2. Chapter Two: Literature Review

2.1 Linear Elastic Fracture Mechanics

Most engineering structures and components have different types of imperfections and flaws due to the active failure mechanisms, manufacturing processes or even handling. Cracks are initiated at weak or damaged areas like discontinuities in metals, inclusions or second-phase particles, scratches on metal surface, pits and twin boundaries [7]. Yet, when these cracks are subjected to an applied loading, they grow leading to failures.

The problem under investigation is a linear elastic fracture mechanics problem, where the elastic stress intensity factor (K) and Paris law for growth are applicable. According to Fatemi [8] there are some constraints when using linear elastic fracture mechanics (LEFM). Fatemi [8] indicated that for LEFM concepts to hold, the nominal stresses applied in a specific cracked plane should be less than 80% of the yield strength. Also, Fatemi added that the plastic distance ahead of the crack tip, r_y, should be less than 1/8th of the cracked plane thickness and the untracked ligament along the plane of the crack. For that reason, considering elastic-plastic fracture mechanics (EPFM) becomes more important when the nominal applied stresses are greater than the yield strength or when the crack size is relatively large compared to the cracked plane.

According to Bayley [1], for most metallic materials, the size of the inelastic region adjacent to the crack tip is relatively small in comparison with the crack size. For that reason, the amount of material experiencing inelastic behavior is small compared to the overall elastic state of the sample or component. Consistent with Alseyabi [6], fatigue stresses applied to a component leads to a plastic deformation zone ahead of the advancing fatigue crack. When this resulting zone is very small compared to the elastic field, LEFM solutions provide a suitable description

6

for fatigue fracture. In line with Zhang [9], fatigue is a progressive failure under repeated, cyclic or fluctuating loads. For that reason, a stress level less than that required to cause failure under static loading conditions is required to cause failure in fatigue.

A fatigue crack in any solid material could be stressed in three different fracture modes: Mode I (Opening Mode), Mode II (Slide Mode) and Mode III (Tearing Mode). Regardless of the load mode applied, a rising stress distribution will be noted around the crack or material imperfection. In this dissertation, Mode I type of loads will be considered in investigating the impact of fatigue loads on neighboring cracks coalescence, interaction and growth.

2.2 Crack Shape in Fatigue

Understanding crack shape development is essential when it comes to life prediction and health monitoring of engineering structures. According to Paris et al. [10], the Paris law predicts that a crack will propagate in the direction of maximum stress intensity. Also, consistent with Lin et al. [11], regardless of the initial crack shape and size, the crack will always grow towards an equilibrium shape before it grows in different directions.

Many different types of materials flaws and imperfection could possibly form initial cracks that propagate leading to fracture. Three categories of flaws can be found in operating engineering structures:

1. A single crack such as semi-elliptical, corner, circular and embedded cracks

2. Multiple interacting crack, which is the focus of this research

3. Multi-element flaws which characterizes the effect of a flaw in a component on another flaw in a different component

7

According to Leek and Howard [2], surface cracks can be, at least initially, of irregular shapes and orientations. However, it is recommended by many standard practices to characterize a surface crack by projecting it onto the plane normal to the principal stress and to assume the crack to be semi-elliptical in shape, having the dimensions of the rectangle that fully encloses it.

Another important aspect of characterizing neighboring cracks is the distance between the planes of the cracks. When this distance approaches zero, meaning that the two cracks exists on the same plane, then there are two coplanar cracks. Otherwise, when the two cracks are not in the same plane, they are called non-coplanar cracks. The focus of this research is semi-elliptical coplanar cracks as illustrated in Figure 2.1:
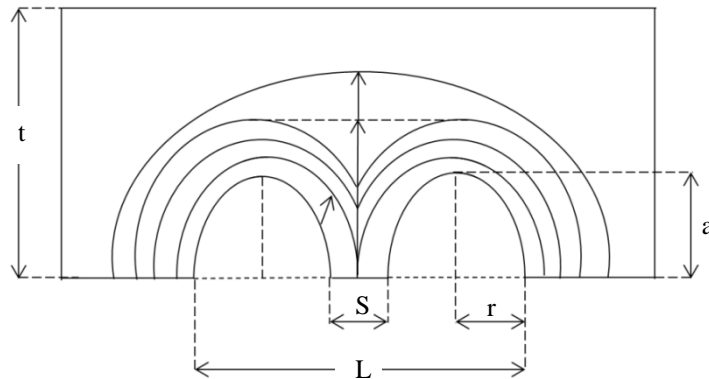
Figure 2.1: Neighboring racks nomenclature illustration

One example of a failure mechanism that induces clusters of initial cracks, which are subject MSD is pitting corrosion. Pitting corrosion is a localized form of corrosion that occurs when a corrosive medium attacks a metal causing a local breakdown of protective surface film forming small holes or pits on the material surface. These pits are formed having different shapes and dimensions. For that reason, corrosion pits were categorized according to their shape as: through pits and sideway pits [12]. Configurations of the different types of pits are illustrated in Table 2.1:

Table 2.1: Different corrosion pit shapes. Adapted from [12]

Through Pits (Elongated)		Sideway pits (Widened)	
Shallow deep		Horizontal grain attack	
Vertical grain attack		Undercutting	
Narrow deep		Subsurface	
Elliptical			

Nuhi et al. [13] also investigated the dimensional growth of corrosion pits and their density under different corrosive conditions. He found that the variation in pit dimensions (i.e., depth and radius) had an average standard deviation of 20% of the recorded mean pit depth and radius.

2.3 Stress Intensity Factor of a Single Semi-elliptical Crack

Stress intensity factor (SIF) is a fundamental quantity used to describe the stress field near crack fronts [1]. SIF depends mainly on crack geometry, boundary conditions and the nature of applied load. As there is an infinite combination of geometries, boundary and loading conditions, exact solutions are often unavailable. Hence SIF solutions for interacting surface cracks of different geometries are not widely studied.

Many efforts were directed towards studying single crack SIF. One of the first single cracks SIF approximations was developed by Irwin [14]. Many approximations followed Irwins' work taking the form of both discrete values and continuous equations and are discussed by Leek [15].

One of the acceptable SIF approximate expressions for a single semi-elliptical crack was proposed by Newman and Raju [16] [17] due to their accuracy, ease of use, and wide ranging applicability. As stated by Newman and Raju [18] [16], comparing their Finite Element Method (FEM) solutions for semi-elliptical surface cracks to experimentally determined fracture data, Newman and Raju ranked the highest amongst other solutions in terms of accuracy. Their solutions were able to correlate 95% of the data analyzed within ±10% error. According to Leek [15], an examination of different solutions of the SIF of a single crack shows that the solution provided by Newman and Raju [16] [17] has a good accuracy and is applicable over a wide range of semi-elliptical cracks.

Newman and Raju SIF solutions for a single crack are defined as follows [16] [17]:

$$0 \leq \frac{a}{r} \leq 2 \qquad \frac{r}{b} < 1 \qquad 0 \leq \emptyset \leq \pi \qquad (2.1)$$

where the variables are defined in Figure 2.2.
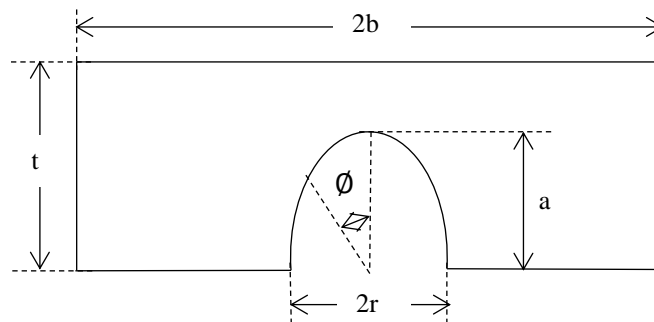
Figure 2.2: Single surface crack illustration

Newman and Raju proposed the following close form equation as a solution for the SIF [19]:

10

$$K_I = (\sigma_t + H\sigma_b)\sqrt{\pi\frac{a}{Q}}\, F\left(\frac{a}{t}, \frac{a}{r}, \frac{r}{b}, \varnothing\right) \tag{2.2}$$

$$F\left(\frac{a}{t}, \frac{a}{r}, \frac{r}{b}, \varnothing\right) = \left[M_1 + M_2\left(\frac{a}{t}\right)^2 + M_3\left(\frac{a}{t}\right)^4\right] \cdot g \cdot f_\varnothing \cdot f_w \tag{2.3}$$

$$f_w = \left[\sec\left(\frac{\pi c}{2b}\sqrt{\frac{a}{t}}\right)\right]^{\frac{1}{2}} \tag{2.4}$$

Newman and Raju's effort in developing equations for the SIF for a semi-elliptical surface crack in a finite plate subject to remote tension and bending loads were obtained in two main stages. The first set of equations was fitted to the finite element results developed for an aspect ratio, a/r, values less than or equal to unity as listed below [17]:

$$Q = 1 + 1.464\left(\frac{a}{r}\right)^{1.65} \tag{2.5}$$

$$M_1 = 1.13 - 0.09\left(\frac{a}{r}\right) \tag{2.6}$$

$$M_2 = -0.54 + \frac{0.89}{0.2 + \dfrac{a}{r}} \tag{2.7}$$

$$M_3 = 0.5 - \frac{1}{0.65 + \dfrac{a}{r}} + 14\left(1 - \frac{a}{r}\right)^{24} \tag{2.8}$$

$$g = 1 + \left[0.1 + 0.35\left(\frac{a}{t}\right)^2\right](1 - \sin(\varnothing))^2 \tag{2.9}$$

$$f_\varnothing = \left[\left(\frac{a}{r}\right)^2 \cos^2\varnothing + \sin^2\varnothing\right]^{\frac{1}{4}} \tag{2.10}$$

The equations for tension and bending loads for aspect ratios greater than unity are listed below [19]:

11

$$Q = 1 + 1.464 \left(\frac{r}{a}\right)^{1.65} \tag{2.11}$$

$$M_1 = \sqrt{\frac{r}{a}} \left(1 + 0.04 \left(\frac{r}{a}\right)\right) \tag{2.12}$$

$$M_2 = 0.2 \left(\frac{r}{a}\right)^4 \tag{2.13}$$

$$M_3 = -0.11 \left(\frac{r}{a}\right)^4 \tag{2.14}$$

$$g = 1 + \left[0.1 + 0.35 \left(\frac{r}{a}\right)\left(\frac{a}{t}\right)^2\right](1 - \sin(\emptyset))^2 \tag{2.15}$$

$$f_\emptyset = \left[\left(\frac{r}{a}\right)^2 \sin^2 \emptyset + \cos^2 \emptyset\right]^{\frac{1}{4}} \tag{2.16}$$

2.4 Cracks Interaction and Coalescence

The service life of engineering structures or components can potentially introduce many small sub-critical flaws that may jeopardize the structural integrity of the system. Inspection intervals are usually directed at the presence of a single crack, but may be inadequate in the presence of multiple crack interaction. A safety assessment of a structure that contains neighboring cracks in close proximity must take crack interaction into consideration as it could introduce a major reduction in a components' service life.

A conceptual comparison between multiple cracks and single crack growth in an aviation application is shown in Figure 2.3. A significant increase in the rate of crack growth was concluded due to the effect of crack interaction and coalescence.
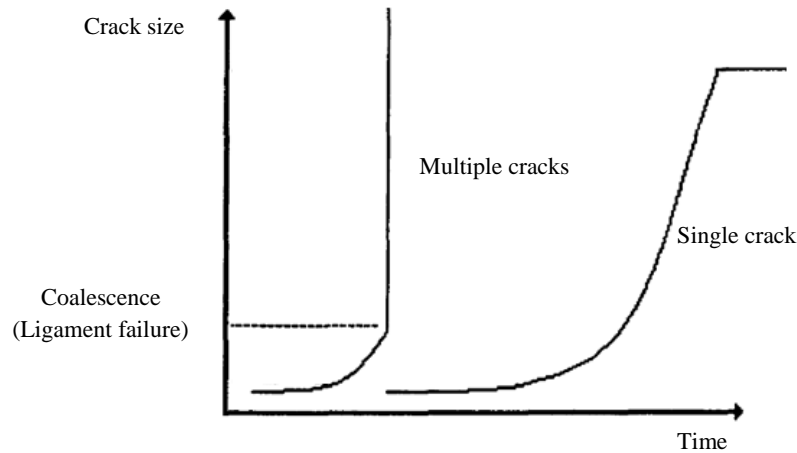
Figure 2.3: Single vs. multiple cracks growth in an aviation application. Adopted from "Multiple-Site and Widespread Fatigue Damage in Aging Aircrafts" by S. Pitt and R. Jones, 1997, Engineering Failure Analysis Journal [20]

Bayley [1] defined crack coalescence as the process of two independent cracks growing together and joining to form a single crack. Consistent with DeBartolo and Hillberry [21], crack propagation rate is influenced by neighboring cracks and their proximity. During propagation, cracks interact with each other even if the crack tips do not touch each other.

2.4.1 Different Stages of Neighboring Cracks Interaction and Coalescence

Various researchers have studied crack interaction and coalescence including: Harrington [22], Leek and Howard [23] [2] [15], Sobojeyo [24], Kishimoto [25], Twaddle [26], and O'Donoghue [27]. Most of their research was directed toward understanding the coalescence mechanism of two neighboring surface cracks.

According to Leek and Howard [23] and DeBartolo and Hillberry [21], the process of two adjacent and coplanar cracks interaction, coalescence and growth is governed by four main stages as illustrated in Figure 2.4:

13

1. Separate phase: The separation distance between the cracks is large enough for interaction to be completely negligible

2. Pre-coalescence phase: initially, neighboring cracks grow independently. However, the interaction starts and increases as the crack tips approach each other.

3. Re-characterization: the inner tips of the neighboring cracks come into contact forming a single concave crack. The crack grows more at the concave position, leading to the ligament failure. At the end of this stage, there is one enveloping crack present.

4. Post-coalescence phase: begins immediately after the two cracks are re-characterized as one and ends when the crack has resumed a uniform shape and continues to propagate as it did before interaction began.
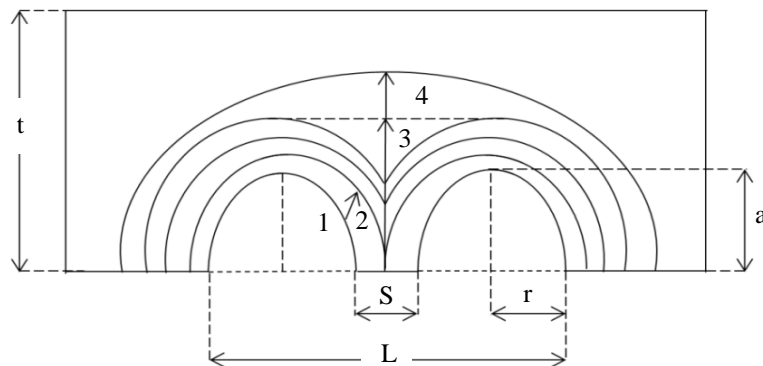
Figure 2.4: Crack growth stages: 1: Separate phase 2: Interaction phase 3: Re-characterization phase 4: Post-coalescence phase

[21]

According to Leek and Howard [23], during phase one of interaction, the neighboring cracks are treated independently meaning that they have no impact on each other's SIF. Also, in phase three, one single enveloping crack is formed and the single crack SIF analysis is used. However, the second phase, which is the interaction stage, is the stage when the proximity of neighboring cracks affects their respective stress fields. Experimental data and finite element simulations done by Soboyejo et al. [24] and Kishimoto et al. [25] showed that the concave crack front in

14

phase three has a high SIF value approximated by twice the SIF around the rest of the cracks due to the rapid failure of the ligament between the two cracks. This rapid failure of the ligament explains also the fast transition from phase two to phase three in this process.

Researchers have yet to reach an agreement on a threshold that indicates the start of crack coalescence. According to Forsyth [28], two cracks will grow together when the plastic zones around the cracks first overlapped. Chang [29] assumed that the cracks would coalesce when the distance between the two cracks was less than 7% of their total length. Chaussumier et al. [30] proposed that the coalescence of cracks is detected when their lengths increased by its crack tip when the plastic zone is large enough to interact with other neighboring cracks. Melin [31] stated that two neighboring cracks don't meet tip to tip but instead deviate slightly and meet either sub-surface or by a small tear at the surface. However, a more accurate identification of coalescence could be concluded by identifying the ligament failure. Swift [32] first proposed a ligament yielding criterion to specify when ligament failure occurs. The ligament failure is predicted when plastic zones around the neighboring cracks come into contact. Also, the failure mode was observed by Moukawsher et al. [33] and appeared to be due to the yield failure of the ligament. Jeong et al. [34] presumed that the stress field at each of the neighboring cracks tip results in yielded volumes. These volumes coalesce in the ligament before linkup, but the constraint of the surrounding material will prevent perfectly plastic deformation. Therefore, the load is focused towards the center of the ligament. When the stress in the ligament surpasses the yield strength approaching the tensile strength, ligament failure is predicted to occur.

According to Leek and Howard [3], there are three main factors that affect crack interaction and coalescence:

15

1. Separation distance between neighboring cracks

2. The shape and relative size of each crack

3. Thickness of the section in which the cracks lie

These factors should be taken into consideration when studying cracks interaction and coalescence for different applications, especially for simulations and experimental work.

According to Leek and Howard [2], when two coplanar cracks grow towards each other, before the cracks meet, either the SIF at the tip of closet proximity will reach the fracture toughness of the material leading to failure of the ligament between the cracks, or the plastic zones around the crack tips will come together invalidating the elastic analysis. Moreover, Melin [31] added, when the cracks grow towards each other, they tend to avoid meeting directly. He showed analytically that it is energetically unfavorable for them to do so. Therefore, that advocates that the crack tips will deviate as if to grow past each other when they become close and join up by tearing of the ligament between the places of the crack tips. So in order to simplify such situations, the failure of a certain engineering structure including interacting cracks could be predicted by setting a certain safety requirement like:

- Sudden increase in the SIF that implies the completion of the coalescence process and the formation of a single enveloping crack of a significant increase in dimension

- Crack front concave shape change to a convex shape caused by the ligament failure

- Surface cracks linkage

- Cracks fronts growth rate

2.4.2 Different Models of Cracks Interaction and Coalescence

Different assessment methods of neighboring crack interaction and coalescence have been investigated in order to identify a method that is reliable and reasonably conservative to further understand the phenomenon from a reliability/integrity stand point. Neglecting the effect of neighboring crack interactions on the SIF could lead to an overly conservative life prediction model and assessment of structure integrity. Leek and Howard [23] compared models that did not account for crack interactions and found that the safety margins achieved by such models induce overly conservative results of up to 37%. Also, Kuang [35] indicated that numerical results indicate that the residual strength of a MSD cracked panel may be overestimated by 40% when using a method which does not consider neighboring cracks interaction and coalescence.

According to Leek and Howard [2], the ASME boiler and pressure vessel code [36], section XI, articles IWA-3000 and IGA-3000, and the BSI PD6493 [37] are considered the most widely known methods for assessing interacting surface cracks. But, after tentatively investigating these methods both theoretically and practically, it was found that these models yield unrealistic overly conservative and perhaps unsafe crack growth predictions as it assumes a geometric condition to define cracks coalescence excluding the impact of neighboring cracks interaction and coalescence on the SIF [23] [15]. Moreover, the same author added that both model accuracy and justification of their methods are unknown.

Another widely accepted assessment method of interacting neighboring cracks was proposed by Iida [38]. The method neglects neighboring cracks interaction by having no measure of interaction effect on the SIF in its analysis. When the cracks inner tips are predicted to touch, an immediate semi-elliptical enveloping crack drawn through the outer tips of the two coalescing cracks and through the deepest point of the deeper crack is assumed. This method was used in

the literature as a basis for both experimental and simulation work by many researchers including Kishimoto et al. [25] and Sobojeyo et al. [24].

According to Leek and Howard [2], the method proposed by Iida [38] is a simple and realistic assessment method of neighboring cracks growth. However, it is not clear whether this method safely accounts for interaction on its own or whether safe assessments are obtained due to other factors in the growth calculations such as SIF approximations or even the material constants used. For that reason, the search for more reliable well defined models that defines a detailed process, logic and analysis was one of the main tasks in this research.

Two of the most widely used and accepted assessment methods of interacting neighboring cracks were developed by Leek and Howard [3] [23]. Both methods were based on quantifying cracks interaction and incorporating this quantification into the SIF and fatigue crack growth calculations. The Cracks Interaction Factor (CIF) was widely studied using finite element and numerical analysis by many researchers including Murakami et al. [4] [5], O'Donoghue et al. [27] and Leek and Howard [3] [15].

The first method developed by Leek and Howard [3] [15], denoted by Leek and Howard I, was based on developing cracks interaction factors which are considered as correction factor that quantifies the effect of neighboring cracks interaction on the SIF. Cracks interaction leads to an increase in the stress intensity around neighboring cracks when compared to single cracks. The SIF was corrected for the neighboring cracks interaction and coalescence as follows:

$$SIF_{neighboring\ cracks} = \gamma \times SIF_{single\ crack} \tag{2.17}$$

Where the cracks interaction factor (CIF) is defined as follows:

$$\gamma = \frac{K_I'}{K_I} \qquad (2.18)$$

The CIF used in this method was found using the solutions of Erdogan [39] and Yokobori et al. [40] for the elastic interaction factors of through cracks in an infinite plane under tensile load. Leek and Howard [3] corrected these CIF values in order to use it for cases of interacting semi-elliptical surface cracks. However, as the original CIF work addresses through cracks, this method had a mild emphasis on the crack front CIF while it focused more on the CIF at the crack tips. Moreover, this method can be cumbersome for crack growth calculations as it has many different calculation steps.

Leek and Howard found that the method developed earlier was complex. For that reason, they have developed another assessment method, Leek and Howard II [23] [15], which is derivative of the previous assessment method. This method is straightforward in application, consistently conservative and has an acceptable amount of realism. The same CIF concept discussed in the previous model was used for the formulation of this model. However, this model was based on developing interaction factor values associated with specific dimensional criteria describing cracks interaction and geometrical development. The method proposes a percentage increase in the SIF around neighboring crack for certain geometrical conditions. This percentage increase in the SIF is applied uniformly to all SIF values around neighboring cracks until the two cracks coalesce forming a single enveloping crack.

However, since the CIF approaches infinity when cracks become close at a certain separation distance, the maximum SIF obtained by the use of CIF becomes larger than that obtained by assuming an enveloping crack. For that reason, this point was considered to be the point at which the ligament between neighboring cracks fails forming a bigger enveloping crack.

19

According to Leek and Howard [2], Leek and Howard I and II have a realistic basis in taking measure of the whole crack geometry and theoretical evidence in their CIF formulation. For that reason, it was concluded that the two models are appropriate for use in the SIF simulations, as they provide realistic and safe interaction predictions.

Leek and Howard solutions, I [3] and II [23], were based on integrating Newman and Raju [16] [17] SIF solutions for single semi-elliptical cracks along with Erdogan [39] and Yokobori [40] solutions for the CIF. Nevertheless, the CIF proposed by Erdogan [39] and Yokobori [40] covers identical cracks. Savin [41] has proposed solutions for the CIF for non-identical cracks, but in this research, it was challenging to use such solutions as it requires high computational power and adds unnecessary complications to the analysis.

The modeling work in this research was formulated based on a combination of conclusions provided by the previously discussed models. Fundamentally, Newman and Raju SIF solutions for a single semi-elliptical crack SIF [16] [17], neglecting interactions model of Iida [38] and the CIF model of Leek and Howard [23] were used to formulate a model that could be used to compute the crack front SIF.

2.5 Fatigue Crack Growth

Developing a crack growth rate model used for life prediction applications could be relatively simple when the level of model prediction conservatism is irrelevant. However, providing accurate fatigue crack growth predictions using a realistic crack interaction model is one of the main aims of this research.

In order to design the optimum reliable fatigue design models, proper characterization of fatigue crack growth rate, da/dN, using appropriate loading parameters is critical. According to Suresh

[42], fatigue crack growth is a process of localized damage accumulation. Crack growth consists of a localized deformation around the crack front with a deformation proportional to the applied external load.

Estimations of fatigue crack growth rate aim to quantify the intrinsic resistance of the material or structure under various conditions of stresses and geometries [43]. Fatigue crack growth is characterized as follows:

$$\frac{da}{dN} \propto \sigma_s{}^p a^q \tag{2.19}$$

where p and q are empirical constants.

According to Paris, Gomez and Anderson [44], LEFM characterizes the rate of fatigue crack growth based on the SIF range:

$$\Delta K = K_{max} - K_{min} \tag{2.20}$$

Hence, the change in the SIF is defined as illustrated in the equations below:

$$K_{max} = F' \sigma_{s,max} \sqrt{\pi a} \tag{2.21}$$

$$K_{min} = F' \sigma_{s,min} \sqrt{\pi a} \tag{2.22}$$

$$\Delta K = F' \Delta \sigma_s \sqrt{\pi a} = F' \left(\sigma_{s,max} - \sigma_{s,min} \right) \sqrt{\pi a} \tag{2.23}$$

Paris, Gomez and Anderson [44], related the fatigue crack growth rate, da/dn, to the SIF with a power law relationship commonly known as the Paris equation:

$$\frac{da}{dN} = C(\Delta K)^n \tag{2.24}$$

Paris added that C and n are empirical constants subject to the material microstructure, cyclic load frequency, waveform, environment, temperature, and the stress ratio.

The Paris equation can be used to find the crack growth rate in both the surface and through the thickness. The through thickness crack growth rate could be obtained by:

$$\frac{da}{dN} = C_a(\Delta K)^n \tag{2.25}$$

On the other hand, the surface crack growth rate could be obtained using the following equation:

$$\frac{da}{dN} = C_c(\Delta K)^n \tag{2.26}$$

Newman and Raju [16] showed that the variation in fatigue resistance along the crack front is due to the variation in the stress field. Different crack growth coefficients, C_a and C_c, are used, which yield an improved prediction of the shape development of cracks. Newman and Raju [16] proposed the following correlation between the two coefficients:

$$C_c = 0.9^n C_a \tag{2.27}$$

The Paris equation is one of the most simplistic models to use because it covers a wide spectrum of materials and fatigue test conditions.

Walker modified the Paris law to account for the mean stress effect with $R \geq 0$ as illustrated below [8]:

$$\frac{da}{dN} = \frac{C(\Delta K)^n}{(1 - R)^{n(1-\lambda)}} \tag{2.28}$$

According to Fatemi [8], λ is an empirical constant that indicates the influence of the loading ratio on the fatigue crack growth in different materials and has a typical value of 0.3 in metals.

In this research, the Paris equation and the Walker equation were used for the crack propagation rate modeling as they are highly reliable and have been vastly used for such modeling purposes in the literature.

So, in a neighboring cracks fatigue problem, the following variables have to be identified in order to find the crack growth rate:

1. Loading conditions: including the applied stress level, loading ratio and frequency
2. Initial cracks geometry and dimensions
3. A valid method of approximating the SIF of a single crack
4. A valid law to calculate the crack growth rate
5. A valid method to account for the cracks interaction effect on the SIF of a single crack

Each of these variables will be defined and explained in this research in order to develop the data scatter required for the probabilistic life prediction model development.

3. Chapter Three: Experimental Work

The main purpose of performing the fatigue testing was to study the fatigue properties of the material with interacting cracks, understand the impact of the neighboring cracks dimensions, evaluate the impact of the loading conditions on the cracks interaction and propagation, and finally gather data for the life prediction model development and validation.

3.1 Testing Material

The material used in the fatigue testing was API-5L Grade B, which is used in the construction of some transport pipelines. An energy dispersive X-ray spectroscopy (EDS) analysis was performed to the samples in order to characterize the elemental composition of the material. EDS is a chemical microanalysis technique used in conjunction with scanning electron microscopy (SEM). The EDS technique detects x-rays emitted from the sample during the bombardment by electron beams to characterize the elemental composition of the analyzed volume [45]. Carlton et al. [46] investigated the accuracy and precision of EDX. In their tests, their experimental measurements mean values were estimated with relative errors within ±5% and relative standard deviations less than 5%, which shows high reliability in analyzing a material elemental composition. The elemental composition of the material used is illustrated in Table 3.1:

Table 3.1: Elemental composition of API-5L Grade B

Element	Si	Cr	Mn	Fe	Co	Cu	Total
Weight %	0.18	0.20	0.86	82.35	0.41	0.09	84.09
Atomic %	0.44	0.26	1.04	97.71	0.47	0.09	-

Moreover, in order to define the precise yield strength of the material for an accurate testing conditions determination, a tensile test was performed. The yield strength was found to be 300 MPa approximately. The stress strain curve produced is illustrated in Figure 3.1:
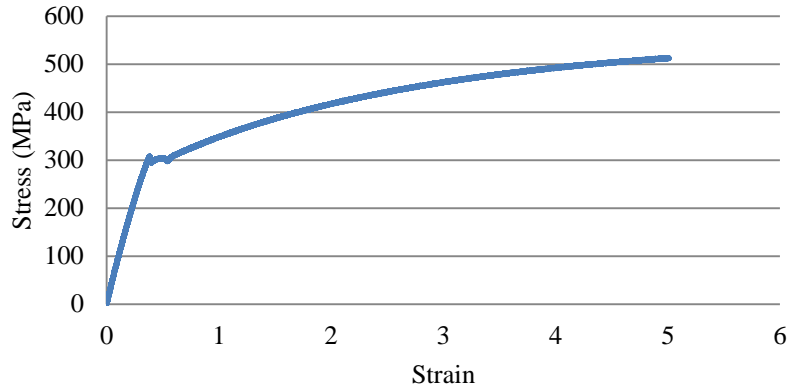
Figure 3.1: Plot of strain versus Stress for API-5L grade B

3.2 Testing Samples

Specimens with two adjacent initial cracks, simulating material defects and flaws, were considered for the crack coalescence experiments. The rectangular dog-boned shaped specimens have a thickness t and width 2W. The sample dimensions (i.e., designed according to the ASTM standard E466-07) are illustrated in Figure 3.2:
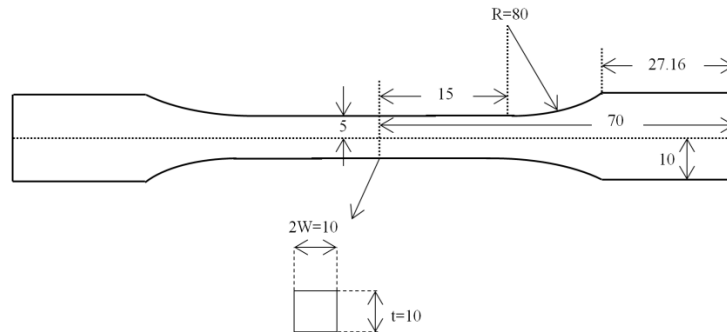
Figure 3.2: Sample dimension, all dimensions are in mm, sample thickness is 10mm

The material and the samples machining was done in Metal Samples [47] which specializes in manufacturing standard testing coupons and samples different types of tests using the latest metal cutting technologies.

3.3 Notches Design

The samples were notched in order to simulate material defects and flaws. The notches were designed according to the ASTM standard E740/E740M and machined using an electric discharge machining (EDM). EDM is usually used to induce notches, as it is a firm machining option for manufacturing geometrically complex and hard material parts that are difficult to machine by conventional machining processes [48]. Other machining options include using slit saw to induce the initial notches [2], however, such techniques induce unnecessary residual stresses around the notch and has less accuracy and precession.

Looking at the cross section of the test specimen, the notches are semi-elliptical in shape with a thickness of 0.1 mm, this geometry will assure a vertical growth of the crack, which leads to an idealized interaction between the two cracks. This is illustrated in Figure 3.3 :

Figure 3.3: 3D illustration of the notches, initial cracks

As corrosion pits are considered major flaws in engineering structures, especially in the oil and gas industry, the geometry of such flaws were considered for the experimental work. Using the findings of Nuhi et al. [13], the variation of pits sizes resulting from exposure a carbon steel material to different corroding environments showed that the maximum average pit size was

0.0163 μm with a standard deviation of 0.0032 μm. So the standard deviation makes 20% of the mean value. These variations in the pits sizes and geometry were considered in the design of the notches in this work.

In this experimental work, the notches are semi-elliptical and coplanar. Three main variables were considered for designing the neighboring cracks notches: depth, diameter and spacing. Eleven different notch combinations, as illustrated in Figure 3.4, were considered in order to have a complete representation of pitting corrosion flaws. However, the dimensions were amplified for accelerated testing purposes.
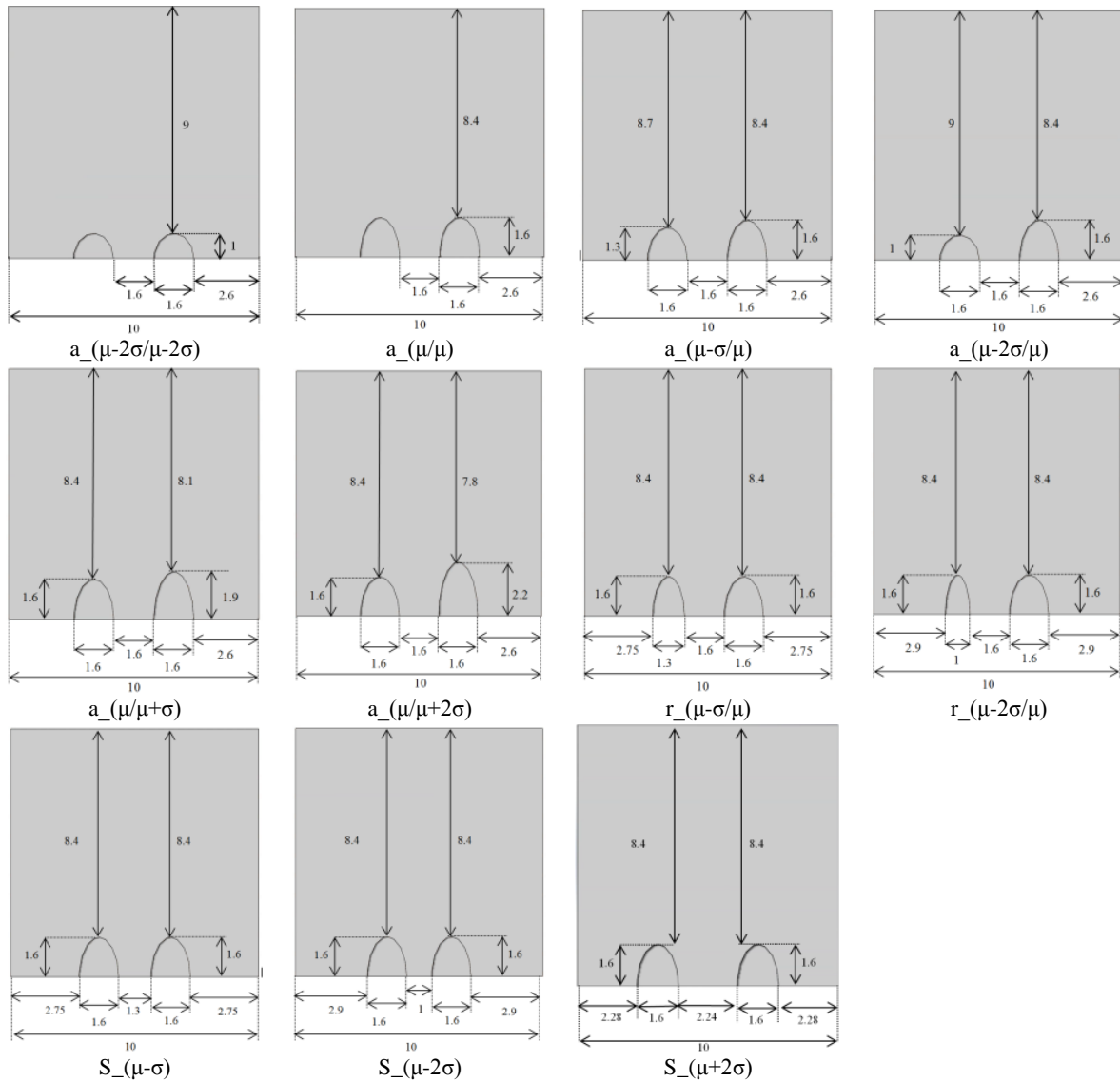
Figure 3.4: Different cracks notch, geometries (mm)

For simplification and reference purposes, each notch geometric shape was given a code that is introduced in Figure 3.4. The parameter μ is the initial notch size predetermined for accelerated testing purposes and the parameter σ is the standard deviation, which is 20% of μ. All experiments were compared to the reference geometry a_(μ/μ) for clarification purposes. For the crack notch geometry and dimensions at the start of each test, refer to Appendix A.

3.4 Experimental Procedure

Determining the number of cycles required for crack interaction, coalescence and failure are essential outcomes of the experimental work. This data will be the building blocks of the probabilistic life prediction model describing crack coalescence phenomenon. For that reason, a comprehensive experimental plan was designed to cover a wide range of crack geometries and loading conditions.

This research investigates the effect of three main variables on cracks interaction, coalescence and growth: cracks dimensions, applied load and the loading ratio. The samples with the variable dimensions will be tested under constant loading conditions. However, one specific geometry, $a\_(\mu/\mu)$, was tested under multiple stresses and loading ratios. The different fatigue testing conditions are illustrated in Table 3.2:

Table 3.2: Fatigue experimental testing conditions

Loading cycles				Marker band cycles				Load frequency (Hz)
Stress (MPa)		Loading ratio	# of cycles	Stress (MPa)		Loading ratio	# of cycles	
Max	Min			Max	Min			
270	27	0.1		270	215			
280	28	0.1		280	220			
	14.5	0.05	10000			0.8	2000	2
290	29	0.1		290	230			
	58	0.2						

A total of nineteen fatigue tests, including four duplicate tests, were performed according to the loading conditions shown in Table 3.2 using the standard dog bone samples. For a summary of the tests performed, refer to Appendix B.

The specimens were tested under constant amplitude uniaxial loading. The fatigue cycles consisted mainly of loading blocks and marker blocks. The loading blocks are the primary reason for crack propagation. On the other hand, the marker blocks were primarily used as a

benchmarking technique to show crack shape progression during the fatigue testing. This allows for a better understanding of the nature of interactions between the two cracks.

According to Willard [49], one of the methods to monitor the fatigue crack front history after testing is to use the marker bands technique. Willard [49] defined marker bands as groups of microscopic striations that when generated in the proper fashions are readily identifiable by optical and scanning electron microscopy.

The marker block consists of load cycles with the same maximum stress applied; however, the minimum stress was increased to 80% of the maximum stress. According to Terrell [50], it was observed that marking block with high stress ratio yields a better marking impression, which is of better visibility. A typical loading ratio used in marker blocks varies from 0.5 to 0.8.
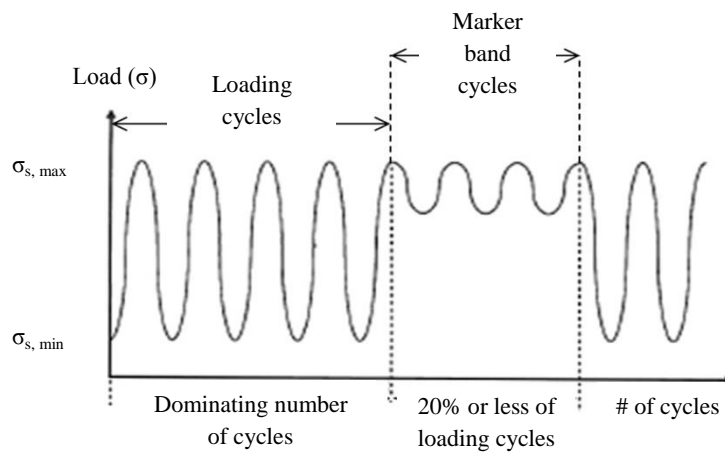
Figure 3.5: Plot of number of cycles versus applied load, a load patter illustration of the maker band technique. Adopted from "Effect of Cyclic Frequency on the Fatigue Life of ASME SA-106-B Piping Steel in BWR Environments" by J. Terrell, 1988, Journal of Material Engineering **[50]**

Other researchers like Leek and Howard [2] stated that changing either the loading ratio or the load frequency could induce marker bands. However, as there is still a debate in the literature on

the load frequency effect on crack growth, this research used variable loading ratio to induce the marker bands.

The loading cycle was sinusoidal in waveform with a frequency of 2 Hz. According to Terrell [50], for API-5L grade B or A106, there is no effect of load frequency on the fatigue life of notched samples at room temperature.

The experiments were carried out at room temperature in air and fatigued on an MTS 311.11 load frame. The machine is of a variable capacity of up to 100 kN. An Instron 8800 controller controlled the load sequences used in the experiments. A real time optical microscope was used to monitor the surface crack length during the fatigue process. The experimental layout and the microscope positioning are illustrated in Figure 3.6:
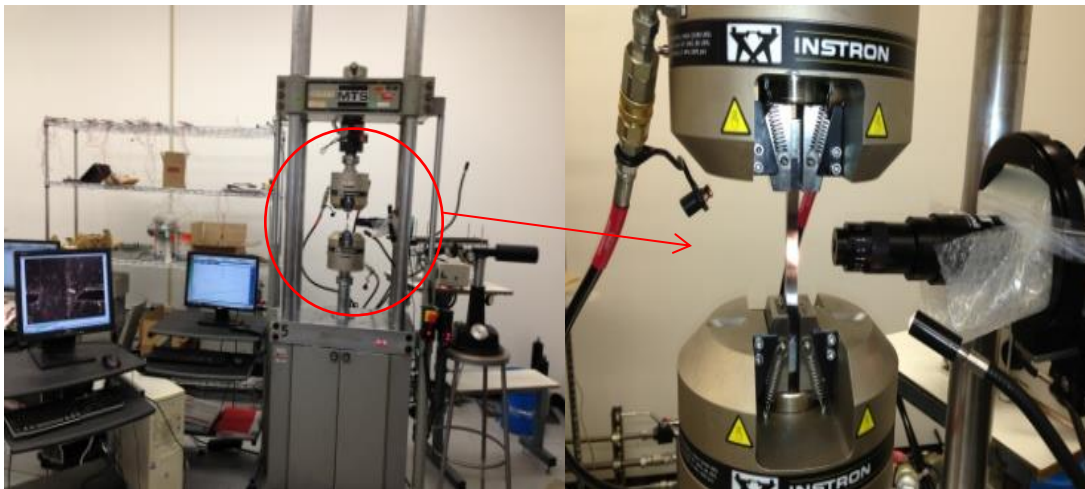
Figure 3.6: MTS machine load frame experimental layout along with the microscope installation and positioning relative to the test section

The start of each test was defined when the surface cracks had initiated and grown providing useful data. Similarly, the end of each test was defined as when no more useful data could be obtained. This happens when the surface cracks approaches the sample edge. However, the

31

samples were fatigued until failure and completely broken to avoid breaking it in a brittle manner and affecting the fracture surface, which is the main source of elucidating crack growth data.

3.5 Experimental Data Analysis

In order to develop a data scatter out of the fatigue experiments, failed samples have to be analyzed and information has to be elicited. The fatigue experiments provide two main sources of data:

2. Surface crack measurements at different number of cycles
3. Crack depth measurements, marker bands

Relating the surface crack length to the crack depth at different number of cycles provided the scatter required for the modeling efforts. For identical cracks growth measurements, either of the two neighboring cracks could be measured for growth, as they propagate having a similar growth rate. However, in non-identical cracks cases, the bigger crack was monitored for growth, as it will be the dominating flaw as proven by the experimental work. A more detailed discussion of this process will be presented next.

3.5.1 Surface Crack Measurement

Surface crack measurements were conducted using an optical microscope. The microscope continuously captured pictures of the sample surface during the fatigue experiment. This process was done in two main stages: before and after crack coalescence.

The microscope was focused on the area between the two cracks, as illustrated in Figure 3.7, to take surface crack measurements before coalescence.
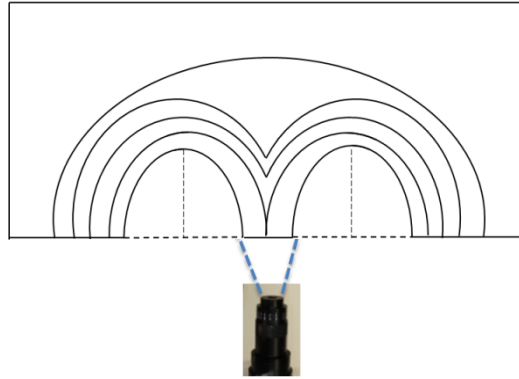
Figure 3.7: Surface crack growth data gathering, before coalescence

Right at the point of coalescence, when the two surface crack tips touch, the microscope was moved to capture the surface crack growth on the other side of the notch towards the sample edge as illustrated in Figure 3.8.
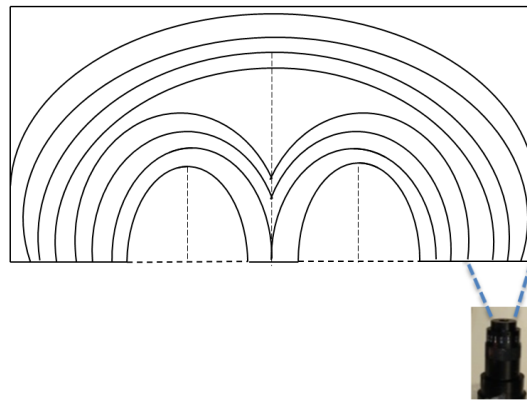
Figure 3.8: Surface crack growth data gathering, after coalescence

In all experiments, the microscope was focused on the bigger crack. As the crack dimension affects the SIF around the crack tips and front, a faster crack growth rate was expected at the bigger crack.

After each experiment, high quality images were used for analysis and image processing. Each picture provided the number of cycles it took to achieve a certain crack growth. Moreover, these

pictures were used to measure the surface crack growth, using image-processing software called ImageJ. The software allowed for the correlation of the pixels of an image to the crack diameter or the sample width which allowed measuring the surface crack length.

Other researchers like Leek and Howard [2] have used a traveling microscope to measure the surface crack length. Although traveling microscopes were widely used for such measurements, optical microscopy shows high levels of accuracy as image-processing softwares offer high accuracy measurements.

3.5.2 Crack Depth Measurement

Both SEM fractography and optical microscopy were used to analyze the fracture surface of the failed samples. SEM was used to get a closer look at the marker bands and confirm their existence. A series of SEM fractography images are shown in Figure 3.9.
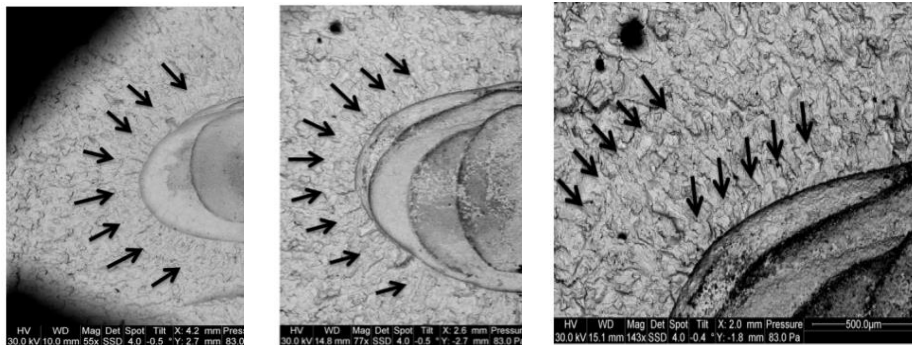
Figure 3.9: SEM images of the fracture surface, marker bands illustration

Although the SEM images show the marker bands clearly, optical microscopy yielded clearer fractography images that are easier for image processing. For that reason, optical microscopy was used as the standard method for fracture surface imaging.

34

Post-failure crack growth measurements were further conducted using quantitative fractography, which involved locating the marker bands on the failed sample fracture surface using an optical microscope. Marker bands similar to the ones conceptually illustrated in Figure 3.10 were located and used to measure the crack depth. Knowing the surface crack length and the associated number of cycles from the surface crack measurements, a correlated depth measurement could be made in order to find the crack depth at that surface crack length and number of cycles.
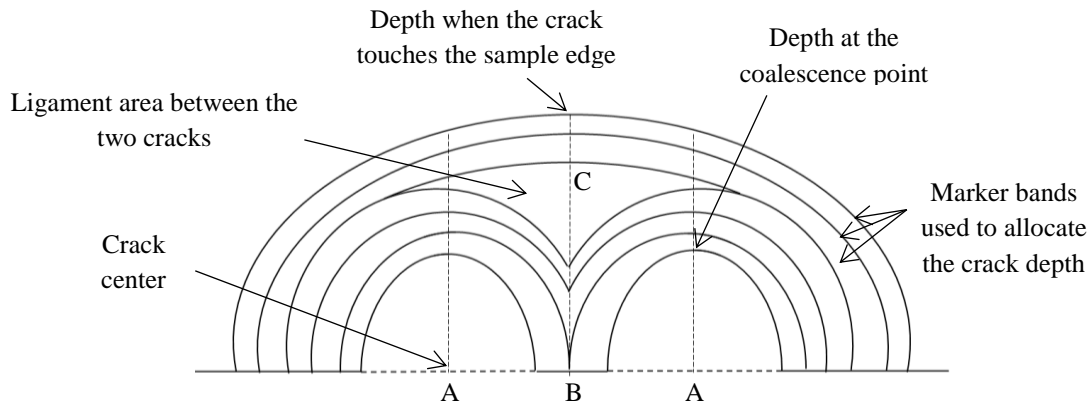
Figure 3.10: Marker bands illustration

The same image-processing software, ImageJ, used for the surface crack measurements was used for the fracture surface analysis. The crack depth measurements were performed at the point of maximum depth of the bigger notch, A_i points as illustrated in Figure 3.10, until an enveloping crack is formed after coalescence. Then the depth measurements were made at the maximum depth of the enveloping crack, C_i points. The crack center before coalescence is located at point A. However, the crack center shifts to point B right after coalescence to account for the bigger enveloping crack geometrical development.

3.6 Experimental Results

In this section, a summary of the findings and conclusions made after performing the experimental work is presented. Different measurements of the surface crack growth between the two cracks were recorded and correlated with the number of cycles and crack depth. A real time microscopy method was employed during the fatigue tests to keep a record of the surface crack growth. An illustration of the surface cracks growth before coalescence is shown in Figure 3.11:

c= 0.86 mm	c= 0.96	c= 1 mm	c= 1.03 mm
N= 59400	N= 62160	N= 70680	N= 78960
dc/dn= 9.89E-10	dc/dn= 7.34E-10	dc/dn= 4.28E-9	dc/dn= 4.40E-9

c= 1.07 mm	c= 1.12 mm	c= 1.16 mm	c= 1.19 mm
N= 85320	N= 93840	N= 102240	N= 105480
dc/dn= 5.41E-9	dc/dn= 5.7E-9	dc/dn= 5.54E-9	dc/dn= 8.12E-9

c= 1.36 mm	c= 1.37 mm	c= 1.41 mm	c= 1.6 mm
N= 112200	N= 113520	N= 116040	N= 117480
dc/dn= 2.5E-8	dc/dn= 6.14E-9	dc/dn= 1.77E-8	dc/dn= 1.31E-7
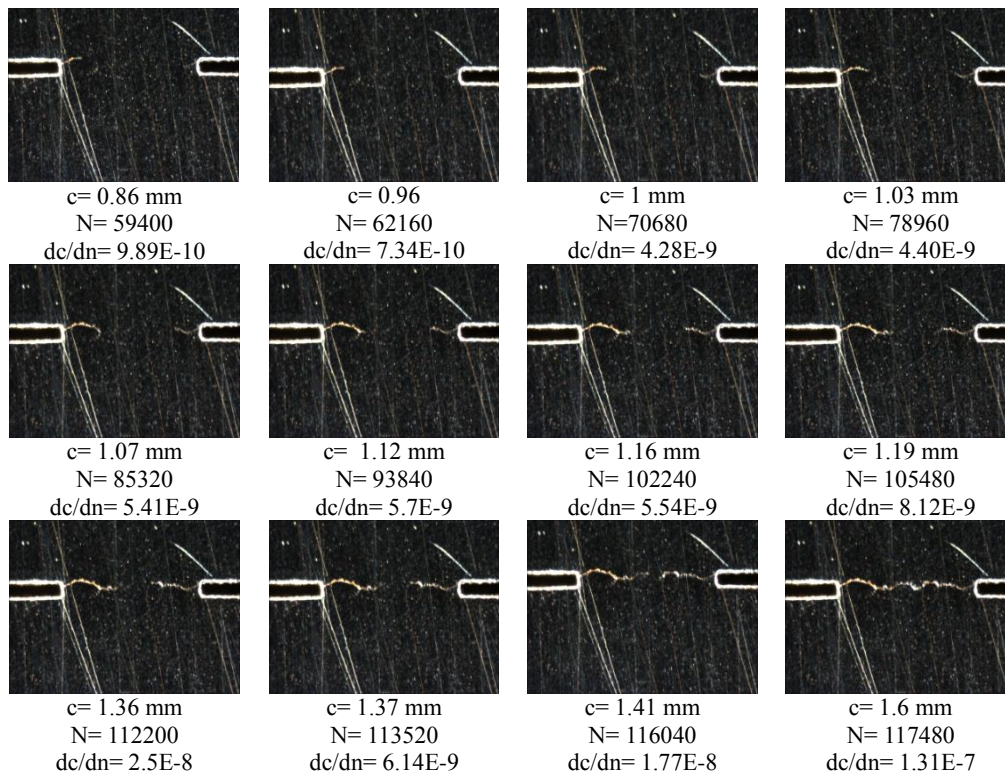
Figure 3.11: Surface crack growth before coalescence, σ_s=270 MPa, f=2 Hz

One main conclusion from the experiments was that the surface crack growth rate between the two cracks, dc/dn, was increasing as result of the cracks interaction effect on stress intensity. As the two surface cracks approach each other, the stress intensity factor increased leading to an increasing surface crack growth rate.

On the other hand, a different surface crack behavior was noticed after cracks coalescence. The surface crack growth rate decreased gradually until it got closer to the sample edge where the sample corner edge effect on stress intensity factor became effective. This led to an increasing crack growth rate as the crack propagates toward the sample edge. An illustration of the surface cracks growth after coalescence and until failure is shown in Figure 3.12:

c= 3.31 mm	c= 3.44 mm	c= 3.72 mm	c= 3.81 mm
N= 141840	N= 143880	N= 148080	N= 150480
dc/dn= NA	dc/dn= 6.23E-8	dc/dn= 6.68E-8	dc/dn= 3.76E-8

c= 3.90 mm	c= 3.91 mm	c= 4.47 mm	c= 5 mm
N= 154440	N= 156600	N= 158640	N= 160320
dc/dn= 2.28E-8	dc/dn= 1.9E-9	dc/dn= 2.74E-7	dc/dn= 3.2E-7
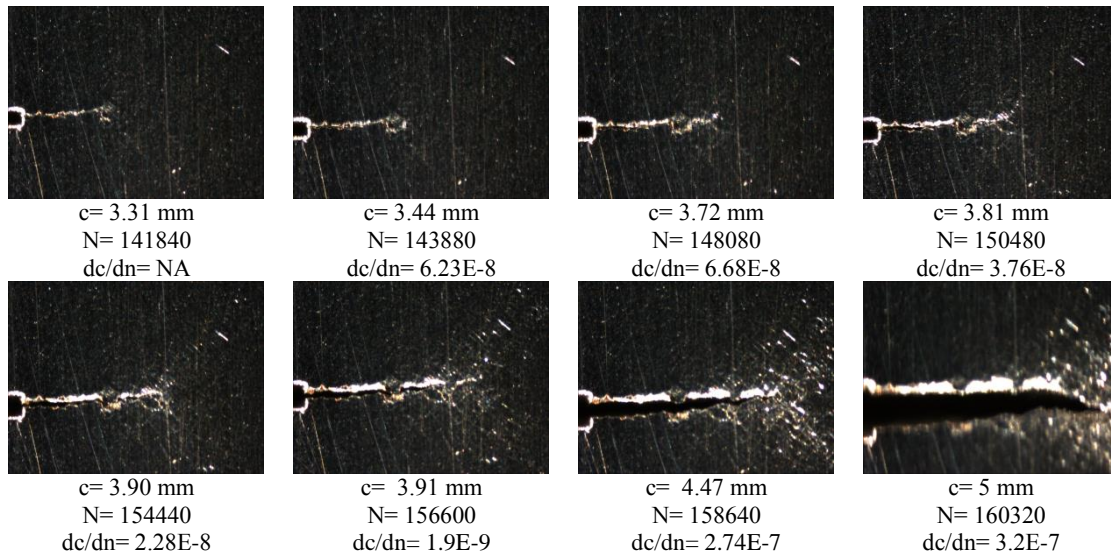
Figure 3.12: Surface crack growth after coalescence, σ_s=270 MPa, f=2 Hz

On the other hand, in order to find the crack depth growth rate, marker bands were used to find the depth at different number of cycles. The fracture surface of eight different fatigued samples using the marker band technique is illustrated in Figure 3.13. Each fracture surface was analyzed using ImageJ and the crack depth was found at different number of cycles by correlating the surface crack measurement performed earlier on the sample surface with the depth measurement performed on the fracture surface.

| a_(μ-2σ/μ) | a_(μ-σ/μ) | a_(μ/μ) | a_(μ/μ+2σ) |
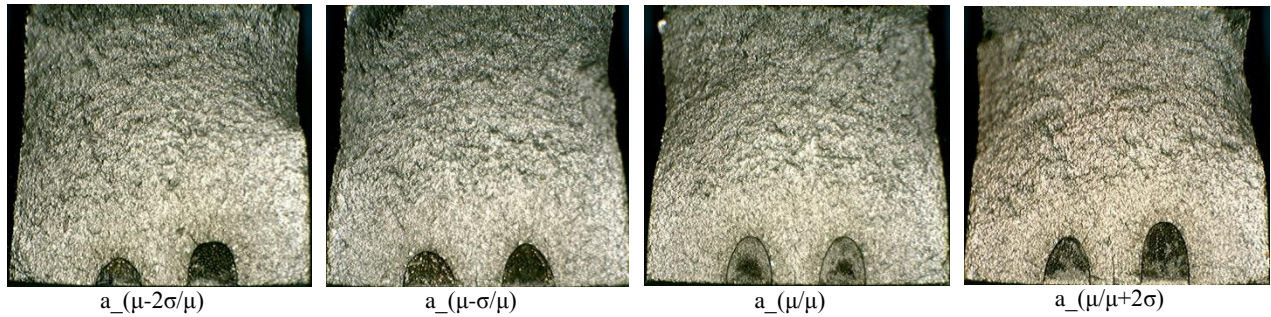
Figure 3.13: Fracture surface microscopic images; marker bands illustration, σ_s=290 MPa, LR=0.1, F=2 Hz

Different materials respond differently to the marker bands technique depending on their ductility. API-5L grade B showed high ductility, however, the marker band contours were relatively clear on the fracture surface.

Most of the tests followed the same patterns when it came to the crack depth behavior. The two cracks would coalesce at an approximate depth of 2.1-3.1 mm depending on the neighboring cracks dimensions. Moreover, when the surface cracks reached the sample tip, which is defined as failure in this case, the crack had an average depth of 4.5mm. These measurements were fairly consistent along the range of variables used in the experiments.
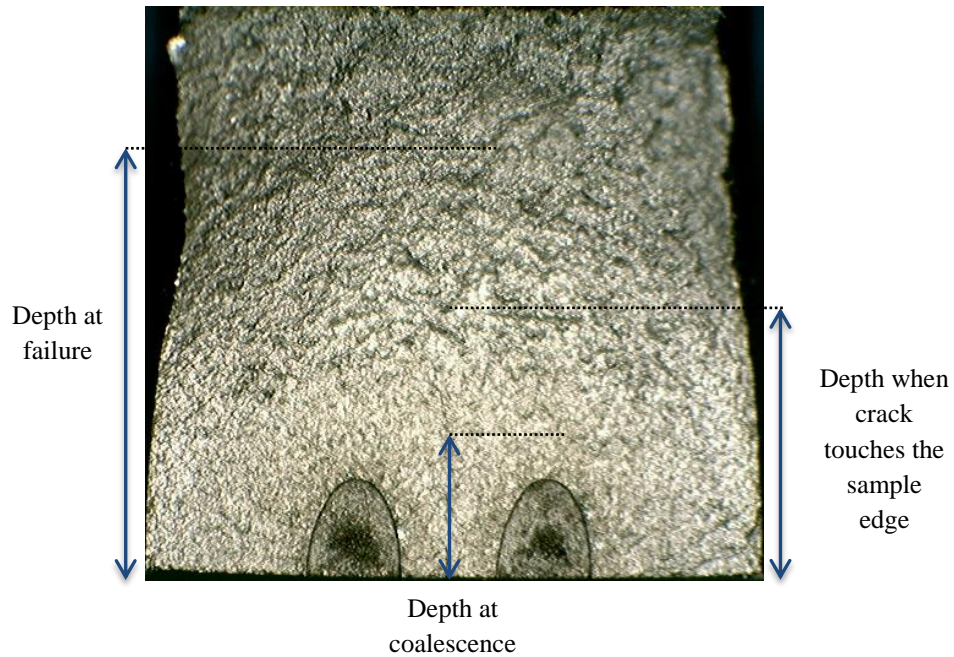
Figure 3.14: Crack depth Measurement using Image J software

As shown in Figure 3.14, the failed samples were cut and analyzed under the optical microscope; the fracture surface showed some marker bands which were used for the depth measurements. The fracture surface was then analyzed using Image J, to find the crack depth. An example of the experimental data collected is demonstrated in Appendix C.

By combining and analyzing all of the performed measurements, information and results about crack interaction, coalescence and growth were found. The kind of data that could be obtained from the suggested methodology is illustrated in Figure 3.15:
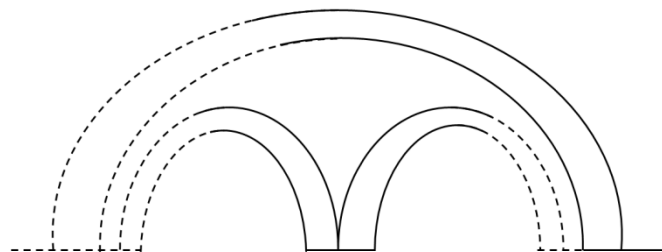
Figure 3.15: Illustration of the data obtained from the experimental work

39

The solid lines indicate that information about the crack depth and radius are possible to measure. However, the dashed lines correspond to the area were information are not available and measurements are not possible. Yet, using more than one camera during the test to capture the surface cracks growth would provide a more complete profile of measurements.

Also, the heat treatment due to the EDM notching has affected the crack growth rate near the cracks in the heat-affected zone. For that reason, the first six measurements of crack growth were neglected and not used in the modeling development. Likewise, the last six measurements before failure were also neglected as this research focuses on region II of crack growth.

3.6.1 Neighboring Cracks Dimensional Variability Effect on Crack Growth

One of the main variables in this work was the neighboring cracks dimensional variability. The main purpose of varying the cracks dimensions is to understand the impact of the crack dimensions variability on cracks interaction and growth. Crack depth, diameter and spacing were varied, as previously illustrated in Figure 3.4 and tested under the same loading conditions.

The first dimension tested was the neighboring cracks depth. In this part of the experimental work, the cracks radius and spacing were kept constant. Moreover, all the tests performed to examine the cracks dimensions were performed under the same loading conditions with a maximum stress of 290 MPa and a loading ratio of 0.1.

In order to understand the effect of the cracks' depth variability, one of the cracks was kept at a constant depth of 1.6 mm while the other cracks' depth was varied. The bigger crack growth and development was monitored for the crack growth data generation and modeling purposes.

One of the main findings of this section is that increasing the depth of one of the neighboring cracks by one standard deviation (i.e., 20% of the initial crack depth) accelerates failure by

almost 23% compared to the reference geometry (i.e., a_(μ/μ) having two identical cracks). This acceleration effect is due to the increased stress intensity between the two cracks and at the crack front which led to a faster ligament failure and crack growth. However, increasing the depth of one of the neighboring cracks by two standard deviations had a similar failure time to the one standard deviation depth increase case, which indicates similar stress intensity between the two cracks disregarding the greater difference in depth.

On the other hand, decreasing the depth of one of the neighboring cracks by one standard deviation, a_(μ-σ/μ), decelerates failure by nearly 10 % compared to the reference geometry. This deceleration is due to reduced stress intensity between the cracks leading to slower interaction and growth. Yet, decreasing the depth of the one of the neighboring cracks by two standard deviations yielded very similar results to the one standard deviation depth decrease case showing a very similar behavior to the increasing depth experiments. A summary of the findings of different experiments discussed earlier is illustrated in Figure 3.16:
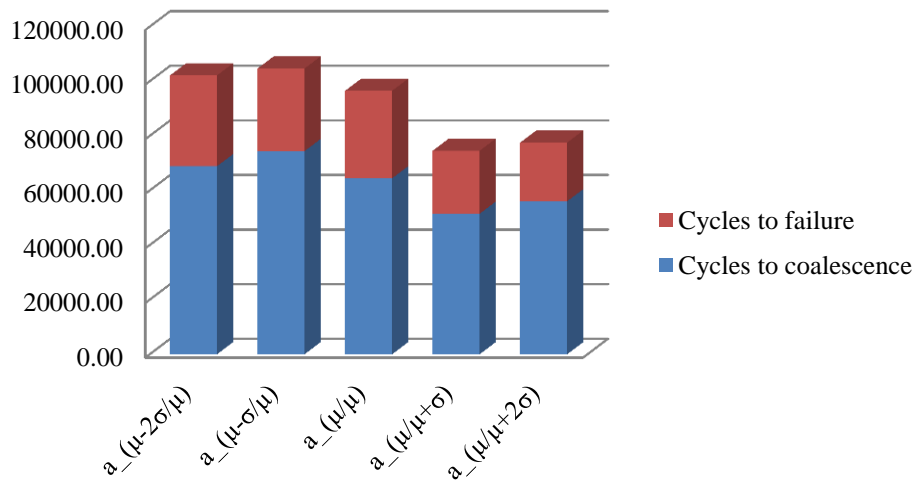
Figure 3.16: Impact of the neighboring cracks depth on the number of cycles to coalescence and failure

41

In order to confirm the importance of the initial cracks depth, one test was performed for a sample with two smaller notches, a_(μ-2σ/μ-2σ), and then compared to the average coalescence and failure time of the previously discussed experiments. A significant increase in the failure time was noticed as illustrated in Figure 3.17:
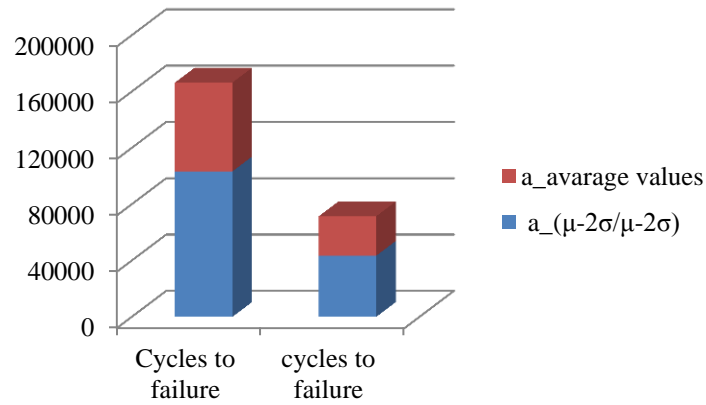
Figure 3.17: Initial neighboring cracks depth significance and impact on time to calescence and failure

The crack depth measurements were plotted against number of cycles along with an illustration of the associated experimental measurement uncertainty in Figure 3.18 for a better understanding of the role of initial neighboring cracks depth on crack growth. The experimental measurement uncertainty was quantified in this work, as detailed in chapter six section 6.2, and was found to be around 17% with 95% confidence.
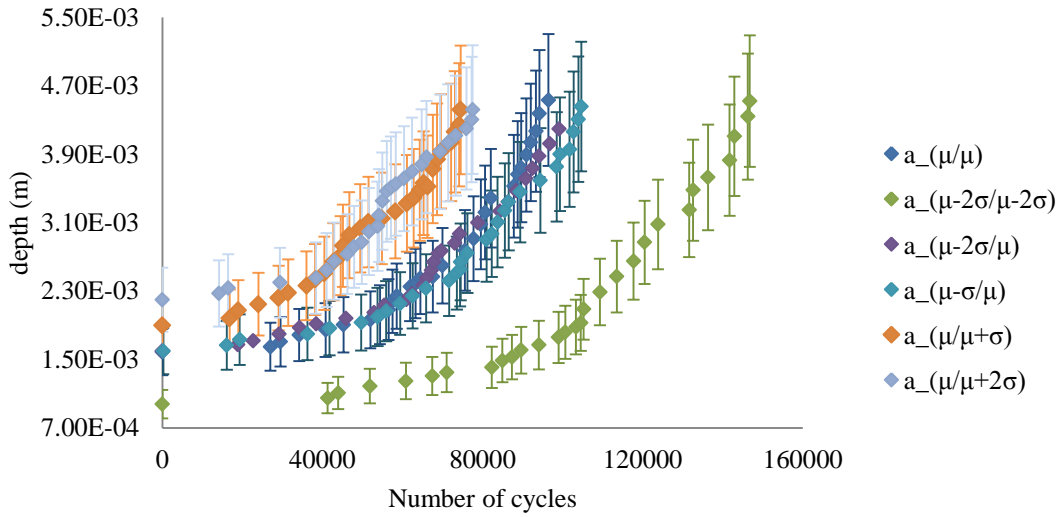
a)
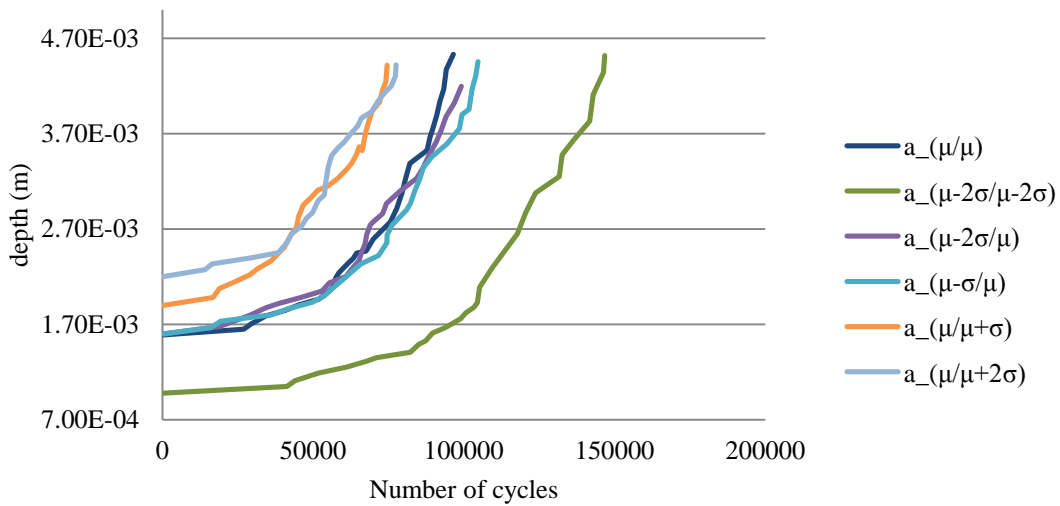
b)

Figure 3.18: Plots of the number of cycles versus crack depth measurements of neighboring crack of variable initial depth, a) Crack depth measurements along with the associated uncertainty at different number of cycles, b) A series of crack growth curves using the mean crack growth measurements

Another dimension tested in this work was the neighboring cracks radius. In this part of the experimental work, the notches had a constant depth and spacing, however, one of the neighboring cracks radius was varied. As illustrated in Figure 3.19, decreasing the radius by

43

either one or two standard deviations did not affect the sample failure significantly compared to the reference geometry. This is observed due to the mild impact of the neighboring cracks radius on the SIF at the crack tip which directly impact the rate of crack growth.
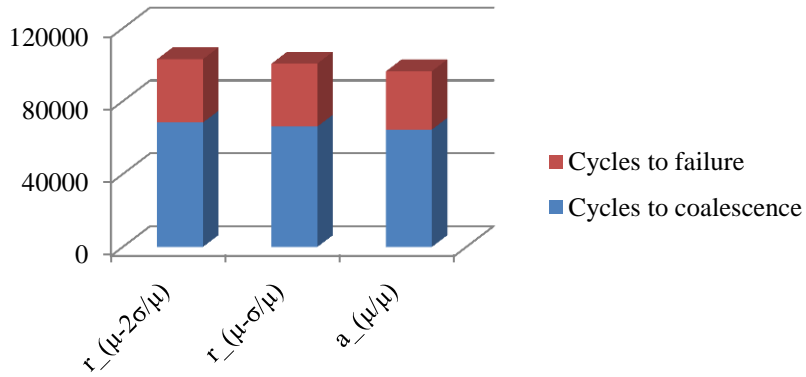
Figure 3.19: Impact of the neighboring cracks radiuses on the number of cycles to coalescence and failure

A slight difference in crack growth rate behavior between the three different cases was observed as shown in Figure 3.20 plots:
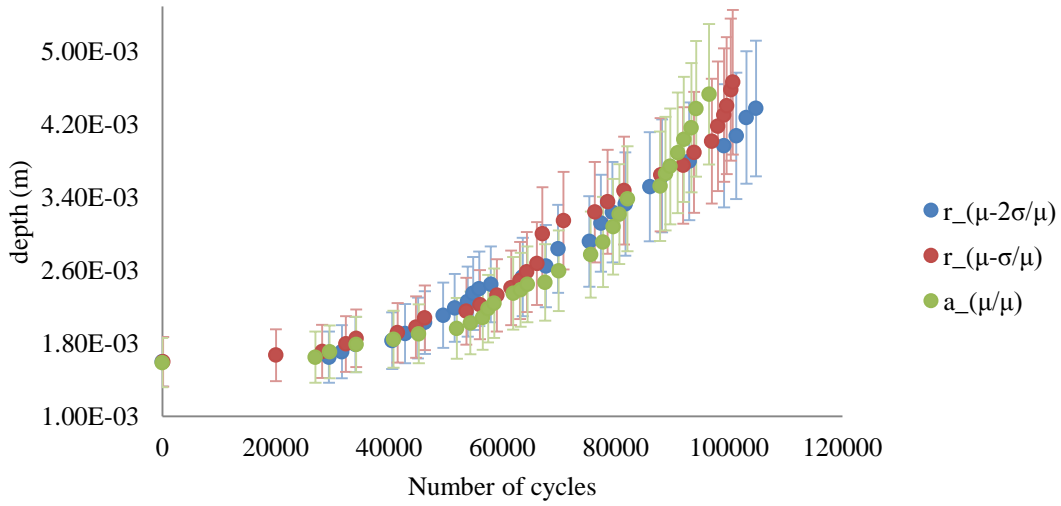
a)
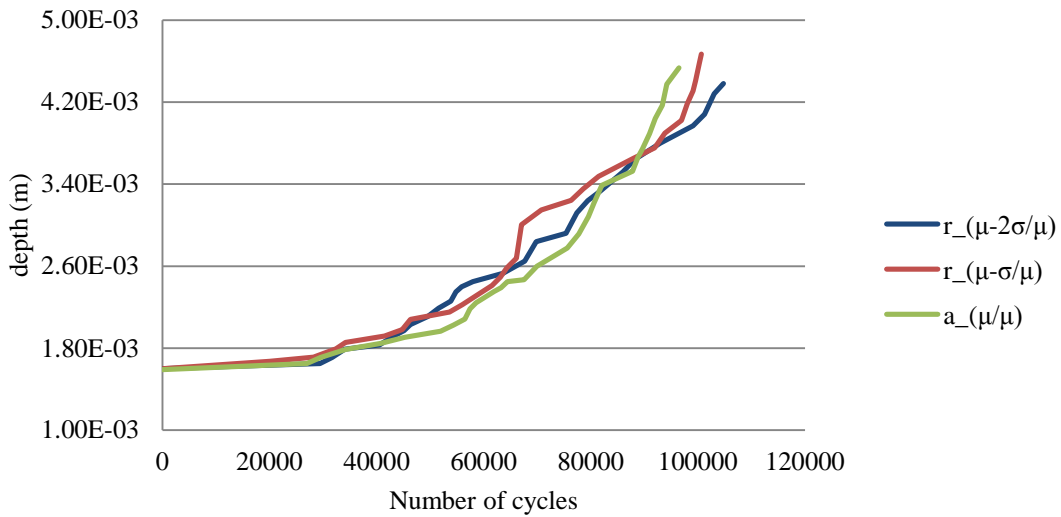
b)

Figure 3.20: Plots of the number of cycles versus depth measurements of neighboring crack of variable initial radius, a) Crack depth measurements along with the associated uncertainty at different number of cycles, b) A series of crack growth curves using the mean crack growth measurements

According to Murakami et al. [5], spacing between neighboring cracks plays a major role in their interaction and coalescence. One of his major conclusions is that if there is a space that allows the existence of a third crack between the two cracks, then the interaction effect between the two

45

cracks at that specific geometric condition is negligible. This statement was investigated experimentally in this research as illustrated in Figure 3.21. A significant increase in the number of cycles to failure was observed when the two cracks were located further apart supporting Murakamis' conclusion.
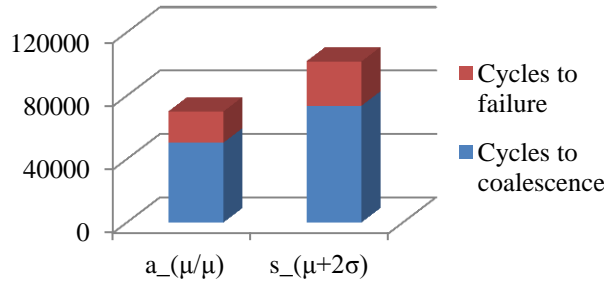
Figure 3.21: Increased neighboring cracks spacing effect on cycles to coalescence and failure

Moreover, two tests were performed with smaller spacing compared to the reference geometry in order investigate how that would accelerate failure. As seen in Figure 3.22, spacing has mainly influenced the number of cycles to coalescence, meaning a faster ligament failure.
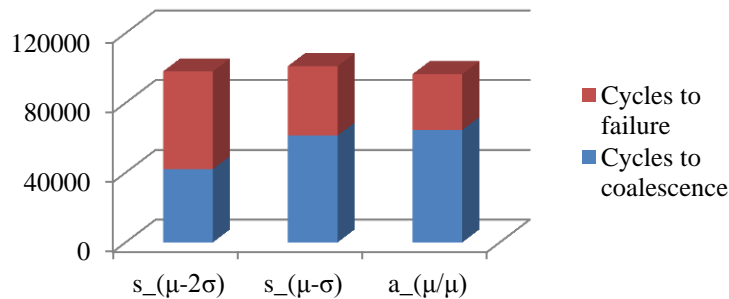
Figure 3.22: Impact of the neighboring cracks spacing on the number of cycles to coalescence and failure

A main reason for this result is that by decreasing the distance between the two cracks, the distance between the outer crack tips and the sample edge increases. As the surface crack growth rate between the two cracks is much faster than it is at the outer crack tip, more time is needed to

46

achieve total failure of the specimen which compensates for the time difference due to the faster time to coalescence caused by the smaller spacing. The crack growth measurements at different number of cycles for different spacing geometries are illustrated in Figure 3.23 plots:
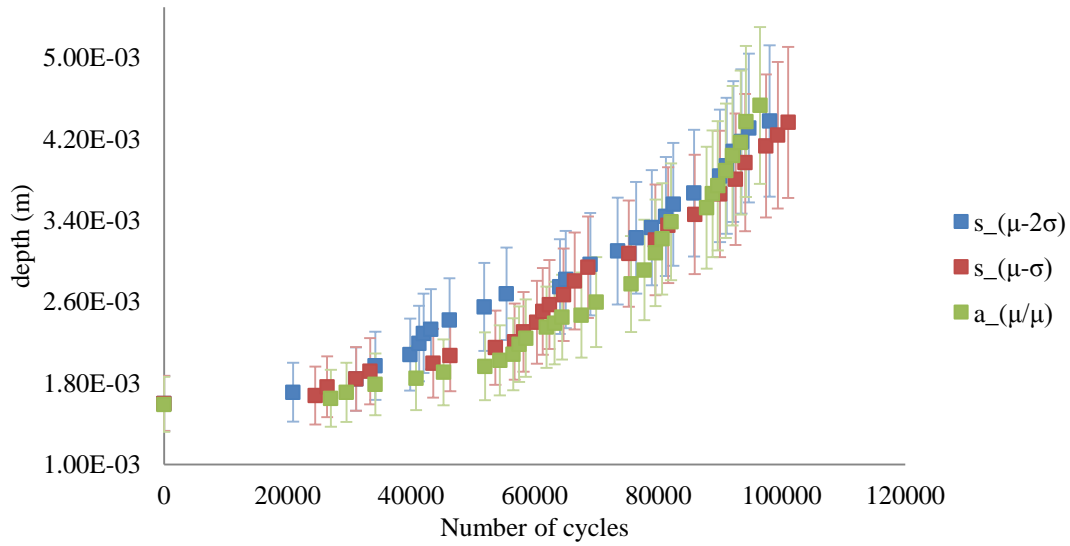
a)
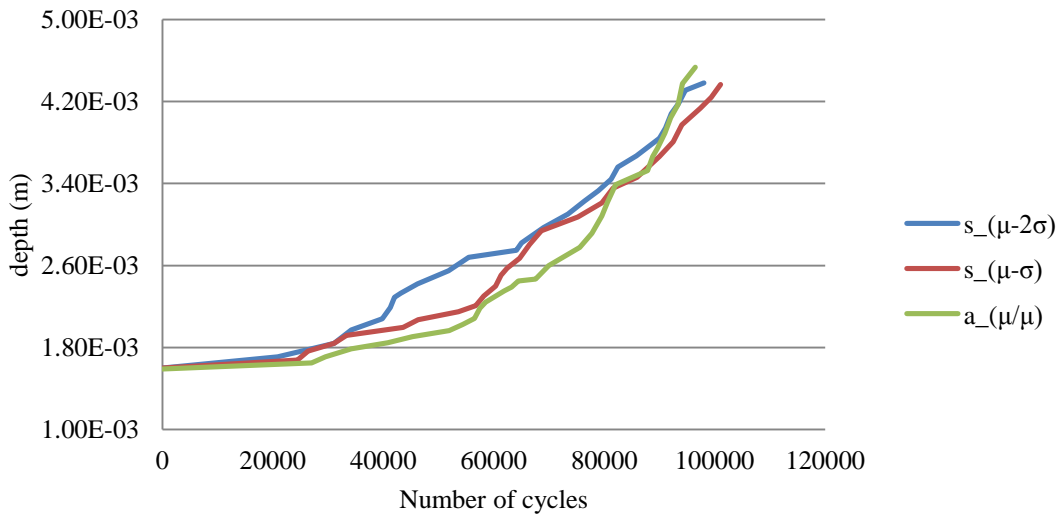
b)

Figure 3.23: Plots of the number of cycles versus depth measurements of neighboring crack of variable initial spacing, a) Crack depth measurements along with the associated uncertainty at different number of cycles, b) A series of crack growth curves using the mean crack growth measurements

47

3.6.2 Loading Conditions Effect on Neighboring cracks Growth

As loading conditions play a major role in determining the life of engineering structures, different loading conditions were considered in this research. Applied stress and loading ratio are the two main loading variables considered. In this section of the experimental work, the geometry was kept constant and all tests were performed using the reference geometry $a_{(\mu/\mu)}$.

In order to test the effect of stress on both times to coalescence and failure, the reference geometry was tested under a constant loading ratio of 0.1 at three different stresses. As illustrated in Figure 3.24, both times to coalescence and failure decrease by increasing stress.
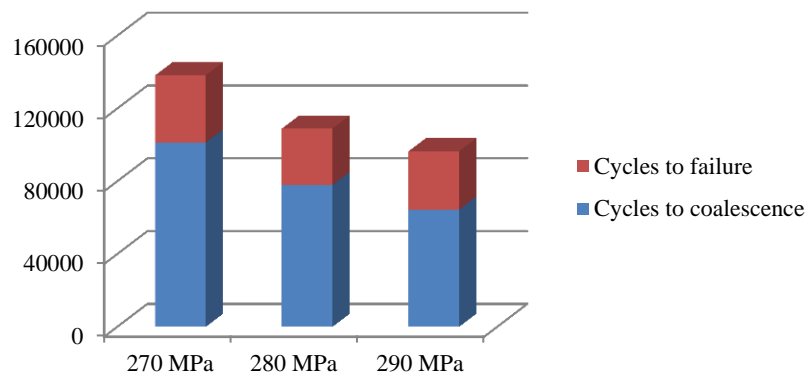
Figure 3.24: Impact of the different stress levels on the number of cycles to coalescence and failure

A similar crack growth behavior was observed at the three different stresses. However, the crack propagation rate was faster with higher stresses as illustrated in Figure 3.25 plots:
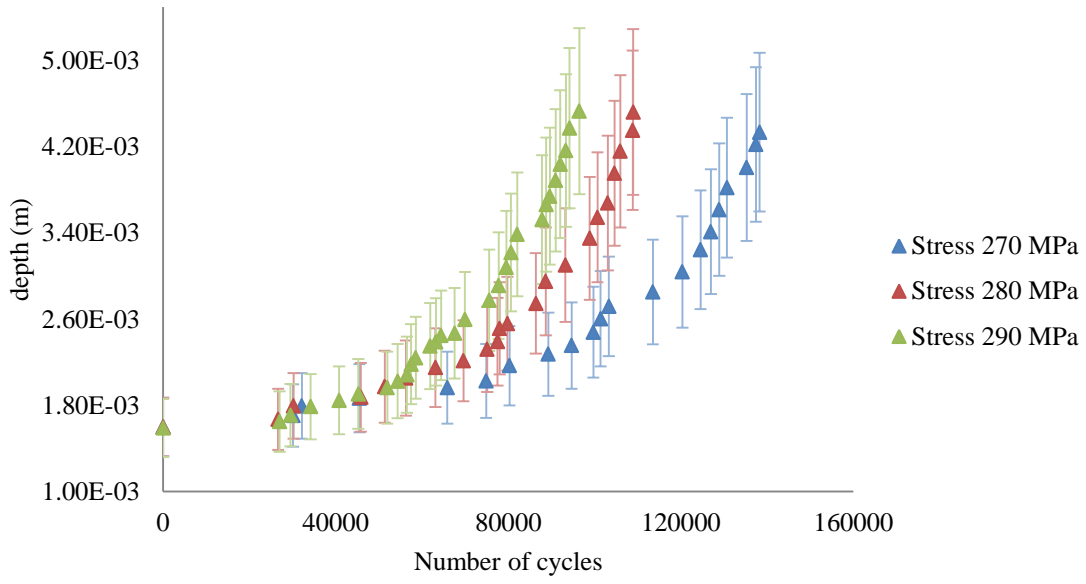
a)
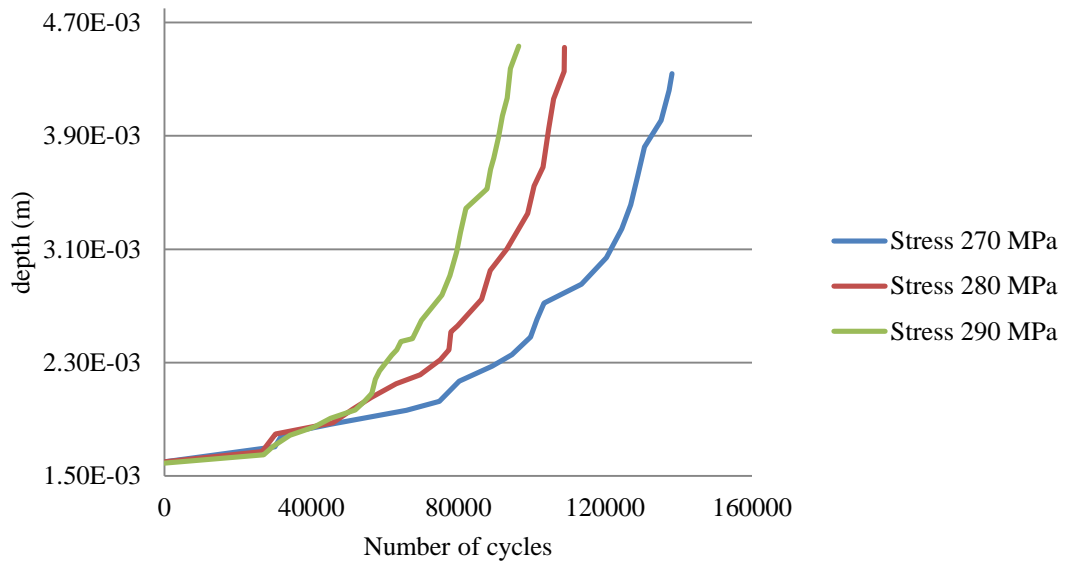
b)

Figure 3.25: Plots of the number of cycles versus depth measurements of neighboring crack at different stress levels, a) Crack depth measurements along with the associated uncertainty at different number of cycles, b) A series of crack growth curves using the mean crack growth measurements

On the other hand, In order to test the loading ratio effect on both times to coalescence failure, the reference geometry was tested under a constant stress of 290 MPa and at three different loading ratios. Both times to coalescence and failure increased by increasing the loading ratio as illustrated in Figure 3.26:
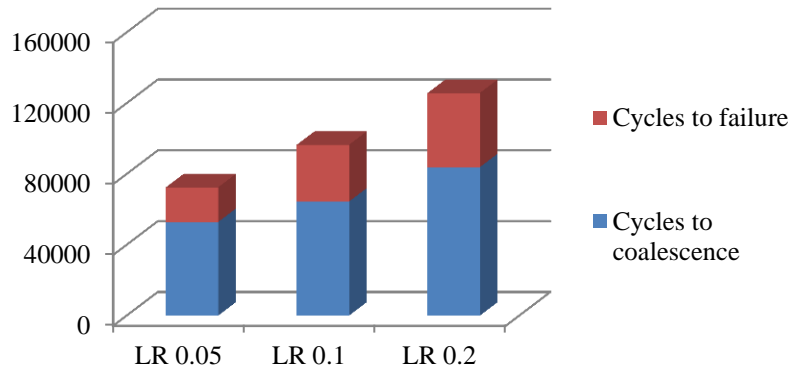
Figure 3.26: Impact of different LR on the number of cycles to coalescence and failure

In other words, as the loading ratio decreases, a faster crack growth rate was observed as illustrated in Figure 3.27 plots:
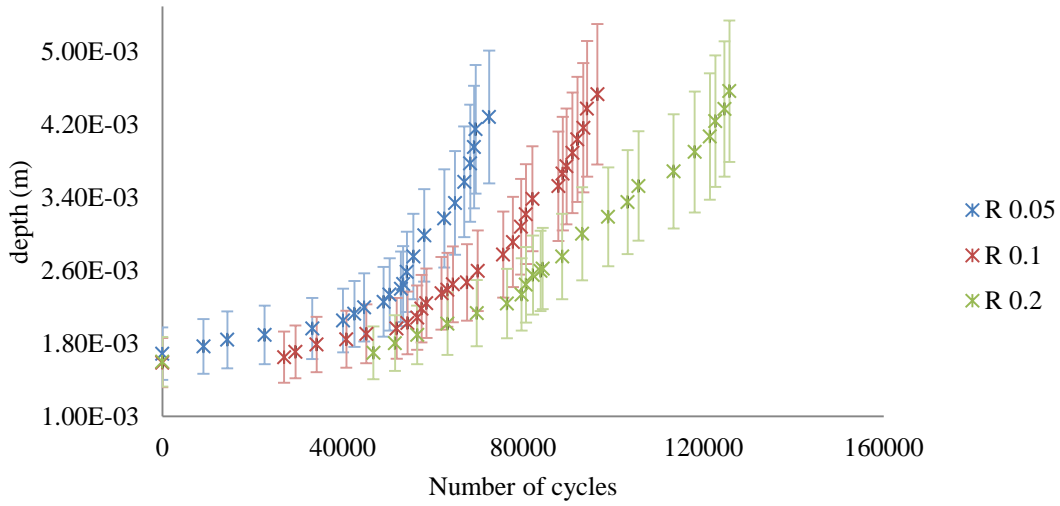
a)
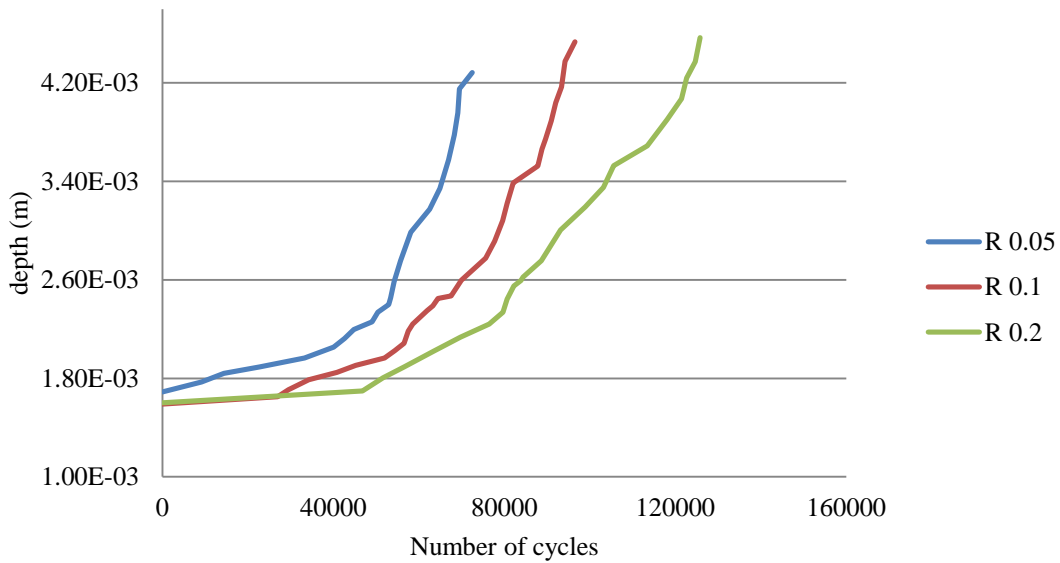
b)

Figure 3.27: Plots of the number of cycles versus depth measurements of neighboring crack at different loading ratios, a) Crack depth measurements along with the associated uncertainty at different number of cycles, b) A series of crack growth curves using the mean crack growth measurements

The reason for these findings is the direct impact of the loading conditions on the stress field around the cracks. Higher applied stresses and lower loading ratios yields a higher stress distribution around the cracks which eventually led to faster ligament failure and crack growth.

51

The crack growth experimental measurements were used for the life prediction model development and validation as will be discussed in Chapters five and six respectively. The different crack depth measurements and their associated number of cycles were used to find the crack growth rate, which was used as a basis for the modeling efforts.

4. Chapter Four: SIF Simulation

Stress intensity factor is a fundamental quantity used to describe the stress field near crack tip [1]. It depends mainly on crack geometry, boundary conditions and the nature of applied load. As there is an infinite combination of geometries, boundary and loading conditions, exact solutions are often unavailable. Hence SIF solutions for interacting surface cracks of different geometries are not widely studied.

One of the most acceptable SIF approximate expressions for a single semi-elliptical crack was proposed by Newman and Raju [16] [17] due to their acceptable accuracy, ease of use, and wide ranging applicability. As stated by Newman and Raju [18] [16], comparing their FEM solutions for semi-elliptical surface cracks to experimentally determined fracture data, their work has ranked the highest amongst other solutions in terms of accuracy. Their solutions were able to correlate 95% of the data analyzed within ±10% error.

Afterwards, many researchers have investigated the SIF around multiple neighboring cracks. Simulation work done by Murakami et al. and verified by Leek and Howard [3] [23] was performed to investigate how the existence of neighboring cracks could affect the SIF at crack tips and front. The end result of the simulation work is a correction factor that adjusts the SIF to take into account the effect of the neighboring cracks interaction and coalescence. Cracks-interaction leads to an increase in the SIF values compared to its values in a single crack growth in all three direction of crack growth.

Leek and Howard [3] based their simulation efforts on integrating Newman and Raju [16] [17] SIF solutions for single semi-elliptical cracks along with Erdogan [39] and Yokobori [40]

solutions for the CIF of two identical cracks. Also, they suggested the use of Savin [41] solutions of the CIF of non-identical cracks.

An illustration of the points at which the SIF was computed for the data scatter development required in this research is shown in Figure 4.1. However, performing a comprehensive simulation to find the SIF at the coalescence points and further understand the ligament failure behavior is still vital in understanding neighboring cracks interaction, coalescence and growth.
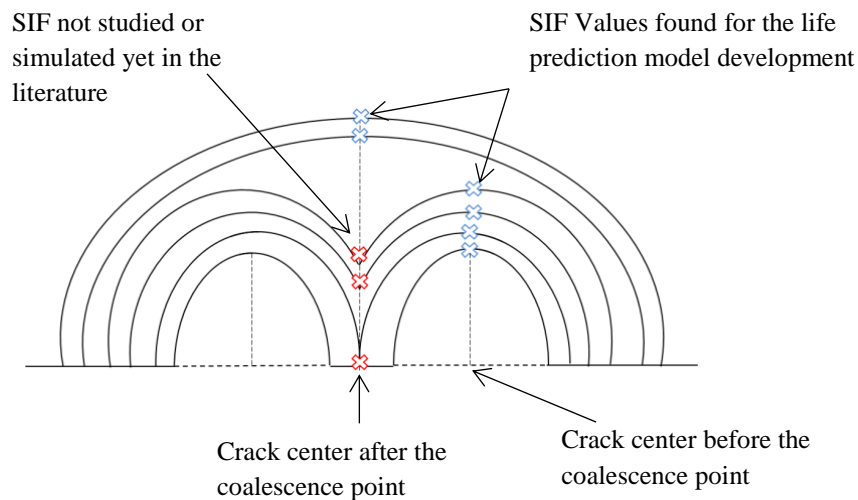
Figure 4.1: Specific geometrical points at which SIF was calculated

However, for engineering structures inspection and health management, it is in fact more realistic and easier to have a model of crack growth that addresses the crack front growth rather than coalescence point growth, as it could be validated by actual inspection measurements throughout the structure life.

4.1 Crack Front SIF Simulation

In order to find the SIF at the crack front, Newman and Raju solutions of the SIF of a single semi-elliptical crack [16] [17] coupled with the CIF developed by Leek and Howard models [15]

[23] were used. However, the uncertainties associated with this model predictions of crack front SIF were not quantified and are recommended for future work. A discussion of this methodology is illustrated in this chapter.

4.1.1 Single Semi-Elliptical Crack SIF Simulation

Newman and Raju solutions [16] [17] were used to develop a computer program that covers a wide range of semi-elliptical crack dimensions. The code was written using MATLAB R2013a to model the SIF at the crack front. In order to find the SIF at the crack front, three main variables have to be defined before and after coalescence:

1. Crack depth at each increment of growth

2. Crack radius at each increment of growth

3. Loading conditions:

    a. Maximum stress

    b. Loading ratio

These variables are the main input variables to Newman and Raju [16] [17] SIF equation beside other geometrical constants like the sample thickness and width. The input data were obtained from the experimental measurements of surface cracks length and depth. So, for each crack development data set, the SIF was obtained for each increment of growth in order to develop a da/dn vs. ΔK data scatter. For more information about the code, refer to Appendix D.

After obtaining the crack front SIF values for the bigger of the neighboring cracks, it was corrected using Leek and Howard [15] [23] CIF model based on their geometrical development which was identified experimentally.

4.1.2 SIF Correction Using the CIF

As Leek and Howard II [23] method addresses identical cracks, an assumption was made in this research that in the case of having two non-identical cracks, they are assumed to be identical and equal to the bigger crack for the CIF analysis. As shown earlier in the experimental results section in this work, it was found that increasing or decreasing the depth or the radius of one of the neighboring cracks by one or two standard deviations had a similar impact on both cycles to coalescence and failure. For that reason, introducing this assumption will have an acceptable accuracy when used for the SIF computation.

For each test, the crack front SIF was obtained for the bigger of the neighboring cracks and then corrected using the correction factors illustrated in Table 4.1. This method specifies geometrical conditions based on the cracks interaction and coalescence development providing a percentage increase in the SIF value anywhere around the crack. The corrected SIF value is then computed using equation (2.17).

Table 4.1: Conditions for a particular increase in SIF of a single crack due to interaction of two identical cracks under tension load: a/t ≤ 0.8, 0.1 ≤ a/r ≤ 2.0, r/w ≤ 0.31 **[23]**, refer to Figure 2.4 for the nomenclature or the list of nomenclature

If $S/\bar{r} >$	or if $S/\bar{a} >$	or if $S/\bar{r} \times S/\bar{a} >$	Correction factor
1.61	7.72	5.952	1.05
0.91	4.14	1.715	1.10
0.48	1.61	0.295	1.20
0.31	0.57	0.122	1.30
0.22	0.32	0.061	1.40
0.16	0.25	0.035	1.50
0.13	0.19	0.021	1.60
0.10	0.15	0.013	1.70
0.08	0.12	0.009	1.80
0.07	0.10	0.006	1.90
0.06	0.09	0.005	2.00

The crack front SIF was recalculated after each increment of growth until the two cracks touched. When the cracks were predicted to touch, a single enveloping crack was immediately

assumed with new dimensions and a shift of the crack center to the coalescence point. When the enveloping crack was assumed, then Newman and Raju solutions [51] were used to continue computing the SIF at the enveloping crack front.

4.2 SIF Simulation Results

Newman and Raju SIF solutions [16] [17] were used to develop a computer program that computes the SIF around a single semi-elliptical crack for a wide range of dimensions. The code was written using MATLAB R2013a to compute the SIF at the crack front of the bigger of the neighboring cracks. Afterwards, these SIF values were corrected using the correction factors proposed by Leek and Howard II [23] to account for the neighboring cracks interaction effect on the stress intensity.

However, in order to understand how neighboring cracks interactions affect the crack front SIF, a comparison was made between two cases: a SIF analysis assuming a negligible effect of neighboring cracks interactions and a second case that accounts for these interactions. This comparison is illustrated in Figure 4.2. Also, an example of the simulation data is exemplified in Appendix E.
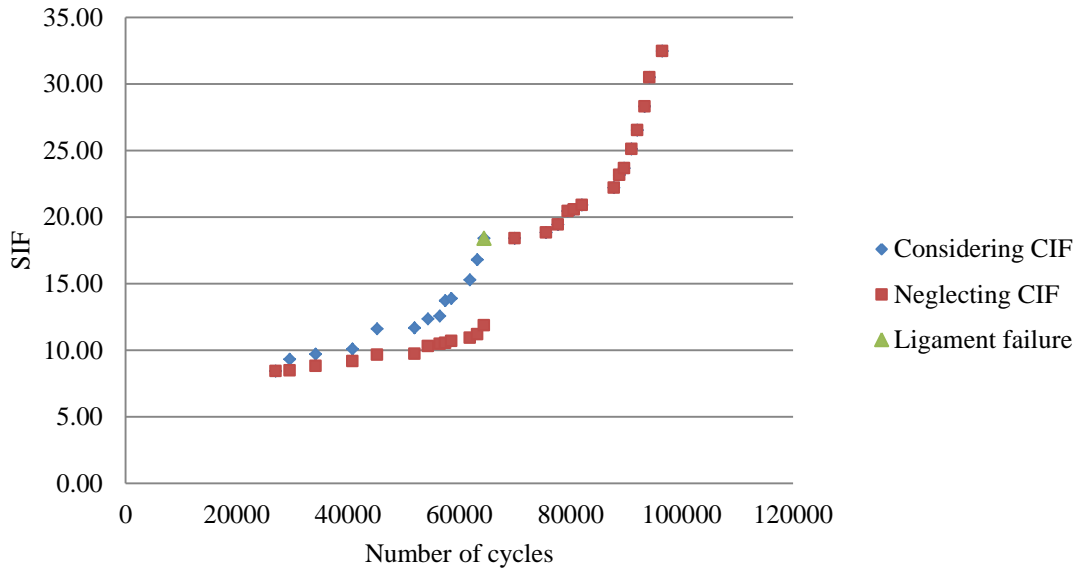
Figure 4.2: Plot of the number of cycles versus crack front SIF, an illustration of the impact of the CIF on SIF analysis, a_(μ/μ), σ_s=290 MPa, LR=0.1

Neglecting the CIF introduces a significant discontinuity in the crack front SIF values when the two cracks achieve coalescence forming a single enveloping crack. Furthermore, no information could be drawn about the ligament failure when such interactions are neglected.

4.2.1 Cracks Dimensional Variability Effect on the Crack Front SIF

The crack front SIF variations due to dimensional variability of the neighboring cracks were investigated in this work. The impact of the neighboring cracks depth and the neighboring cracks separation distance on the crack front SIF was investigated.

It was found that increasing the depth of one of the neighboring cracks or both of them yields higher stress intensity around the cracks as illustrated in Figure 4.3:
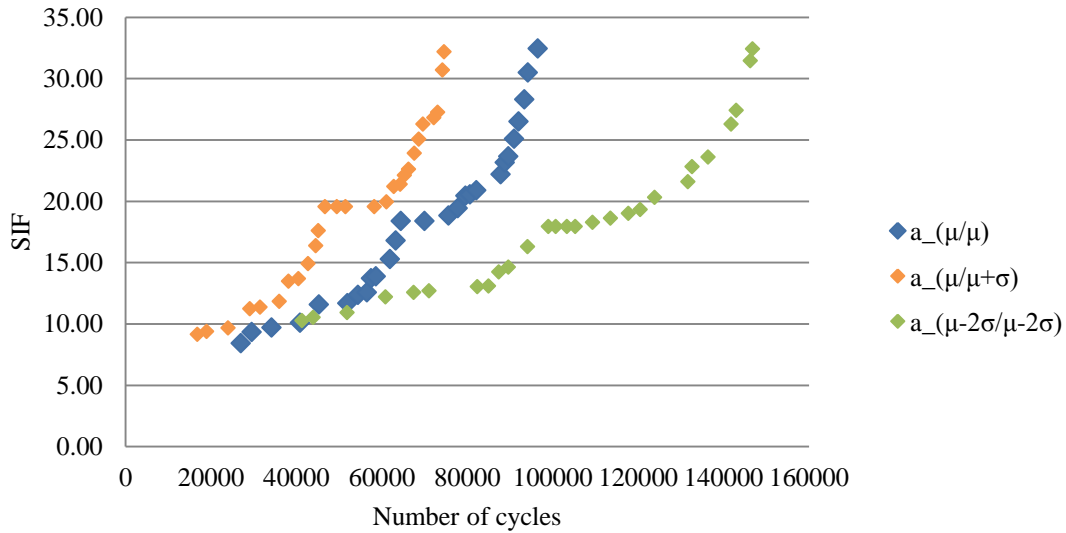
Figure 4.3: Plot of the number of cycles versus crack front SIF of neighboring cracks of variable initial depth

When cracks coalescence is achieved, a change in the SIF development behavior is observed due to the ligament failure and the formation of a bigger enveloping crack. This sudden increase in the crack dimension caused a rapid increase in the crack front SIF values.

On the other hand, the separation distance between neighboring cracks was found to play a significant role in defining the stress concentration around the cracks. Smaller separation distances yielded higher stress intensity between the neighboring cracks causing faster coalescence and ligament failure as illustrated in Figure 4.4. This result was found to be in agreement with the experimental observations discussed earlier on the impact of the neighboring cracks on both cycles to coalescence and failure.
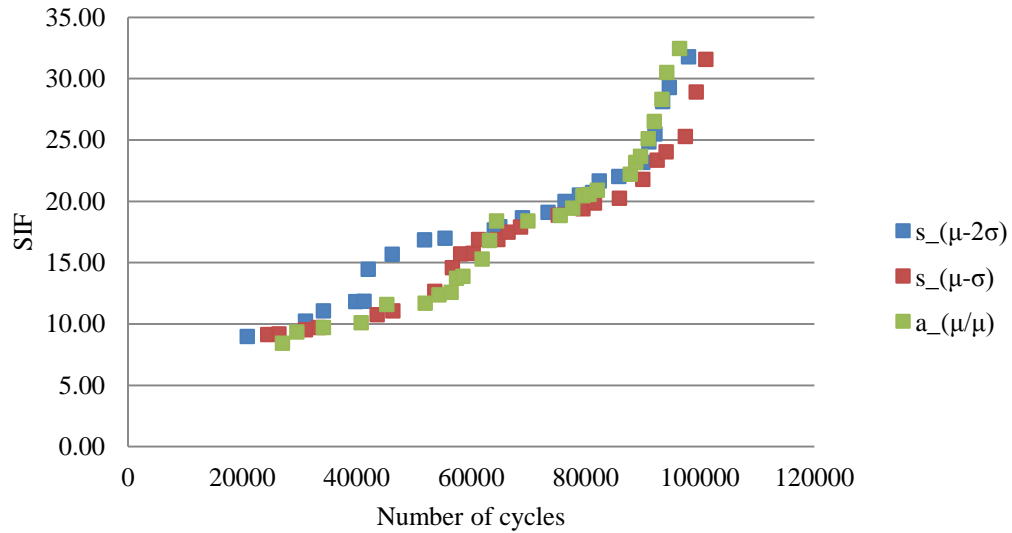
Figure 4.4: Plot of the number of cycles versus crack front SIF of neighboring cracks of variable initial spacing

4.2.2 Loading Conditions Effect on the Crack Front SIF

Loading conditions have a direct impact on the stress field surrounding the neighboring cracks. For that reason, different stress levels and loading ratios impact on the crack front SIF were investigated in this work. A similar crack front SIF behavior was observed at different stress levels. However, higher stresses yielded higher stress intensity as shown in Figure 4.5:
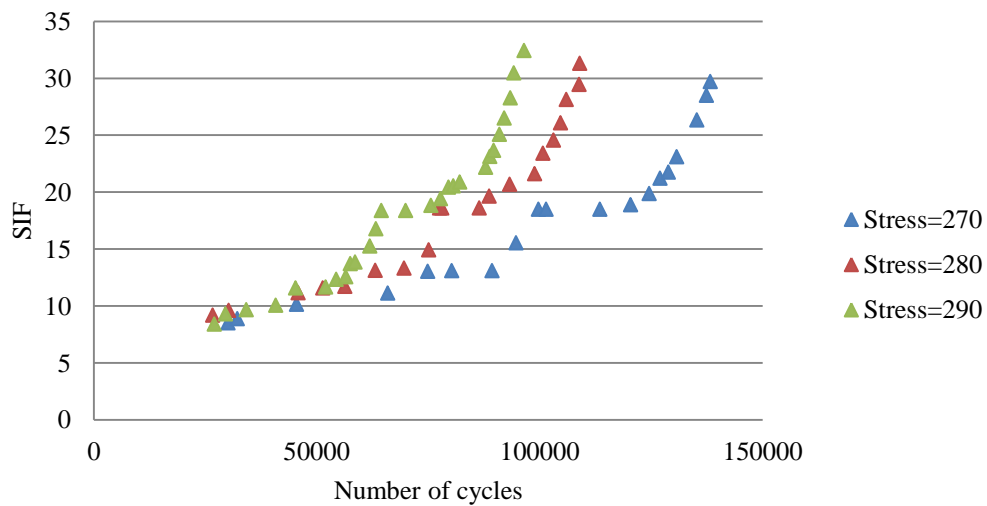
Figure 4.5: Plot of the number of cycles versus crack front SIF of neighboring crack at different stress levels, stress in MPa

60

Similarly, changing the loading ratio at a given stress level had a visible impact on crack front SIF. On contrary to the different stress levels impact on stress intensity, lower loading ratios yields higher crack front SIF value as illustrated in Figure 4.6.
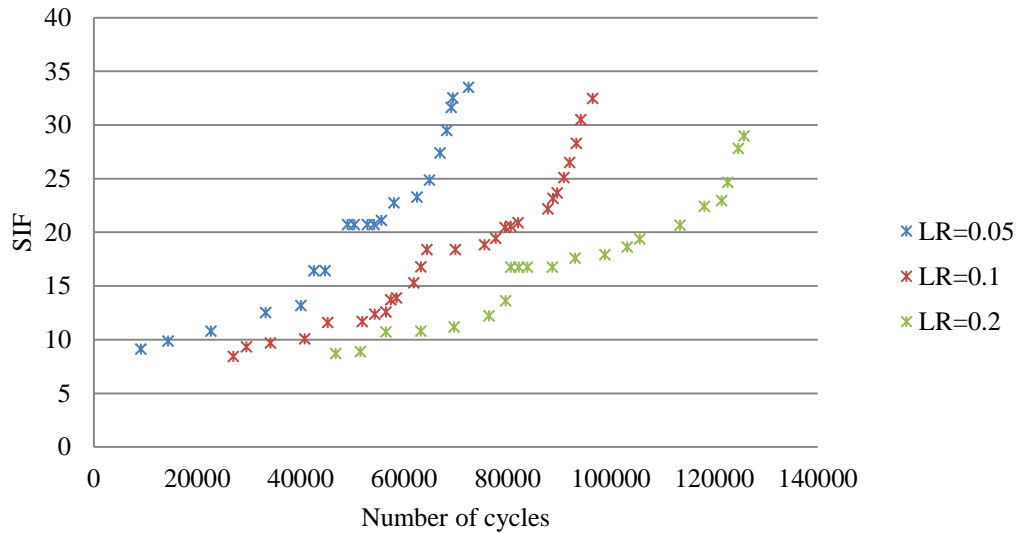
Figure 4.6: Plot of the number of cycles versus crack front SIF of neighboring crack at different loading ratios

4.3 Ligament Failure

In both experimental and simulation efforts performed in this research, the impact of different loading conditions on the time to ligament failure was investigated. According to Leek and Howard [23], as the two cracks approach each other; the CIF values increase rapidly. So, there will always be a certain dimensional criterion at which the maximum SIF obtained by the use of the CIF method becomes larger than that obtained by assuming an enveloping crack (i.e., assumed to be condition at which ligament failure occurs). However, in reality, many factors affect number of cycles to ligament failure. Leek and Howard [23] indicated that the neighboring cracks shapes and dimensions, type of material and the nature of loading conditions are some of the determining factors of ligament failure.

61

Swift [32] first proposed a ligament yielding criterion to specify when ligament failure occurs. He predicted ligament failure to occur when plastic zones around the neighboring cracks come into contact. Other researchers like Moukawsher et al. [33] and Jeong et al. [34] have also tried to come up with identification methods of the ligament failure by investigating the yielding of the ligament. However, no discussion of any correlations between the neighboring cracks dimensional variability or the loading conditions with ligament failure were discussed.

In this research, the impact of loading conditions on time to ligament failure was only investigated due to the limited number of tests performed. The criterion of ligament failure proposed by Leek and Howard was also investigated and validated experimentally in this work.

The impact of the different applied stress levels on the time to ligament failure was first investigated in this work. It was found that higher applied stress levels had linear accelerating impact on the time to ligament failure. Also, a good agreement between the experimental and simulation results was found as illustrated in Figure 4.7:
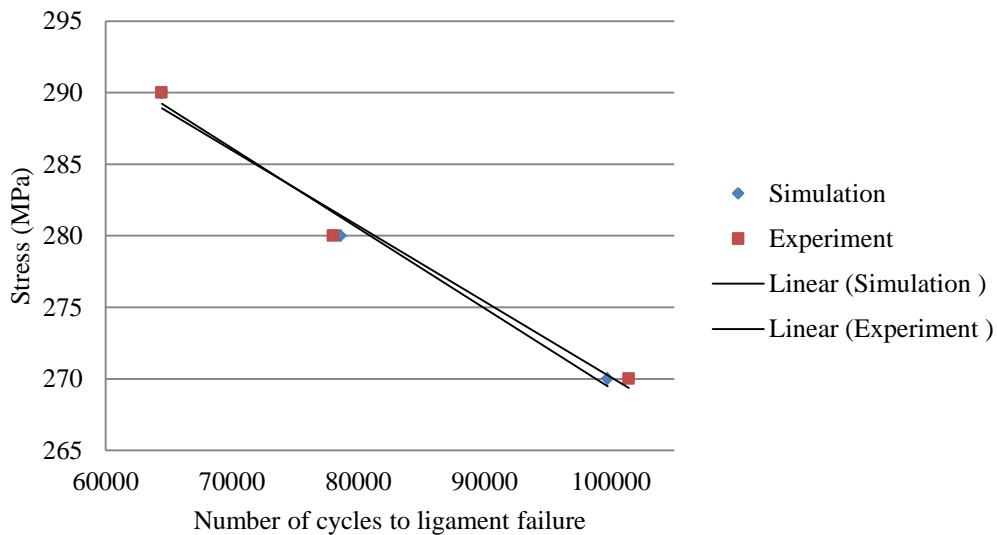
Figure 4.7: Plot of number of cycles to ligament failure versus applied stress

Similarly, it was found that lower loading ratios had the same accelerating impact on the ligament failure. Furthermore, good agreement between the experimental and simulation results was observed as illustrated in Figure 4.8:
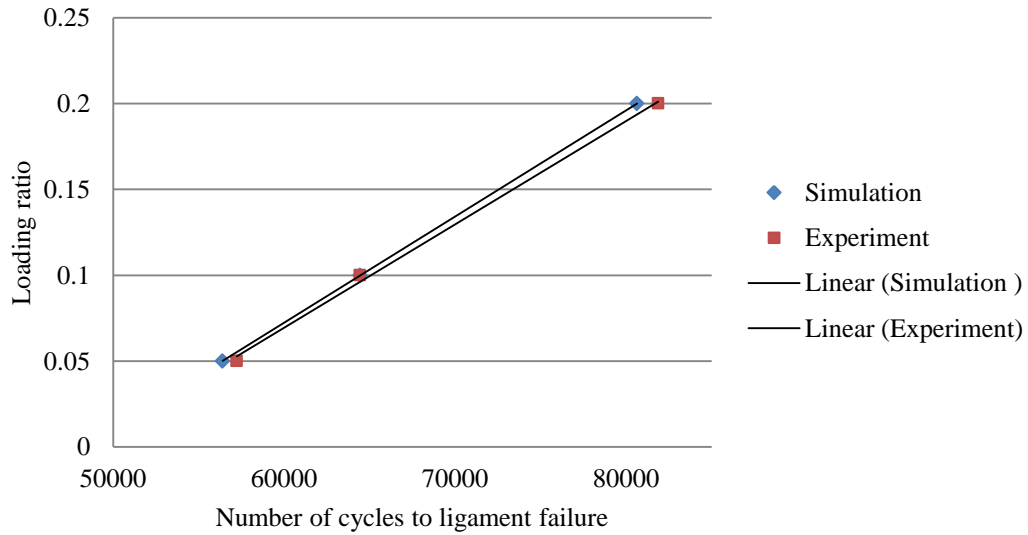
Figure 4.8: Plot of number of cycles to ligament failure versus loading ratio

In line with Jeong et al. [34], higher stresses and lower loading ratios leads to an increased loading on center of the ligament leading to faster failure. For that reason, the stress field around the ligament is directly influenced by the nature of the applied loading conditions. However, further investigations are required in order to understand the impact of the neighboring cracks dimensional variability on the time to ligament failure.

5. Chapter Five: Model Development

This chapter discusses the probabilistic crack growth modeling approach followed in this research. The proposed models incorporate experimental and simulation results for a better understanding of the neighboring cracks interaction, coalescence and growth.

5.1 Modeling Assumptions

This section presents the foremost assumptions employed in developing the life prediction model. Some of the assumptions were made based on the SIF analysis performed in this research, while others were made based on the nature of the experimental and modeling efforts performed. Yet, uncertainties due to these assumptions are not quantified and should be analyzed as part of the future research. The following is a list of the assumptions used in this work:

1. The initial cracks shapes are assumed to be semi-elliptical. Also, cracks will grow keeping their semi-elliptical shape until coalescence is achieved. However, the cracks aspect ratios change as their dimensions change

2. Crack initiation is not considered in the modeling efforts in this research, only crack growth was considered

3. The models developed addresses coplanar surface cracks. Non-coplanar and embedded cracks were not considered in this work

4. Interaction, coalescence and growth of two neighboring cracks were addressed in this work. The model developed does not address multiple cracks interaction and growth

5. When the inner tips of the neighboring cracks touch, a single enveloping semi-elliptical crack is formed due to the rapid ligament failure

6. Non-identical cracks are assumed to be identical and equal to the bigger crack for the CIF computation

7. The crack growth measurements were performed on the bigger of the neighboring cracks before coalescence

8. The SIF was computed at the crack front of the bigger of the neighboring cracks before coalescence

9. The material is assumed to be homogeneous and isotropic

5.2 Computational Methodology and Procedure

One of the main objectives of this research is to develop a model with minimum number of parameters capable of predicting crack growth of neighboring cracks. Most of the reviewed models in the literature address growth of a single crack. However, in reality, cracks don't exist unaccompanied all the time. For that reason, probabilistic modeling was used to model fatigue cracking of two neighboring cracks in order to identify and explore how interaction and coalescence affect crack growth and have an end model that describes this phenomenon.

Probabilistic modeling of mechanistic fatigue models is quite challenging. Selecting the simplest PPoF fatigue model form was one of the important factors to be taken in account to facilitate the probabilistic analysis. Also, the selection of an appropriate probabilistic modeling procedure was a critical step in this research. The flowchart of modeling steps undertaken in this research is illustrated in Figure 5.1:

```
┌─────────────────────────────────────┐
│  Perform a comprehensive literature  │
│ survey about the failure mechanism   │
│  in order to obtain an initial form  │
│       of the model proposed          │
└─────────────────────────────────────┘
                  ⇩
┌─────────────────────────────────────┐           ┌──────────────────┐
│   Select an appropriate PoF model    │           │      Prior       │
└─────────────────────────────────────┘           │ distributions of │
                  ⇩                                │   the uncertain  │
┌─────────────────────────────────────┐           │    parameters    │
│      Define the model parameters     │────┐      └──────────────────┘
└─────────────────────────────────────┘    │      ┌──────────────────┐
                  ⇩                         └──────│  Values for the  │
┌──────────────┐  ┌────────────────────────┐      │   deterministic  │
│ Evidence data│  │ Gather data to estimate│      │    parameters    │
│ sources like:│──│ the model uncertain    │      └──────────────────┘
│material tests│  │ parameters: evidence   │
│simulation,   │  │ data to update these   │
│  field data  │  │ parameters             │
└──────────────┘  └────────────────────────┘
                  ⇩
┌─────────────────────────────────────┐
│  Employ the Bayesian analysis to     │
│  update the uncertain parameters     │
│ distributions using the evidence     │
│            available                  │
└─────────────────────────────────────┘
                  ⇩
┌─────────────────────────────────────┐
│  Quantify the model bias and         │
│  uncertainties and employ a          │
│     suitable validation method       │
└─────────────────────────────────────┘
```

Figure 5.1: Flow diagram of the computation methodology employed in this research. Adopted from "Accelerated testing, ENRE 641" By M. Modarres, 2008 **[52]**

5.2.1 Physics-of-Failure Model Selection

A comprehensive literature review was performed to investigate the different fatigue crack growth models of neighboring cracks; however, it was found that most of the research performed was directed towards understanding the physics behind cracks interaction and coalescence rather than modeling crack growth. Yet, these models helped identifying the main factors influencing neighboring cracks growth. Chapter 2 summarized the most popular cracks interaction and coalescence models and the most widely accepted PoF crack growth models.

Two PoF models were considered in this work. The first model was based on the Paris Law equation; however, it was modified in order to account for the loading ratio effect by adding a correction factor to the equation. On the other hand, the second model was based on the Walker equation. The ease of use, simplicity, wide acceptance in the literature and reasonable number of parameters were the main criteria behind selecting the two crack growth models. A summary of the models inputs, output and mathematical representation is summarized in Table 5.1:

Table 5.1: A summary of the PoF models used in this research, inputs, outputs and mathematical representation

	Modified Paris law equation	Walker equation
Model inputs	Stress Intensity Factor (ΔK)[1] Loading ratio	
Model output	Crack growth rate (da/dN)	
Mathematical representation	$\frac{da}{dN} = f(\Delta K, LR \mid C, n, LR_0, m)$	$\frac{da}{dN} = f(\Delta K, LR \mid C, n, \lambda)$
Equation	$\frac{da}{dN} = C\Delta K^n \left(\frac{LR}{LR_0}\right)^m$	$\frac{da}{dN} = \frac{C(\Delta K)^n}{(1 - LR)^{n(1-\lambda)}}$

5.2.2 Model Variables

The model variables are a key deciding factor on how the computation will be executed. For that reason, the variables were treated very carefully in this work. Both models considered in this research have two main variables:

1. SIF

2. Loading ratio

However, there are SIF-related variables that were used to identify the SIF at the crack front and the associated CIF used to account for the interaction and coalescence effect. So, all these variables were used in the SIF simulations making them part of the models variables. However,

---

[1] Corrected for the impact of neighboring cracks as illustrated in Chapter 4, section 4.1.2

they are embedded within the SIF term. A summary of all models input variables is illustrated in Table 5.2:

Table 5.2: A summary of the models variables, refer to Figure 2.4 for the nomenclature or the list of nomenclature

Main input variables	Embedded input variables
Stress intensity factor of a single semi-elliptical crack (SIF)	• Crack depth (a) • Crack radius (r) • Cracks spacing (S) • Sample thickness (t) • Half the sample width (b) • Applied stress ($\Delta\sigma_s$)
Cracks interaction factor (CIF)	• Crack depth (a) • Crack radius (r) • Cracks spacing (s)
Loading ratio (LR)	• Maximum applied stress ($\sigma_{s,max}$) • Minimum applied stress ($\sigma_{s,min}$)

5.2.3 Model Parameters

As this research addresses two main PPoF models, variability between the two models parameters was observed. As was shown in Table 5.1, the modified Paris equation model has four main parameters from which three are uncertain parameters (C, n, m) and one is a deterministic parameter (R_0). On the other hand, the Walker model has three main uncertain parameters (C, n, λ). The Paris law coefficients (C and n) were common between the two models. Nevertheless, the parameter associated with the loading ratio term in each equation was different; yet, they still correlated the loading ratio variable to the crack growth rate output.

A literature survey was performed to gather prior information about each parameter used in the modeling development efforts. Many researchers like Beltrao et al. [53], Shi et al. [54], Fernandes [55], Cortie et al. [56], Hamam et al. [57], Beretta et al. [58] and Krishnaprasad et al. [59] have investigated crack growth in carbon steel materials. For that reason, a wide variety of

Paris law coefficients values are available in the literature. Some of these values, presented in Table 5.3, were used in this research to develop prior distributions for these coefficients.

Table 5.3: A summary of the available coefficients of Paris law available in the literature

C		n		Reference
2.06E-11		4.59		Beltrao et al. [53]
6.11E-14		4.42		Shi et al. [54]
5.13E-10		3.61		Fernandes [55]
3.00 E-10		2		Cortie et al. [56]
No value provided		3		Hamam et al. [57]
4.53 E-10		2.09		Beretta et al. [58]
1.13 E-10		2		Krishnaprasad et al. [59]
μ	2.33E-10	μ	3.10	
σ	2.41E-10	σ	1.19	

This data obtained from the literature search was later introduced to a different program, ReliSoft-Weibull ++ 5.32, in order to find the best distribution that fits the data. It was found that the normal distribution best fits the data of both coefficients as illustrated in Figure 5.2 and Figure 5.3:
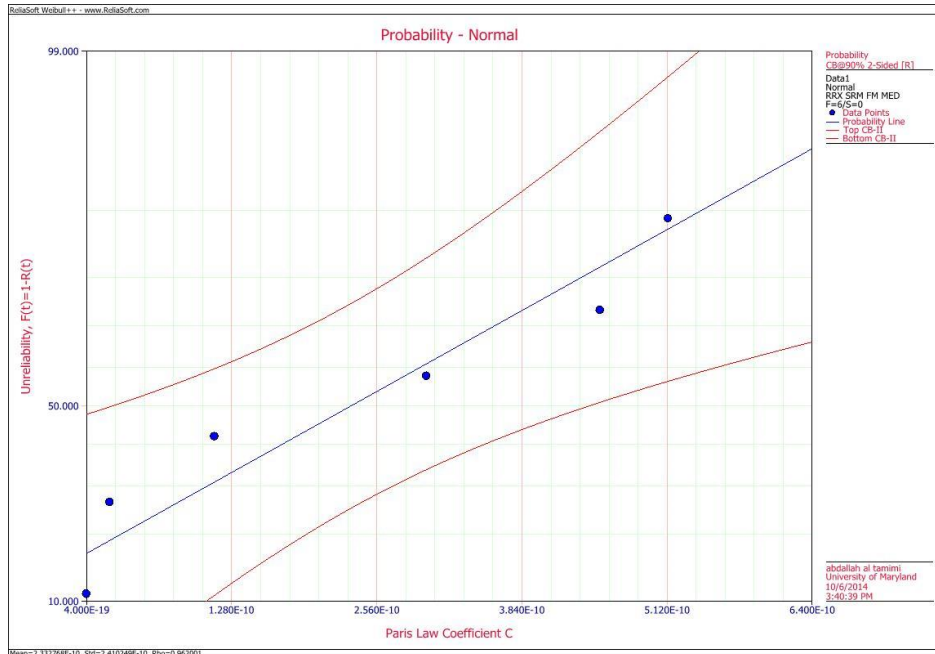
Figure 5.2: The normal distribution of the Paris equation coefficient C based on the prior data available in the literature

69
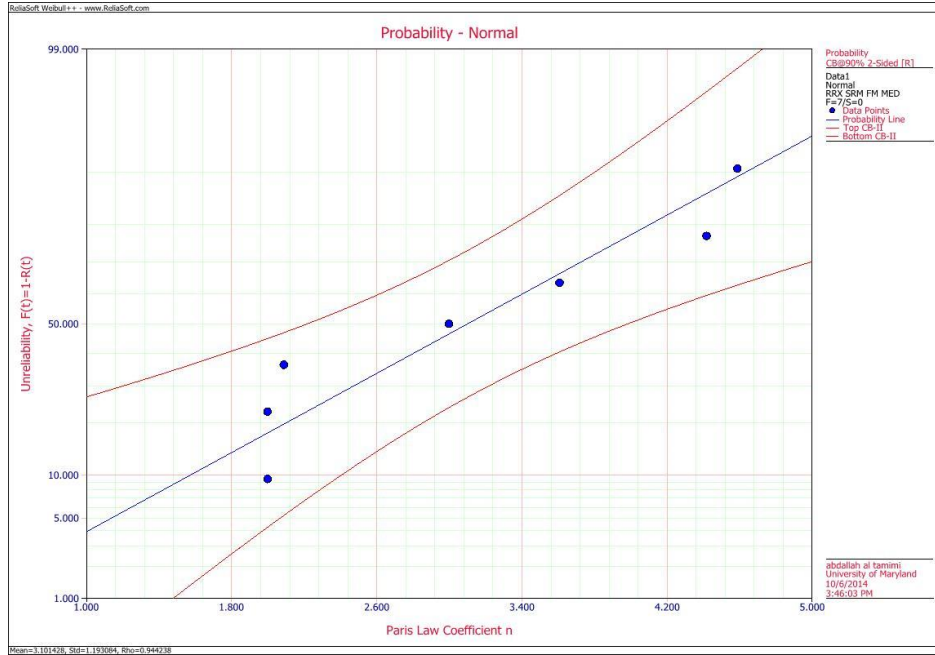
Figure 5.3: The normal distribution of the Paris equation coefficient n based on the prior data available in the literature

In the modified Paris law model, two other parameters had to be investigated. As the loading ratio correction factor was introduced in this work, no prior information was available for the uncertain parameter m. For that reason, a uniform distribution with values ranging from -5 to 5 was assumed in the Bayesian analysis performed. On the other hand, the other parameter, R_0, was a normalizing parameter to make the correction factor a dimensionless quantity. Accordingly, this parameter was considered as a deterministic parameter with a value of 0.1167 which is the mean value of loading ratios used in the experimental work in this research.

Similarly, the Walker model has one uncertain parameter, λ, which correlates the loading ratio variable with the crack growth rate. Dowling et al. [60] have investigated this parameter for different grades of steel. These values, presented in Table 5.4, were used to develop a prior distribution of the parameter λ.

70

Table 5.4: Values of the λ parameter in the Walker equation for different grades of carbon steel [60]

Steel grade	λ
SAE 1015	0.7352
GSMnNi63	0.8113
Ck45	0.6949
SAE 4130	0.6903
49MnVS3	0.8492
17MnCrMo33	0.6575
50CrMo4	0.7776
42CrMo4	0.7781
AISI 4340	0.6497
SAE 4130	0.5457
300M	0.4157
SAE 1045	0.4839
SAE 1045	0.4286
SAE 1045	0.5245
μ	0.6459
σ	0.1434

Again, the software program ReliSoft-Weibull ++ 5.32 was used in order to find the best distribution that fits the λ parameter values obtained from the literature. It was found that the normal distribution was found to best fit the data as illustrated in Figure 5.4:
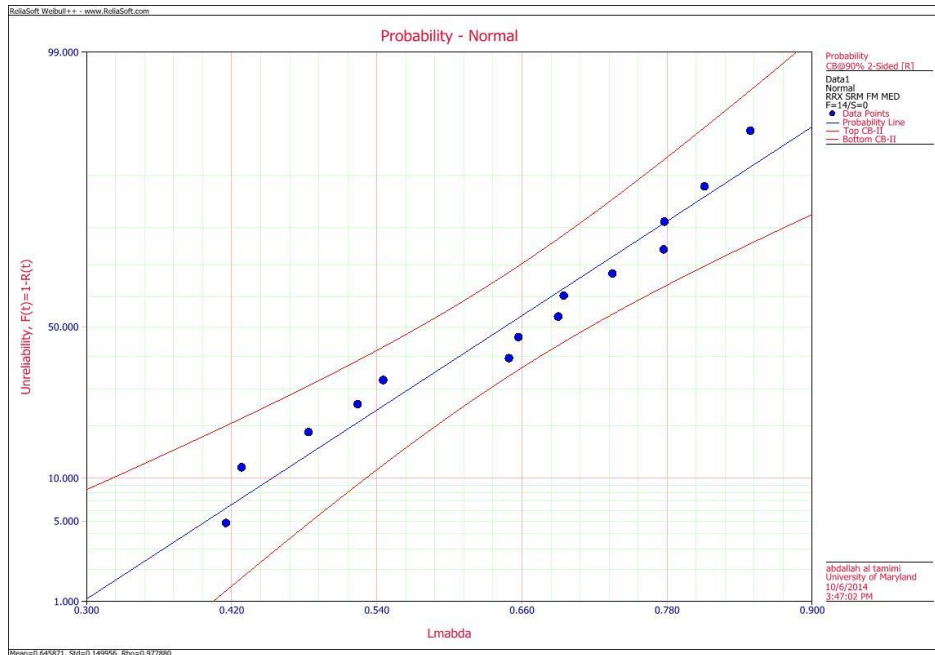
Figure 5.4: The normal distribution of the Walker equation coefficient λ based on the prior data available in the literature

Based on these literature survey estimations, prior distributions of the uncertain parameters of both models were assumed and used along with the evidence data gathered in this research to define an updated posterior distributions of these parameters.

5.2.4 Evidence Data Handling

This section discusses how the data scatter developed in this research will be employed in the modeling technique. Two main steps are required to develop the PPoF models previously discussed as illustrated in Figure 5.5:
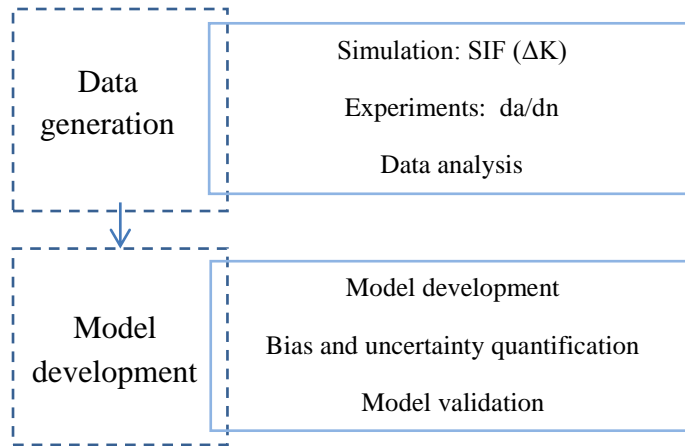
The data scatter developed in this work has been split into two main sets:

1. Model development data set

2. Bias and uncertainty quantification and model validation data set

Each model development stage requires an independent data in order to avoid or minimize the bias and avoids overlapping results. The first set of data was used to update the model uncertain parameters distributions. On the other hand, the second set of data was used to quantify the uncertainty and validate the proposed model.

5.3 Model Development

In order to shape the final form of the models, estimation of the models uncertain parameters is required. As this research tries to develop two different models of crack growth, this section will discuss how each model was developed.

There are an infinite number of possible fatigue experiments and simulations to perform to fully understand the nature of interactions between neighboring cracks and model the associated cracks growth. Therefore, obtaining crack growth data for such interacting cracks under the

impact of fatigue loading has proven to be difficult, time consuming and expensive. Yet, a great analytical tool that enables the integration of new evidence with the existing prior knowledge and produces an updated knowledge of the uncertain model parameters is the Bayes' theorem. As such, the Bayesian estimation method was applied in this research to estimate the two models parameters by integrating generic data available in literature, experiments and simulations developed in this research.

A Bayesian inference was used to develop the models by estimating the model's parameters with available data. A summary of the Bayesian process used is conceptually illustrated in Figure 5.6:
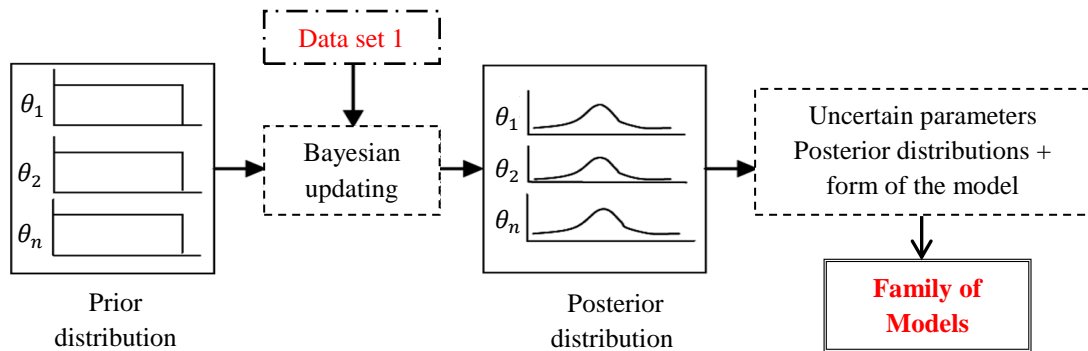
Figure 5.6: Different stages of model development

5.3.1 Modified Paris Law Model

In the Bayesian inference, a subjective prior pdf of each of the model uncertain parameters $f_o(C, n, m)$ was defined based on the literature search as illustrated in section 5.2.4. Subsequently, this prior was combined with the experimental and simulation data in the form of a likelihood function. A sample of this data is illustrated in Appendix F .

The likelihood equation of the crack growth rate was assumed to follow a normal distribution and is illustrated in equation (5.1):

$$L(\text{C}, \text{n}, \text{m}, \sigma | Data) = \prod_{i=1}^{j} \frac{1}{\sigma\sqrt{2\pi}} e^{-\frac{\frac{da}{dN_i} - \left(C\Delta K_i{}^n \left(\frac{R_i}{0.1167}\right)^m\right)}{2\sigma^2}} \tag{5.1}$$

The result is an updated state of knowledge identified as the posterior distribution, $f(\text{C}, \text{n}, \text{m}, \sigma | Data)$. This process is shown mathematically in equation (5.2):

$$f(\text{C}, \text{n}, \text{m}, \sigma | Data) = \frac{L(\text{C}, \text{n}, \text{m} | Data) f_0(\text{C}, \text{n}, \text{m})}{\int_\theta L(\text{C}, \text{n}, \text{m} | Data) f_0(\text{C}, \text{n}, \text{m})} \tag{5.2}$$

To accomplish this task, WinBUGS software program was employed to run the Bayesian analysis. In line with Speigelhalter et al. [61] the WinBUGS program is a windows-based environment for MCMC simulation that is based Bayesian inference using Gibbs Sampling. A wide variety of modeling applications could benefit from using such software. This program has been previously used in uncertainty management works according to Azarkhail et al. [62] [63] as well as accelerated life testing data analysis.

In this research, the WinBUGS platform was used for Bayesian updating and related numerical simulations. For a detailed illustration of the WinBUGS Bayesian inference algorithm used to obtain posterior knowledge of the model uncertain parameters, refer to Appendix G.

After running the developed WinBUGS code, a posterior knowledge of the uncertain parameters C, n and m was obtained. Figure 5.7 summarizes these steps to obtain the posterior distributions of these parameters.
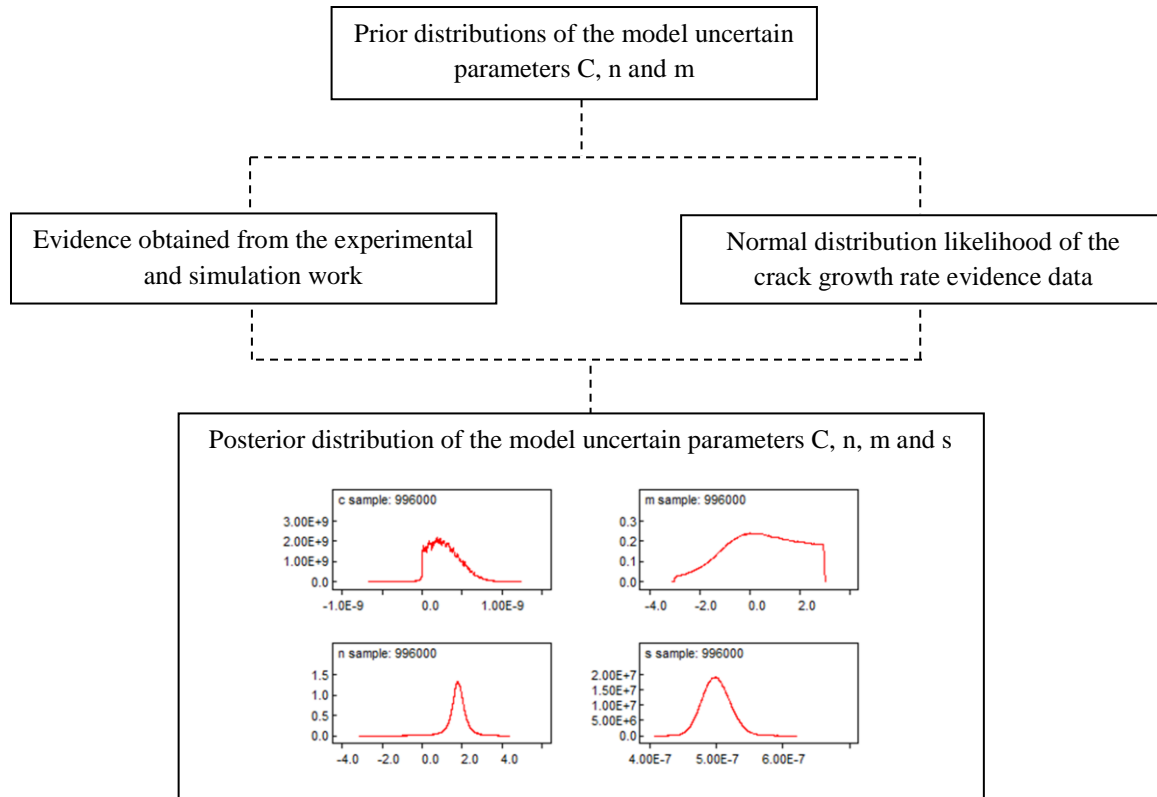
Figure 5.7: Algorithm for the Bayesian approach in the WinBUGS program to obtain an updated knowledge of the modified Paris law model uncertain parameters C, n and m posterior distribution

The final results of the Bayesian updating process of the model uncertain parameters is illustrated in Table 5.5:

Table 5.5: C, n, m and σ posterior distributions as calculated in WinBUGS for 1000000 samples

node	μ	σ	MC error	2.50%	median	97.50%
C	2.86E-10	2.16E-10	2.57E-12	7.81E-12	2.63E-10	7.08E-10
n	1.783	0.4265	0.004802	0.8292	1.793	2.627
m	0.5222	1.43	0.003377	-2.311	0.5396	2.864
s	5.00E-07	2.09E-08	2.36E-11	4.61E-07	4.99E-07	5.43E-07

After developing the knowledge of the model parameters distributions, families of the model could be developed and assessed in order to find the model with least bias and uncertainty. This was done by dividing each parameters' distribution into three equally probable regions and

76

determine the median of each region. Then, the different combinations of these median values yielded different deterministic crack growth rate models as shown in Figure 5.8:
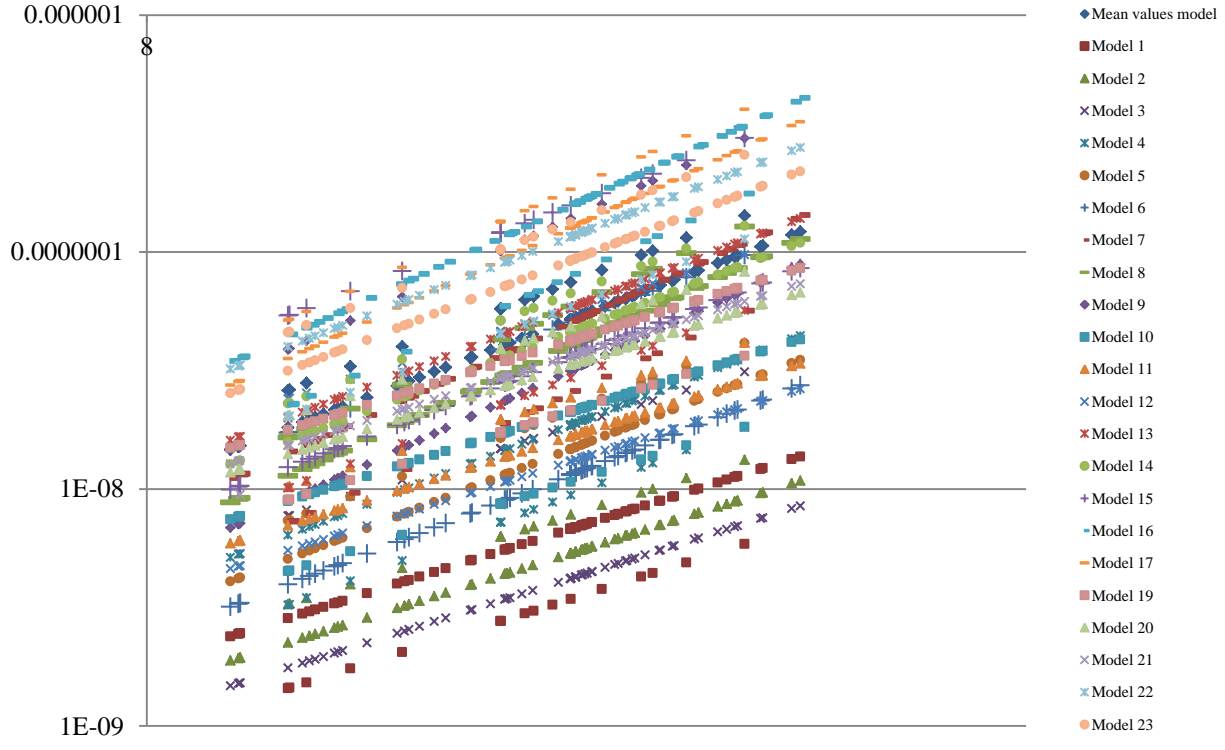
Figure 5.8: Family of the Paris law models describing crack growth rate of neighboring cracks

Each model was then validated using the validation data set in order to find a model with reasonable conservatism and minimal uncertainties. It was found that using the mean values of the posterior distributions of the model parameters yielded the best fit. Moreover, the uncertain parameters correlations were obtained using WinBUGS, however, no correlations were found as illustrated in Figure 5.9:
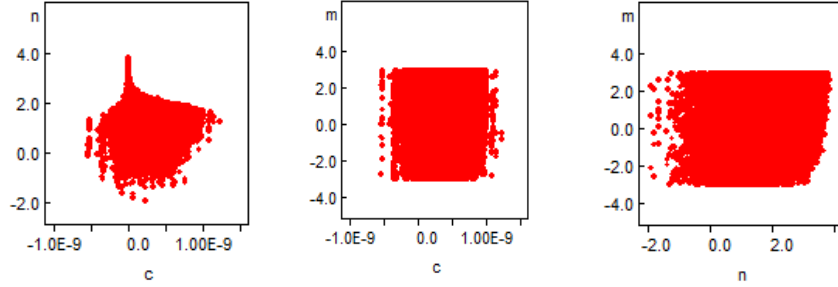
Figure 5.9: Modified Paris law model uncertain parameters correlations as calculated in WinBUGS for 200000 samples

Subsequently, many models were used to generate crack growth rate values for the uncertainty and validation step, discussed next chapter, in order to find a reasonably conservative model that provides crack growth rate predictions with acceptable errors and least uncertainty.

5.3.2 Walker Model

The same procedure followed to develop the modified Paris law model was employed to develop the Walker model. In the Bayesian inference, the prior probability distribution of each of the model uncertain parameters f_0(C, n, λ) was defined. Subsequently, this prior was combined with the evidence data in the form of a likelihood function. The likelihood equation of the crack growth rate was assumed to follow a normal distribution and is illustrated in equation (5.3):

$$L(\text{C}, \text{n}, \lambda, \sigma | Data) = \prod_{i=1}^{j} \frac{1}{\sigma\sqrt{2\pi}} e^{-\frac{\frac{da}{dN_i} - \left(\frac{C\Delta K_i{}^n}{(1-R_i)^{n(1-\lambda)}}\right)}{2\sigma^2}} \qquad (5.3)$$

The result is an updated state of knowledge identified as the posterior distribution, f(C, n, λ, σ |Data). This process is shown mathematically in equation (5.4):

$$f(\text{C}, \text{n}, \lambda, \sigma | Data) = \frac{L(\text{C}, \text{n}, \lambda | Data) f_0(\text{C}, \text{n}, \lambda)}{\int_\theta L(\text{C}, \text{n}, \lambda | Data) f_0(\text{C}, \text{n}, \lambda)} \qquad (5.4)$$

After running the developed WinBUGS code and using the same Algorithm for the Bayesian approach illustrated in Figure 5.7, a posterior knowledge of the uncertain parameters C, n and λ was obtained as illustrated in Figure 5.10:
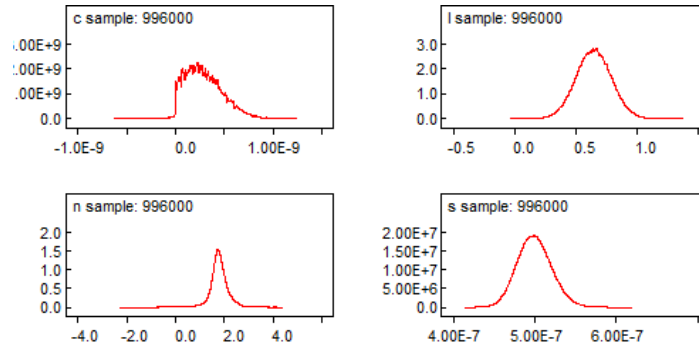
Figure 5.10: Walker model uncertain parameters C, n and λ posterior distribution

The final results of the Bayesian updating process of the model uncertain parameters is illustrated in Table 5.6:

Table 5.6: C, n, λ and σ posterior distributions as calculated in WinBUGS for 200000 samples

node	μ	σ	MC error	2.50%	median	97.50%
C	2.88E-10	2.14E-10	2.63E-12	8.52E-12	2.64E-10	7.07E-10
n	1.785	0.39	0.005095	0.9817	1.773	2.588
λ	0.6473	0.143	3.36E-04	0.3672	0.6471	0.9293
s	4.99E-07	2.09E-08	2.35E-11	4.60E-07	4.99E-07	5.42E-07

The same procedure discussed earlier in the modified Paris law model development was used herein to find a family of Walker models, as illustrated in Figure 5.11, in order to come up with a model with reasonable conservatism and minimal uncertainties.
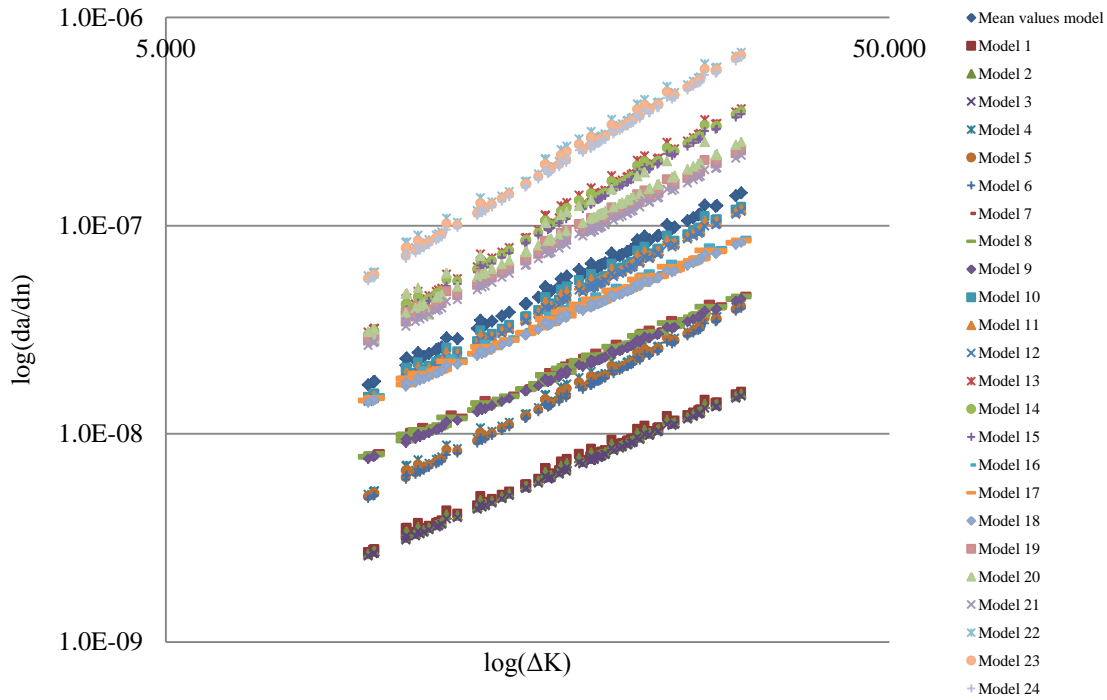
Figure 5.11: Family of the Walker models describing crack growth rate of neighboring cracks

A similar finding was that using the mean values of the posterior distributions of the model parameters yielded the best fit.

The uncertain parameters correlations were obtained using WinBUGS, however, no correlations were found as illustrated in Figure 5.12:
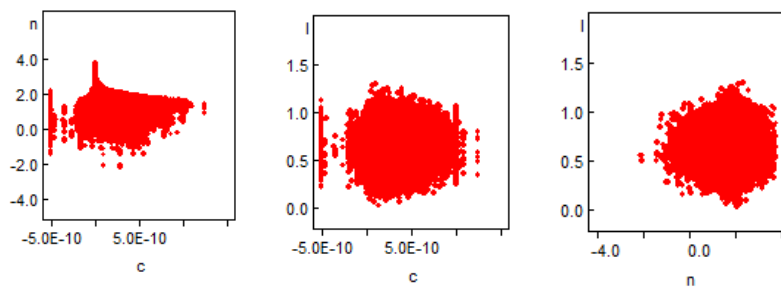
Figure 5.12: Walker equation model uncertain parameters correlations as calculated in WinBUGS for 200000 samples

Similarly, the family of models spawned was used to generate crack growth rate values that will be used in the uncertainty and validation step with the aim of having a reasonably conservative model that provides crack growth rate predictions with acceptable errors and least uncertainty.

6. Chapter Six: Bias and Uncertainty Quantification and Model Validation

Determining and quantifying the different sources of uncertainty and error in this research is a vital step in the model development process. Spotting the light on the major sources of uncertainty and quantifying them using the available statistical tools allows a better understanding of the model prediction capabilities and the associated levels of confidence. Moreover, such analyses give the modeling efforts a higher level of credibility and open the doors for future researchers to improve upon what has been done in this research. Both data used and the models developed in this research have sources of uncertainties. For this reason, this chapter will discuss possible sources of uncertainty along with a proper quantification technique associated with each source of uncertainty.

6.1 Sources of Uncertainty

One of the main aims of identifying sources of uncertainty in any research is to recognize the weakness of certain apparatus, experimental layout, simulation technique or even the model development process. Also, identifying the uncertainties of specific data gathering technique makes the modeling output more reliable.

Two key sources of uncertainties in this research were investigated: stochastic and systematic uncertainties associated with the experimental measurements and epistemic uncertainties associated with the models predictions. A summary of the sources of uncertainty addressed in this work is illustrated in Figure 6.1:
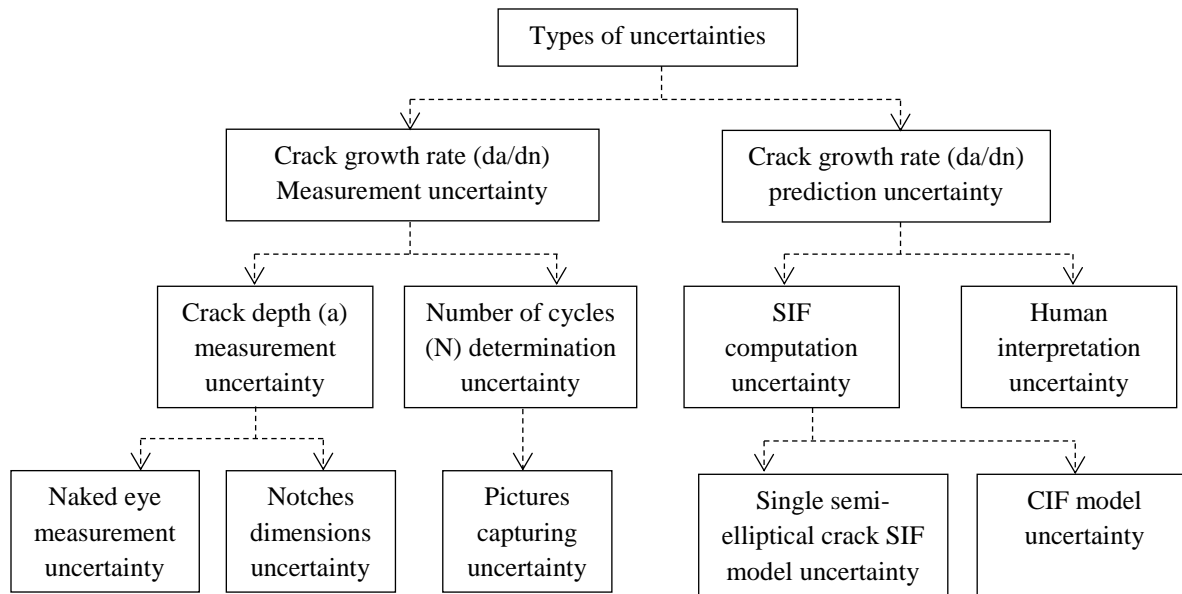
Figure 6.1: Experimental measurement and model prediction uncertainties breakdown

Each category will be addressed separately for a better understanding of the nature of the factors affecting it, and quantified using an appropriate uncertainty quantification technique.

6.2 Sources of Experimental Data Uncertainty

A code of practice established by the European Commission's standards [64] was to standardize a procedure for estimation of uncertainties associated with mechanical tests on metallic materials. This standard was used by Peter [65] to define a procedure for estimating the different sources of uncertainty in fatigue crack growth measurements. A summary of this procedure is illustrated as follows:

1. Identifying the measured variables for which uncertainty is to be estimated

2. Identify all sources of uncertainty in the experimental measurements performed

3. Classify the uncertainties based on their method of quantification

4. Quantify each source of uncertainty

5. Estimate the overall experimental uncertainty

83

The first step of identifying the overall experimental data uncertainty is to identify the measured variables for which the uncertainty is to be estimated. Two main variables were monitored in the experiments performed in this research: the crack size in meters and number of cycles counted.

As a result, an appropriate list of sources of uncertainties that might have a direct or indirect impact on the measurements performed has been prepared. This list was categorized depending on the type of uncertainty and its contribution to the overall uncertainty.

According to the International Organization for Standardization [66], uncertainty is classified into two main categories depending on its type of quantification. The first type, denoted type A, is quantified based on statistical tools when a number of repeated measurements of a certain quantity are available. The Second type, denoted type B, is quantified based on any other appropriate mean of uncertainty quantification like expert judgment, available quantifications from the literature or a manufacturer report. However, an uncertainty could be classified as both type A and B uncertainty as it could be quantified using different quantification methods.

After defining the type of each uncertainty, then it is weighted against its impact on each measurable variable based on the following scale: 0 meaning no contribution, 1 as major contribution.

The different sources of uncertainty associated with the experimental work along with a classification of their types are illustrated in Table 6.1:

Table 6.1: Different sources of uncertainty in the experimental measurements

Source of uncertainty		Type	a	N
Samples Fabrication	Notches dimension	B	1	0
Test procedure	Pictures capturing	A	0	1
Measurements	Naked eye measurement	A	1	0

6.2.1 Quantification of Experimental Data Uncertainty

As mentioned earlier, there are two main uncertain measured quantities in the experimental work performed in this research: crack depth and the associated number of cycles. In this section, different sources of measurement uncertainty were quantified in order to find the overall measurement uncertainty. This was done based on the standard procedure established by the European Commission of standards [64].

All sources of uncertainty contributing in a certain measured variable uncertainty must be expressed in similar units before they are combined. Therefore, all uncertainties should be converted to have a unified unit at the same level of confidence. According to [67], a source of uncertainties is standardized as illustrated in equation (6.1):

$$\sigma^2{}_{standard} = \frac{\sigma^2}{\mu^2}$$

(6.1)

After quantifying all different sources of uncertainty, having the assumption that they all contribute equally to the overall uncertainty; the total uncertainty is quantified as illustrated in equation (6.2):

$$\sigma_{combined} = \sqrt{\sum_{i=1}^{n} \sigma_{standard,i}{}^2}$$

(6.2)

6.2.1.1 Crack Depth Measurement Uncertainty

As discussed earlier, the first source of uncertainty in the crack depth measurement is the test samples fabrication. The test specimens were manufactured using a laser-cutting technique that yields high precision measurements and minimum residual stresses. Moreover, the samples were made using the same batch of API-5L grade B carbon steel in order to avoid any variation in the

material properties across the testing samples. However, inducing the initial notches using the EDM technique had some precision uncertainty, which was addressed in this work. As confirmed by the machine shop, which performed the EDM notching, the dimensions of the initial notches have a precision uncertainty of ±0.1mm.

The second source of uncertainty is the actual crack depth measurements. All crack measurements were analyzed using image-processing software. However, the measurements were performed with the naked eye. For that reason, each measurement was performed twice at two different times in order to reduce the measurements bias.

Performing each measurement twice enabled quantifying the uncertainty associated with the naked eye measurement. A sizing error model (i.e. a model that addresses the correlation between the crack size and the measurement uncertainty) was used in order to quantify the naked eye measurement uncertainty as illustrated in equation (6.3):

$$\Delta_\varepsilon = \left(m_\varepsilon\left(P_{avg}\right) + b_\varepsilon\right).E_\Delta \tag{6.3}$$

A Bayesian inference was used to obtain the model parameters $m_\varepsilon, b_\varepsilon$ and E_Δ. A subjective uniform prior of the model uncertain parameters was introduced. Subsequently, this prior was combined with the experimental data in the form of a normal likelihood function. A sample of this data is illustrated in Table 6.2.

Table 6.2: A sample of the data used in sizing error model development, all measurements are in Pixels

Measurement 1	Measurement 2	Measurement average	Difference between the two measurements
94.0	93.0	93.5	1
97.0	95.0	96.0	2
100.0	101.0	100.5	3

The result of the Bayesian inference is an updated state of knowledge identified as the posterior distribution of the sizing error model parameters m_ε, b_ε and E_Δ. To accomplish this task, WinBUGS software program was employed to run the Bayesian analysis. After running the developed WinBUGS code, a posterior knowledge of the uncertain parameters m_ε, b_ε and E_Δ was obtained as illustrated consecutively in Table 6.3 and Figure 6.2:

Table 6.3: mε, bε and σ posterior distributions as calculated in WinBUGS for 50000 samples

node	μ	σ	2.50%	median	97.50%
m_ε	0.002589	9.35E-04	3.21E-05	7.92E-04	2.58E-03
b_ε	0.7647	0.1431	0.005061	0.4805	0.7654
E_Δ	0.6107	0.03007	1.53E-04	5.55E-01	0.6096
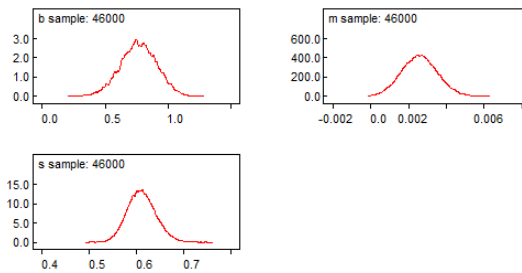
Figure 6.2: Sizing error model uncertain parameters mε, bε and EΔ posterior distribution

As shown in Table 6.3, the parameter m_ε has a mean value of 0.002589 which indicates a mild correlation between the duplicated measurements average and the associated difference between them. The difference between each of the duplicated measurements was then converted into a percentage as a first step of the uncertainty quantification. Subsequently, the overall naked eye measurement uncertainty was obtained by computing the root sum squares of these percentage values. A sample of the data used in quantifying the overall naked eye measurement uncertainty is illustrated in Table 6.4:

Measurement average	difference	Difference percentage (%)
93.5	1	1.07
96.0	2	2.08
100.5	1	0.99

So the standard overall naked eye measurement uncertainty was found to be almost 16%. Other sources of experimental uncertainties were also present in this work; such as test repeatability and sample size uncertainties. However, these sources of uncertainty did not affect the crack measurements or the associated number of cycles determination directly.

6.2.1.2 Crack depth Associated Number of Cycles Determination

The second source of uncertainty comes from the fatigue testing procedure. Starting the camera that captures the surface crack growth and keeps track of the associated number of cycles performed had a minor contribution to the overall experimental measurements uncertainty. Whenever, the fatigue test starts, the camera had to be operated at the same time. However, a lag of less than one second, a mean value of 0.59 sec, was observed in the data. Considering that the load frequency used for the fatigue testing was 2 Hz and the average time to failure is 90000 cycles, this uncertainty could be neglected.

6.2.2 Overall Experimental Uncertainty

After quantifying the different sources of uncertainty in the experimental measurements of crack growth, the combined uncertainty was obtained by computing the root sum squares. A summary of the quantified uncertainties and the associated standard combined uncertainty is illustrated in Table 6.5:

Table 6.5: A summary of the quantified uncertainties and the associated standard combined uncertainty of the experimental measurements of crack growth rate

Source of uncertainty	Uncertainty (%)
Notches dimension	6.25
Naked eye measurement	16.05
Cumulative uncertainty	17.22

6.3 Sources of Model Predictions Uncertainty

The same procedure used to identify the source of uncertainties in the experimental measurement was used to identify the sources of uncertainty in the models developed. However, a different quantification method developed by Azarkhail et al. [62] and Ontiveros et al. [68] was used to quantify these uncertainties.

As the models developed in this work are PPoF life prediction models based on the Paris equation and the Walker equation, the main input variable is the SIF. So, most of the uncertainties associated with the modeling development are directly related to the method of SIF quantification. Also, other sources of uncertainties include the data scatter and the form of the model used to predict crack growth rate.

Table 6.6: Models input variables, their units, symbols and method of quantification

Measured variable	Units	Symbol	Method of quantification
SIF of a single semi-elliptical crack	MPa$\sqrt{m}$	ΔK	Newman and Raju model [16] [17]
Cracks interaction factor	-	N	Leek and Howard model [23]
Loading ratio	-	LR	-

6.3.1 Quantification of Model Uncertainty

This section will discuss the models bias and uncertainty quantification. A comparison between the two models will be addressed in order to find the model with least uncertainty, acceptable conservatism and better representation of the failure mechanism investigated.

A method developed by Azarkhail et al. [62] and Ontiveros et al. [68] to quantify the model uncertainties was used. The bias and uncertainty quantification is based on comparing the model predictions with the experimental results and developing a multiplicative error term that corrects the model prediction for a better representation of the true crack growth rate value as illustrated in Figure 6.3.
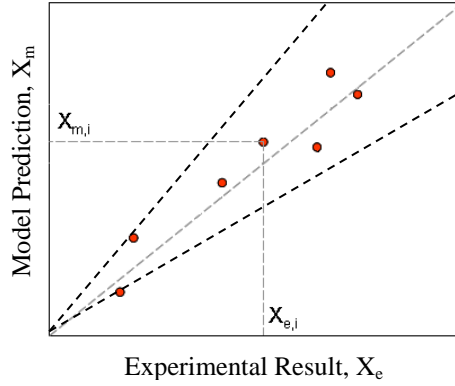
Figure 6.3: Model predictions compared to experimental results. Adopted from "A Bayesian Framework for Model Uncertainty Consideration in Fire Simulation Codes" by M. Azarkhail et al., 2009, 17th International Conference on Nuclear Engineering

[69]

If the model predictions perfectly matched the experimental results, then all the points would lie exactly on the gray dotted line. However, in reality a scatter around that line is observed due to uncertainties in both model predictions and experimental measurements.

In this research, the model prediction and experimental result are considered to be estimations of the true crack growth rate given some error as shown in equations (6.4) and (6.5):

$$\frac{da/dN_i}{da/dN_{e,i}} = F_{e,i} \; ; \; F_e \sim LN(b_e, s_e) \tag{6.4}$$

$$\frac{da/dN_i}{da/dN_{m,i}} = F_{m,i} \; ; \; F_m \sim LN(b_m, s_m) \tag{6.5}$$

90

As the modeling addresses crack growth values; then the model outcome is always expected to be a positive value, for that reason, a multiplicative error model described by a lognormal distribution was assumed.

As the true value of the crack growth rate da/dN_i is unknown, equations (6.4) and (6.5) are combined yielding the following equations:

$$F_{e,i}(da/dN_{e,i}) = F_{m,i}(da/dN_{m,i}) \tag{6.6}$$

$$\frac{da/dN_{e,i}}{da/dN_{m,i}} = \frac{F_{m,i}}{F_{e,i}} = F_{t,i} \tag{6.7}$$

Assuming independency of F_m and F_e, then:

$$F_t \sim LN\left(b_m - b_e, \sqrt{s_m^2 + s_e^2}\right) \tag{6.8}$$

So, the likelihood used in the Bayesian inference is illustrated in equation (6.9):

$$L(F_{t,i}, b_e, s_e | b_m, s_m) = \prod_{i=1}^{n} \frac{1}{\sqrt{2\pi}(F_{t,i})\sqrt{s_m^2 + s_m^2}} e^{-\frac{[ln(F_{t,i}) - (b_m - b_e)]^2}{2(s_m^2 + s_m^2)}} \tag{6.9}$$

Finally, the Bayesian inference was performed, where the relation between the posterior distribution of the model parameter with the likelihood function and the prior evidence is shown in equation (6.10):

$$f(b_m, s_m | F_{t,i}, b_e, s_e) = \frac{L(F_{t,i}, b_e, s_e | b_m, s_m) f_0(b_m, s_m)}{\int (L(F_{t,i}, b_e, s_e | b_m, s_m) f_0(b_m, s_m))} \tag{6.10}$$

The data used in this step of the analysis must be data independent of the data used in the model development step. For a sample illustration of the data used in the uncertainty analysis, refer to Appendix H. Also, for a detailed illustration of the WinBUGS Bayesian inference algorithm used to quantify the models' uncertainty, refer to Appendix I.

6.3.2 Modified Paris Law Model Uncertainty

After running the Bayesian inference algorithm developed by Azarkhail et al. [62] and Ontiveros et al. [68] to quantify the model uncertainties, knowing that the crack growth experimental measurement are not biased and have an estimated uncertainty of 17.22%, See Table 6.5, the modified Paris law mean model (i.e., developed using the mean values of the model uncertain parameters as illustrated in equation (6.11)) multiplicative error was obtained.

$$\frac{da}{dN} = (2.86E - 10)\Delta K^{1.783} \left(\frac{R}{0.1167}\right)^{0.522}$$ (6.11)

A summary statistics for the mean model multiplicative error is illustrated in Table 6.7:

Table 6.7: Modified Paris law mean model uncertainty quantification and validation summary

node	μ	σ	MC error	2.50%	median	97.50%
F_m	0.9494	0.5766	5.89E-03	0.2697	0.8151	2.398
b_m	-0.2013	0.05939	6.58E-04	-31.90%	-0.2006	-8.61%
s_m	0.5407	0.0437	4.62E-04	0.464	0.5378	0.6358

The model uncertainty bounds for the crack growth rate can be determined from the percentiles of F_m. So, the resulting uncertainty upper bound is 140% while the low bound is -73%. In other words, a model user could be 95% confident that the true value resides between 140% higher and 73% lower than what the model predicts. This is shown graphically in Figure 6.4.
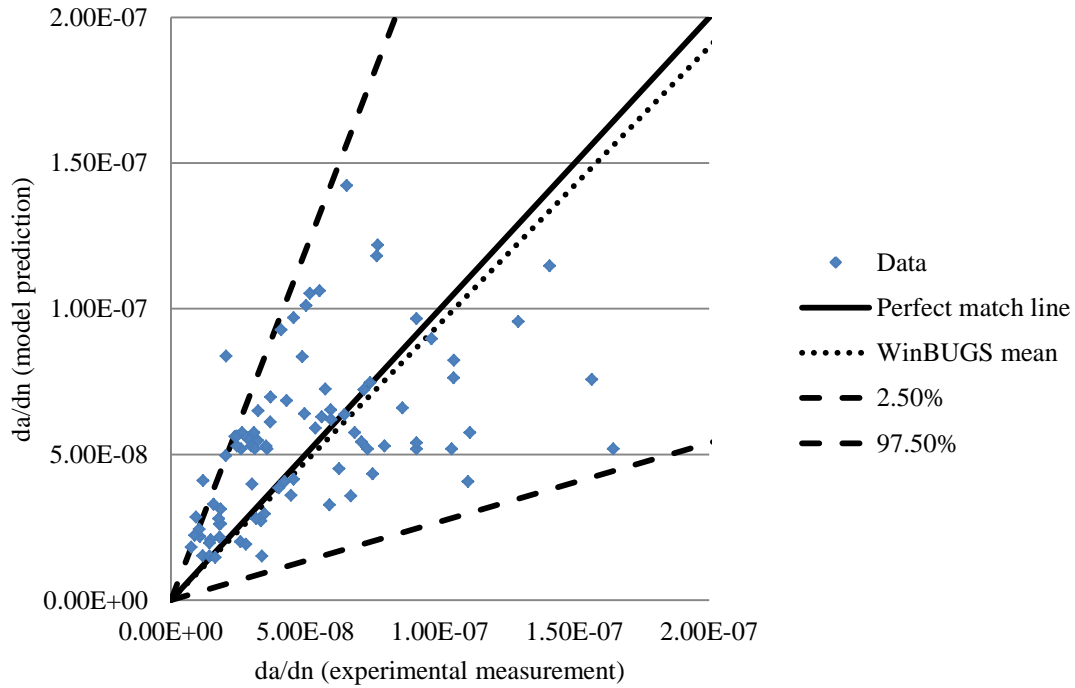
Figure 6.4: Modified Paris law posterior predictive mean model with the uncertainty bounds

When observing the mean value of F_m, the model shows a slight bias, 5%, under predicting the real value. However, it has a wide range of uncertainty. As mentioned earlier, the measurements uncertainty was quantified to be around 17.22% meaning that a considerable portion of the model uncertainty comes from the SIF computation, data scatter and the form of the model used. One way to identify the major source of uncertainty is by validating the SIF computation model and quantifying its uncertainties. Yet, performing more experiments could also better shape the scatter of data and reduce the model uncertainty by providing more evidence for the probabilistic model development.

Nevertheless, as the mean model tends to under predict the crack growth rate, a different model, illustrated in equation (6.12), was found to yield less bias with slight conservatism.

$$\frac{da}{dN} = (2.32E - 10)\Delta K^{1.813} \left(\frac{R}{0.1167}\right)^{0.5385} \tag{6.12}$$

A summary statistics for the mean model multiplicative error is illustrated in Table 6.8:

Table 6.8: Modified Paris law model uncertainty quantification and validation summary

node	μ	σ	MC error	2.50%	median	97.50%
F_m	1.071	0.6337	0.006915	0.3112	0.9256	2.67
b_m	-0.07948	0.05999	6.30E-04	-0.1954	-0.08057	0.03921
s_m	0.5433	0.04376	4.92E-04	0.4652	0.5404	0.6357

This model provides 95% confidence that the true value of crack growth rate resides between 167% higher and 69% lower than what the model predicts. The uncertainty in this model prediction slightly increases; yet, less bias and conservatism are observed. This is shown graphically in Figure 6.5:
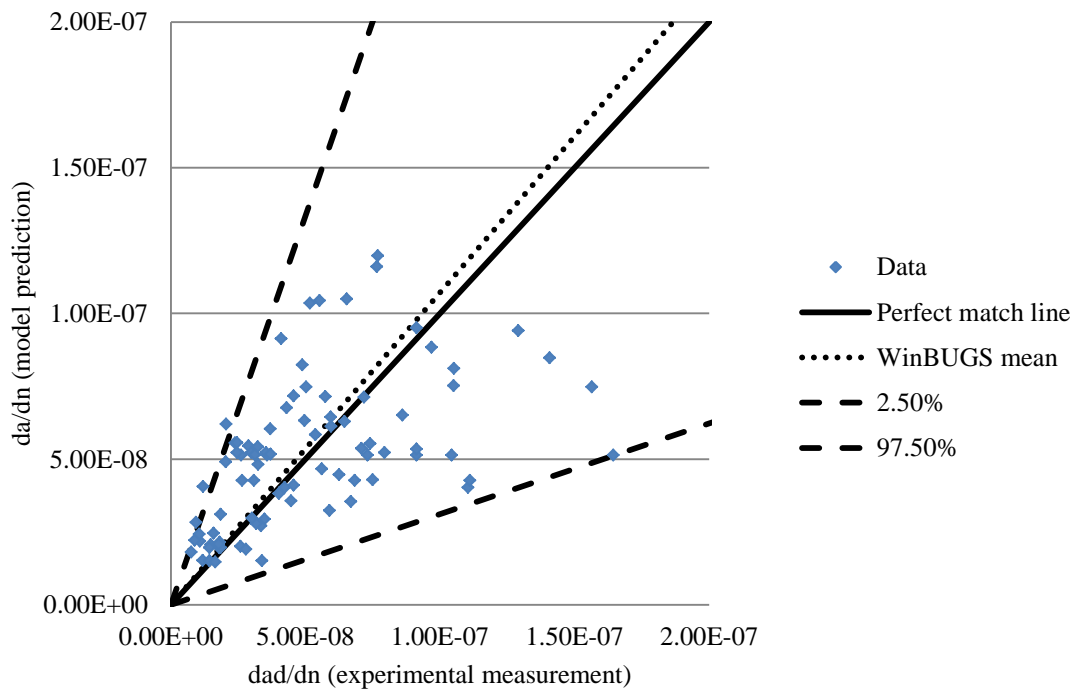
Figure 6.5: Modified Paris law posterior predictive model with the uncertainty bounds

94

6.3.3 Walker Model Uncertainty

Following the same procedure used to quantify the modified Paris law model multiplicative error, the Walker mean model (i.e., illustrated in equation (6.13)) multiplicative error was computed.

$$\frac{da}{dN} = \frac{(2.88E - 10)(\Delta K)^{1.785}}{(1 - R)^{0.630}} \tag{6.13}$$

A summary of the resultant statistics is illustrated in Table 6.9.

Table 6.9: Walker mean model uncertainty quantification and validation summary

node	μ	σ	MC error	2.50%	median	97.50%
F_m	0.8482	0.4786	5.03E-03	0.259	0.742	2.06
b_m	-0.3014	0.05883	5.94E-04	-0.420	-0.301	-0.187
s_m	0.5268	0.04248	4.57E-04	0.451	0.524	0.616

The model predictions were found to provide 95% confidence that the true value resides between 106% higher and 74% lower than what the model predicts. This is shown graphically in Figure 6.6.

Figure 6.6: Walker posterior predictive mean model with the uncertainty bounds

When observing the mean value of F_m, the model shows a bias of 15% under estimating the true value of the crack growth rate. Also, it has a wide range of uncertainty; however, this model yields less uncertainty when compared with the modified Paris law model. Similar to the modified Paris law model, a considerable portion of the model uncertainty comes from the SIF computation, data scatter and the form of the model used.

As the mean model tends to under predict the crack growth rate, a different model, as illustrated in equation (6.14), was found to provide more conservative predictions with less bias, however, it yielded more uncertainty.

$$\frac{da}{dN} = \frac{(2.54E - 10)(\Delta K)^{1.769}}{(1 - R)^{0.648}} \tag{6.14}$$

A summary statistics for the mean model multiplicative error is illustrated in Table 6.8:

node	μ	σ	MC error	2.50%	median	97.50%
F_m	1.011	0.5735	0.006177	0.3099	0.877	2.46
b_m	-0.1282	0.05688	6.05E-04	-0.24	-0.1284	-0.01631
s_m	0.5268	0.04222	4.26E-04	0.4531	0.5244	0.6178

This model provides 95% confidence that the true value of crack growth rate resides between 146% higher and 69% lower than what the model predicts. As the uncertainty slightly increases for this model prediction, yet, less bias and more conservatism are observed. This is illustrated graphically in Figure 6.7:
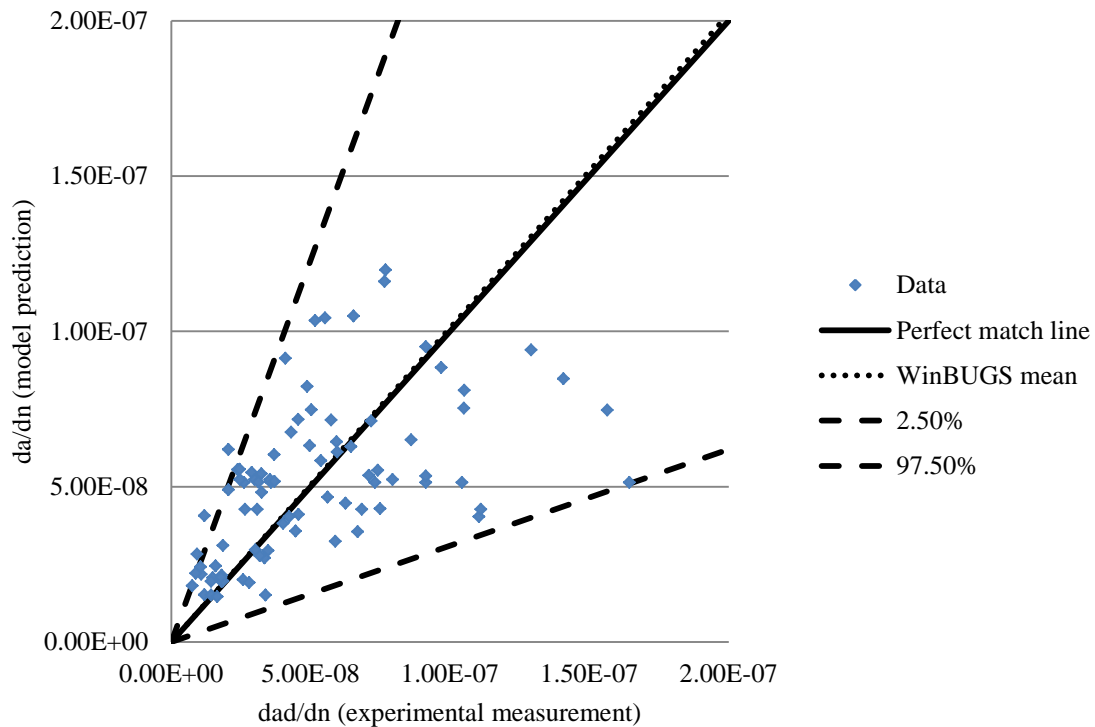
Figure 6.7: Walker posterior predictive model with the uncertainty bounds

6.4 Models Comparison and Bayesian Selection

As illustrated earlier, two crack growth models were developed in this work. The first model was developed based on the Paris law equation of crack growth with an addition of a correction factor

that accounts for the loading ratio effect. On the other hand, the second model was developed based on the Walker equation of crack growth that already incorporates the loading ratio as an input parameter within its formulation.

Both models were estimated using an identical set of data in order to be able to compare their outputs and uncertainties. Yet, as the two models have different forms, selecting a suitable model is important. A comparison between the two models is illustrated in Table 6.11:

Table 6.11: A comparison between the two developed models structure, error and uncertainty

	Modified Paris law model	Walker model
Model form	$\frac{da}{dN} = C\Delta K^n \left(\frac{R}{R_0}\right)^m$	$\frac{da}{dN} = \frac{C(\Delta K)^n}{(1 - R)^{n(1-\lambda)}}$
Model inputs	ΔK, LR	ΔK, LR
Model output	da/dN	da/dN
Uncertain parameters	C, n, m	C, n, λ
Model multiplicative mean error value	-0.2013	-0.3014
Uncertainty lower bound (%)	-73	-74
Uncertainty upper bound (%)	140	106

The modified Paris mean model shows a lower mean error compared to the Walker mean model. However, the Walker mean model shows less output uncertainty. For that reason, a Bayesian selection method was employed in order to identify the better model.

Two main widely used model selection techniques in the literature are the Bayesian Information Criterion (BIC) and the Akaike Information criterion (AIC). However, the BIC method was used in this research. According to Cavanaugh [70], BIC serves as an asymptotic approximation to a transformation of the Bayesian posterior probability of a candidate model. In large sample sets, the model favored by BIC ideally resembles to the candidate model. The Bayesian Information Criterion (BIC) is illustrated in equation (6.15):

$$BIC = n \ln(\sigma^2) + k.\ln(n) \qquad (6.15)$$

Lower values of BIC indicate a higher Bayesian posterior probability, for that reason, the model that scores lower on BIC is better. A comparison between the two models BIC is illustrated in Table 6.12:

Table 6.12: BIC values comparison between the Paris law model and the Walker model

	Modified Paris law mean model	Walker mean model
n	290	290
k	3	3
σ^2	0.292	0.277
BIC	-339.627	-354.732

As both models associated uncertainties were quantified using the same set of data and have the same number of uncertain parameters, the main determining factor in the BIC calculation was the model variance. As a result, the Walker mean model turned out to be the favored model.

6.5 Favored Model Uncertainty Treatment

As the Walker mean model was preferential by the Bayesian model selection method, it was further treated in order to minimize its uncertainty. One way to have a better crack growth rate predictions with reasonable uncertainty is by splitting the model into two main sub-models; the first representing the crack growth rate before coalescence and the second representing it after coalescence as illustrated in Figure 6.8. However, more work has to be done in order to define the coalescence point at which the ligament failure occurs as accurately as possible. It is vital to do more experimental and simulation investigations to be able to come up with a time to ligament failure model which will define the threshold between the two crack growth rate models.
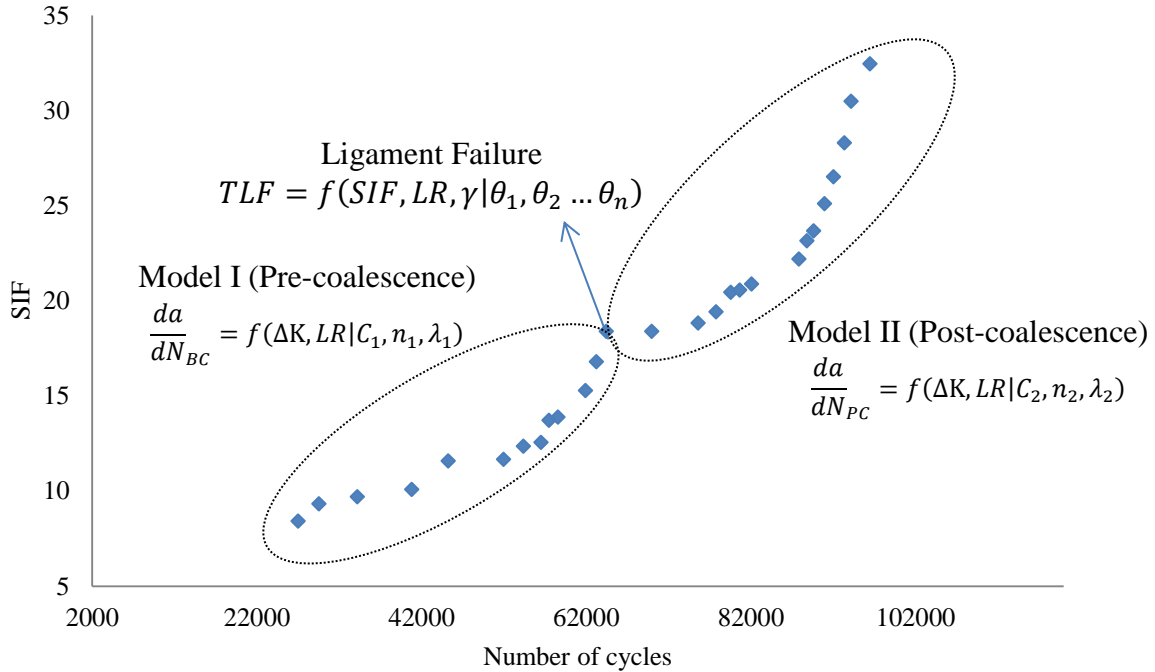
Figure 6.8: A strategy to model crack growth rate at different stages of crack interaction

Even though more data is required for applying such modeling strategy, some work was done in this direction in order to illustrate how such crack growth rate modeling strategy would minimize predictions uncertainties. It was possible in this work to show how splitting the crack growth rate model into two sub-models (i.e. pre-coalescence model and post-coalescence model) minimizes uncertainty; however, the data available was not enough to come up with a time to ligament failure model. Further discussions of this issue are addressed in the recommendations section 7.4.

6.5.1 Pre-Coalescence Crack Growth model

The first step of developing the pre-coalescence Walker model is the Bayesian inference. The same subjective prior pdf of each of the model uncertain parameters $f_o(C, n, m)$ used earlier was used herein. Subsequently, this prior was combined with the crack growth rate experimental data and the crack tip SIF simulation data before coalescence in the form of a normal distribution likelihood function as illustrated earlier in equation (5.1). The result is an updated state of

knowledge identified as the posterior distribution, f(C, n, m, σ |Data). This process was shown earlier mathematically in equation (5.2).

After running the developed WinBUGS code and using the Algorithm for the Bayesian approach, a posterior knowledge of the uncertain parameters C, n and λ was obtained as illustrated in Figure 6.9 and Table 6.13:
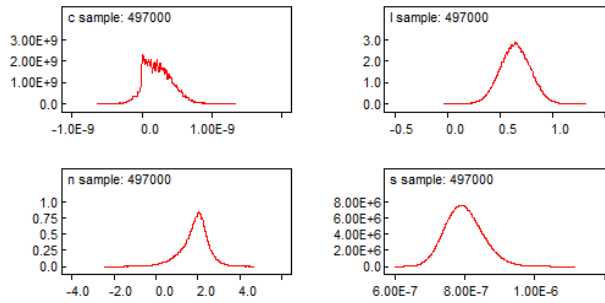
Figure 6.9: Pre-coalescence Walker model uncertain parameters C, n and λ posterior distribution

Table 6.13: Pre-coalescence Walker model uncertain parameters C, n, λ and σ posterior distributions as calculated in WinBUGS for 500000 samples

node	μ	σ	MC error	2.50%	median	97.50%
C	2.29E-10	2.29E-10	2.56E-12	-1.29E-10	2.11E-10	6.63E-10
n	1.85	0.646	0.004976	0.3206	1.933	2.99
λ	0.6468	0.1439	4.36E-04	0.3658	0.6467	0.9278
s	7.98E-07	5.37E-08	8.26E-11	7.01E-07	7.95E-07	9.11E-07

After running the uncertainty quantification algorithm, the model multiplicative error and uncertainty were obtained. A summary statistics for the model multiplicative error is illustrated in Table 6.14:

Table 6.14: Pre-coalescence Walker mean model uncertainty quantification and validation summary

node	μ	σ	MC error	2.50%	median	97.50%
F_m	0.909	0.4838	0.005145	0.2989	0.8062	2.086
b_m	-0.2088	0.08733	8.99E-04	-0.3806	-0.2091	-0.03656
s_m	0.4877	0.06708	7.34E-04	0.3767	0.4803	0.638

The model predictions showed 95% confidence that the true value resides between 108% higher and 70% lower than what the model predicts as shown graphically in Figure 6.10:

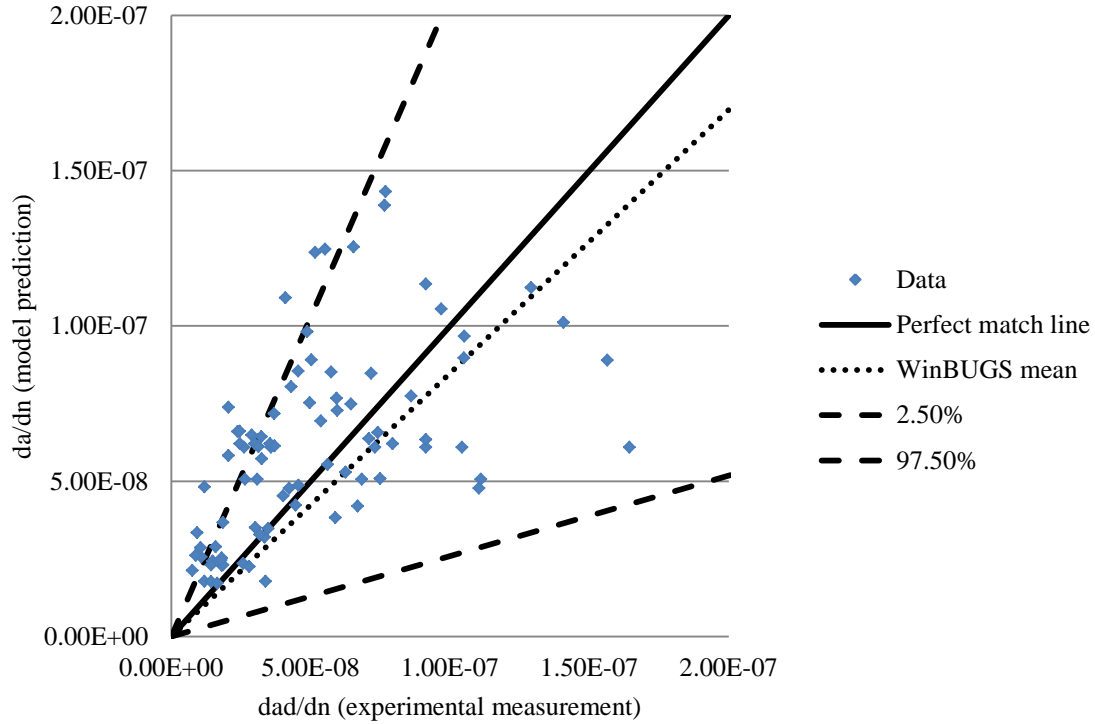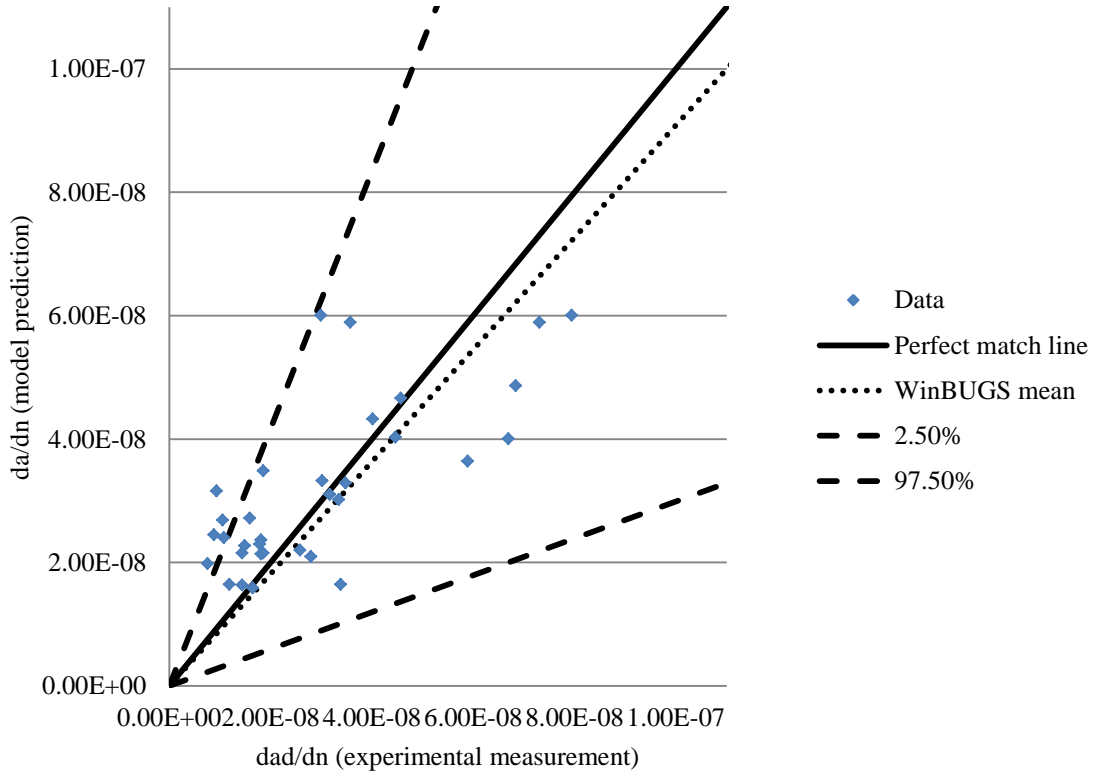Figure 6.10: Pre-coalescence Walker posterior predictive mean model with the uncertainty bounds

When observing the mean value of F_m, the model shows a bias of less than 10% compared to 15% when not considering this distinction between the two phases of neighboring cracks growth (i.e. before coalescence and after coalescence). Also, this model shows similar uncertainty when compared to the Walker model even though the data sets used for the model development and validation were much smaller than those used for developing the Walker model. So, it is likely that using more data to develop and validate the pre-coalescence Walker model will yield less bias and uncertainty.

6.5.2 Post-Coalescence Crack Growth Model

Following the same procedure used earlier for developing the pre-coalescence Walker model, a posterior knowledge of the uncertain parameters C, n and λ was obtained for the post-coalescence Walker model as illustrated in Figure 6.11 and Table 6.15:
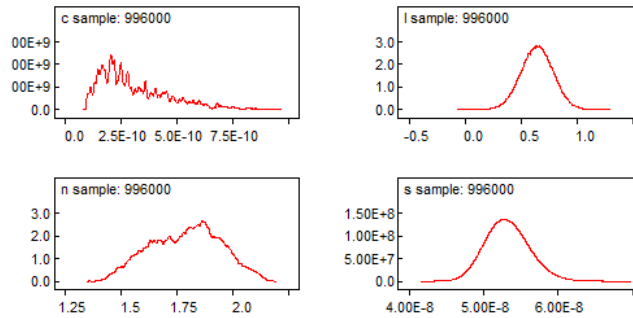
Figure 6.11: Post-coalescence Walker model uncertain parameters C, n and λ posterior distribution

Table 6.15: Post-coalescence Walker model uncertain parameters C, n, λ and σ posterior distributions as calculated in WinBUGS for 500000 samples

node	μ	σ	MC error	2.50%	median	97.50%
C	3.07E-10	1.86E-10	4.92E-12	1.08E-10	2.61E-10	6.96E-10
n	1.788	0.1558	0.004869	1.491	1.8	2.075
λ	0.6436	0.1431	4.44E-04	0.3629	0.6439	0.923
s	5.32E-08	2.95E-09	4.55E-12	4.78E-08	5.30E-08	5.93E-08

A summary statistics for the model multiplicative error and uncertainty is illustrated in Table 6.16:

Table 6.16: Post-coalescence Walker mean model uncertainty quantification and validation summary

node	μ	σ	MC error	2.50%	median	97.50%
F_m	0.8165	4.10E-01	0.38%	29.13%	73.13%	182.50%
b_m	-0.3135	0.07359	7.36E-04	-0.4573	-31.34%	-0.1683
s_m	0.4541	5.58E-02	5.90E-04	0.3608	0.4482	0.5793

The model predictions showed 95% confidence that the true value resides between 83% higher and 71% lower than what the model predicts. This is shown graphically in Figure 6.12:
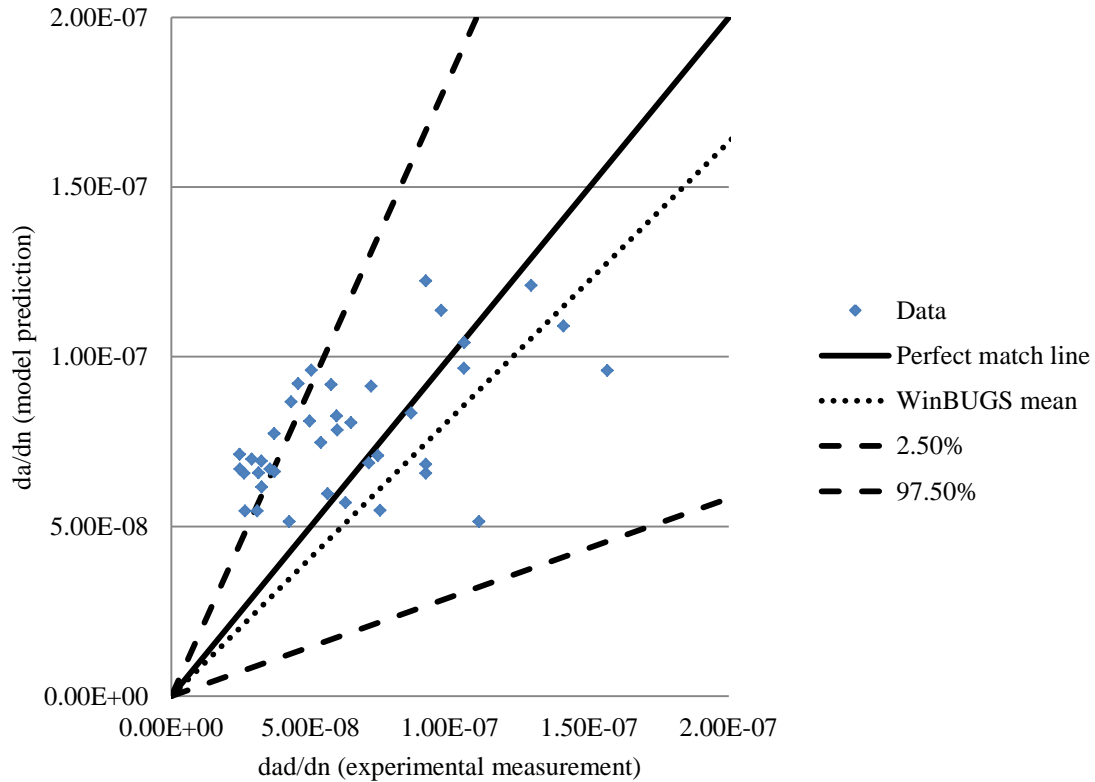
Figure 6.12: Post-coalescence Walker posterior predictive mean model with the uncertainty bounds

When observing the mean value of F_m, the post-coalescence model shows slightly higher bias (i.e. 20%) compared to 15% when not considering this distinction between the two phases of neighboring cracks growth (i.e. before coalescence and after coalescence). However, this model shows less uncertainty when compared to the Walker model even though the data sets used for the model development and validation are much smaller than those used for developing the Walker model. So, it is likely that using more data to develop and validate the pre-coalescence Walker model will yield less bias and uncertainty.

When comparing the two modeling strategies, meaning modeling crack growth rate before and after coalescence in one model versus modeling the crack growth rate before coalescence in one

model and after coalescence in a different model, it was found that the two models strategy yields similar or better bias and uncertainty.

7. Chapter Seven: Conclusions and Recommendations for Future Work

7.1 Conclusions

Many different degradation mechanisms act on engineering structures causing damage. This research focuses on fatigue as the failure mechanism causing degradation and fracture. The main focus of this research was to come up with a more realistic life prediction model of fatigue damage that considers presence of neighboring cracks. As such this developed and validated a multi-site damage probabilistic life prediction model that could be used to assess the integrity of engineering structures susceptible to fatigue in the presence of neighboring cracks. In order to achieve that, both experiments and simulation were performed to produce the data required for the model development.

The experiments were performed to investigate the interaction of two adjacent semi-elliptical cracks of variable dimensions under different cyclic loading conditions. A series of tests were conducted under uniaxial constant amplitude fatigue loads on API-5L grade B steel dog-bone samples. Thus, the Physics of Failure and Fracture Mechanics laboratory at the Center for Risk and Reliability was used to conduct the tests. The impact of the neighboring cracks dimensional variability and the different loading conditions on the cracks interaction, coalescence and growth were investigated.

This work has developed an improved experimental layout and procedure to investigate cracks interaction, coalescence and growth in carbon steel materials. A reliable design of experiment based on improving crack monitoring techniques available in the literature was presented in this work. This was done by using real-time microscopy to monitor the cracks during the interaction and coalescence process, which improved the measurements accuracy. The fractography images

were processed using image processing software to obtain the most accurate measurements possible and assure the consistency throughout the different tests. Moreover, a novel approach was implemented in order to monitor the crack growth stages by correlating the surface crack growth with the crack front growth using different microscopy tools and image processing.

This research offered a more accurate understanding of the effect of neighboring cracks dimensional variability on their interaction, coalescence and growth process. It was found that increasing the depth of one of the neighboring cracks by one standard deviation accelerates failure by almost 23% compared to the reference geometry. This acceleration effect is due to the increased stress intensity between the two cracks and at the crack front which led to a faster ligament failure and crack growth. However, increasing the depth of one of the neighboring cracks by two standard deviations had a similar failure time to the one standard deviation depth increase case, which indicates similar stress intensity between the two cracks disregarding the greater difference in depth. On the other hand, decreasing the depth of one of the neighboring cracks by one standard deviation, $a_{(\mu-\sigma/\mu)}$, decelerates failure by nearly 10 % compared to the reference geometry. This deceleration is due to reduced stress intensity between the cracks leading to slower interaction and growth. Yet, decreasing the depth of the one of the neighboring cracks by two standard deviations yielded very similar results to the one standard deviation depth decrease case showing a very similar behavior to the increasing depth experiments.

Other crack dimensions were also investigated in this work. For example, decreasing the radius of one of the neighboring cracks by either one or two standard deviations did not affect the failure time significantly compared to the case of having two identical cracks. The reason behind that is the mild impact of the cracks radius on the SIF at the crack tip which directly impact the rate of crack growth. Nevertheless, the spacing between the two cracks was found to have an

accelerating effect on the number of cycles to coalescence. Smaller spacing led to faster coalescence which will eventually lead to faster failure. In summary, the dimensional variability of the neighboring cracks shows fundamentally that the bigger crack in depth dominates the crack growth behavior of neighboring cracks due to the increased stress levels at the crack front. Also, faster coalescence leads to faster ligament failure and eventually faster sample failure.

Correspondingly, this research has broadened the state of the art on the effect of different loading conditions on crack interaction, coalescence and growth. Both experiments and simulations were performed to investigate the impact of different loading conditions on cracks interaction, coalescence and growth rate. Higher stresses and lower loading ratios accelerated both cracks coalescence and sample failure. Yet, lower applied stress and higher loading ratio yielded slower coalescence and failure. The reason for that is the direct impact of the loading conditions on the stress field around the cracks. Higher applied stresses and lower loading ratios yields a higher stress distribution around the cracks which eventually led to faster ligament failure and faster crack growth.

Furthermore, simulations were performed to understand the SIF behavior around neighboring cracks in order to justify the faster crack growth behavior. The crack front SIF was investigated using a simulation technique that incorporates the stress intensity factor of a single crack with existing CIF models that accounts for the neighboring cracks interaction and coalescence. A comprehensive summary of the models discussing how the SIF of a single semi-elliptical crack could be corrected for the neighboring cracks interaction effect was performed. A combination of these models were integrated and used to find the SIF values necessary for the probabilistic life prediction modeling purposes.

An improved characterization of the SIF behavior at the crack front during different crack development stages was developed in this research. It was found that increasing the depth of one of the neighboring cracks or both of them yields higher stress intensity around the cracks. On the other hand, the separation distance between neighboring cracks was found to play a significant role in defining the stress concentration around the cracks. Smaller separation distances yielded higher stress intensity between the neighboring cracks causing faster coalescence and ligament failure. When cracks coalescence is achieved, a change in the SIF development behavior is observed due to the ligament failure and the formation of a bigger enveloping crack. This sudden increase in the crack dimension caused a rapid increase in the crack front SIF values. Also, the impact of the loading conditions on the SIF was investigated. The SIF had a very similar development behavior at different stresses before and after coalescence except that increasing the stress and decreasing the loading ratio caused higher stress intensity around the cracks.

This work has also investigated the impact of different loading conditions on the time to ligament failure both experimentally and using simulation. A different strategy of investigating ligament failure was followed, which was identifying when ligament failure occurs rather than how it occur. It was found that higher applied stress levels had linear accelerating impact on the time to ligament failure. On contrary, it was found that lower loading ratios had the same accelerating impact on the ligament failure. The reason for that is that higher stress levels and lower loading ratio imposes more stress on the ligament zone between the cracks leading to faster failure.

Finally, a Bayesian approach was used to construct a multi-site fatigue crack growth rate model coupled with the concept of accelerated life testing in order to estimate the model parameters. The available experimental and simulation data combined with informative prior uniform

distributions of the models parameters was employed in WinBUGS to calculate the posterior estimates of the model parameters. The Bayesian approach also allowed performing proper uncertainty characterization and model validation to account for the model errors and confirm its outputs.

7.2 Recommendations

The following extensions of the research presented in this dissertation are recommended:

- Perform more fatigue tests at a wider variety of stresses and loading ratios to improve model error and reduce its uncertainty

- Investigate the effect of load frequency on the fatigue life of the material as there are some contradicting conclusions in the literature about this issue

- Investigate the dynamic response of neighboring cracks of variable dimensions at arbitrary loading conditions where the stress and the loading ratio are assumed to be arbitrary functions of time

- Validate the model proposed in this research against other grades of carbon or stainless steel for a more global application

- Investigate cracks interaction, coalescence and growth in various corrosive environments (i.e., Corrosion-Fatigue) for a more global application

- Investigate multiple cracks interaction, coalescence and growth and update the model proposed in this research to incorporate these results for a more global application and higher levels of realism

- Further develop the SIF model used in this research by making it probabilistic in nature for a better quantification of SIF computation uncertainty

- Further investigate the ligament failure between neighboring cracks both experimentally and numerically for a better understanding of the failure mechanism

- Develop a time to ligament failure model defining a threshold that distinct the pre-coalescence crack growth phase from the post-coalescence phase

- Further investigate the ligament failure in different grades of steel materials, different neighboring cracks dimensions and at different loading conditions using different testing apparatus (e.g., acoustic emission)

- Improve the CIF computation by accounting for the dimensional variability of the neighboring cracks. However, a suitable model that addresses CIF of non-identical cracks or a proper simulation effort will be required

- Further investigate the correlations between the different model parameters, especially the Paris law equation coefficients

- Account for pit initiation and pit to crack transition in the model developed in this research

- Consider large scale plasticity at the crack front impact on neighboring cracks interaction, coalescence and growth could improve the model predictions

- Add proper sensitivity analysis as it could provide a better understanding of the nature of correlations between the physical parameters of the failure mechanism investigated

- Investigate cases when the neighboring cracks dimensions are larger compared to the specimen dimension. This yields bigger plastic zones around the cracks which require further understanding of the PEFM aspect of the problem when the LEFM concepts are no longer applicable

- Expand the work proposed chapter six, section 6.5, could be a great addition in truly understanding cracks interaction and its impact on crack growth. Modeling crack growth in two different phases (i.e., pre-coalescence and post-coalescence crack growth) side by side with a clear identification of a threshold that distinct the two phases is recommended

- Investigate cracks interaction, coalescence and growth by the use of entropy in the context of classical thermodynamics, Boltzman-gibbs or information entropy

7.3 Prognostic Health Management (PHM) Perspective

The scope of this research topic was defined based on a real problem in the oil and gas transport pipelines. There are many different failure mechanisms acting on oil and gas transport pipelines leading to their failure. For that reason, and in order to insure the safety of such systems, a proper assessment of each failure mechanism should be performed.

Internal degradations, external degradation and various mechanical forces are the main failure causes in piping systems. However, according to National Research Council [71] the pipeline interior is at the highest risk because of its high exposure to the shipped liquids. Corrosion followed by erosion, to a lesser extent, may be considered the main causes of internal degradation. On the other hand, corrosion and cracking are the main sources of external degradation. Other forms of degradation could be caused by the fluid over-pressurization or other external forces acting on the system causing actual mechanical damage.

In order to assure the safe operation of oil and gas transport pipelines, a proper risk assessment procedure should be developed to account for any potential failures. Based on the work done in this dissertation, the following procedure is suggested:

- Define the structure at risk by defining the material, all active failure mechanisms, operating conditions and service history

- Perform a comprehensive assessment of the structure by identifying any week points, welded areas or even more sever operating conditions sections in order to prioritize sections at highest risk

- Gather failure data and classify it based on the causing failure mechanism

- Identify all hazards and risks for each type of failure

- Evaluate the hazards and risk for each type of failure

- Prioritize the risks based on the severity level of each failure

- Investigate possible options for eliminating or controlling hazards and risks

- Design an action plan to control any failure by designing a proper control measures specific to each type of failure

- Review the efficiency of the designed plan by continuously logging the failure

Having a proper risk assessment procedure does not mean eliminating risks. However, different tools could be employed to predict failures. Here comes the need for life prediction models, such as the one developed in this dissertation, to predict failures. Having this kind of predictive models and a proper risk assessment procedure could minimize risks significantly.

One main advantage of probabilistic life prediction models is that it could be continuously updated using the Bayesian approach taking into account real failure data from the fields. This process is illustrated in Figure 7.1:
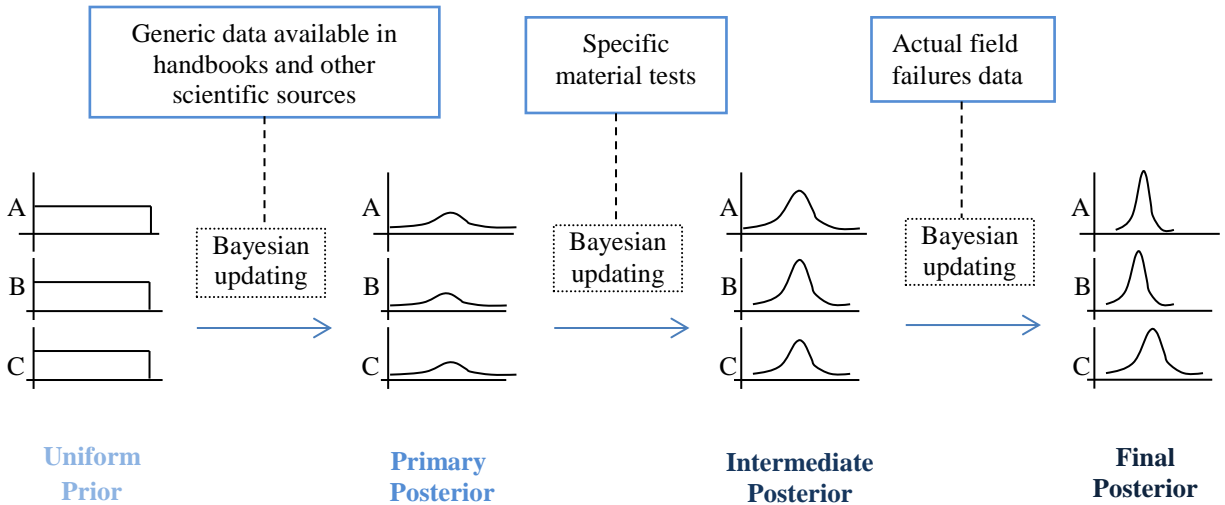
Figure 7.1: Continuous updating of probabilistic life prediction models using different sources of data. Adopted from "Accelerated testing, ENRE 641" By M. Modarres, 2008 [52]

The same life prediction technique could be performed for other failure mechanisms as illustrated in Figure 7.2:
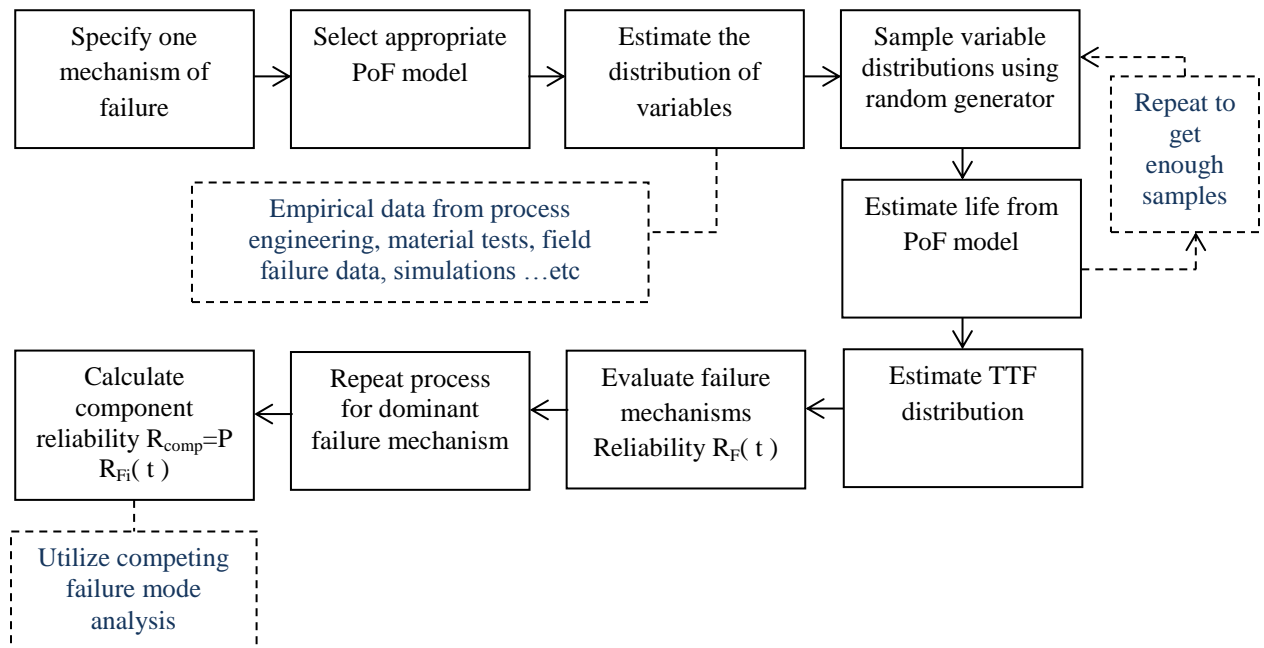
Figure 7.2: Modeling steps of various failure mechanisms probabilistically and its implementation. Adopted from "Accelerated testing, ENRE 641" By M. Modarres, 2008 [52]

114

So, when developing a family of life prediction models of the most dominant failure mechanisms acting on a certain critical engineering structure along with a proper risk assessment procedure, a significant improvement in the production efficiency and the overall system safety is predicted. These tools help guiding the maintenance planning strategies, cultivating a clear path for the integrity management and helping the management make the right decisions.

Appendices

Appendix A

Initial cracks/notches dimensions

Table 0.1: Geometry of the cracks at the start of test, 1 refers to the right crack and 2 refer to the left crack, all dimensions are in mm: refer to Figure 2.4 for explanation of notation

Geometry code	a_1	r_1	a_1/c	a_1/t	r_1/w	a_2	r_2	a_2/c	a_2/t	r_2/w	s	$a_{average}$	$r_{average}$
a_(μ-2σ/μ-2σ)	1	0.8	1.25	0.1	0.08	1	0.8	1.25	0.10	0.08	1.6	1	0.8
a_(μ/μ)	1.6	0.8	2	0.16	0.08	1.6	0.8	2.00	0.16	0.08	1.6	1.6	0.8
a_(μ/μ-2σ)	1.6	0.8	2	0.16	0.08	1	0.8	1.25	0.10	0.08	1.6	1.3	0.8
a_(μ/μ-σ)	1.6	0.8	2	0.16	0.08	1.3	0.8	1.63	0.13	0.08	1.6	1.45	0.8
a_(μ/μ+σ)	1.6	0.8	2	0.16	0.08	1.9	0.8	2.38	0.19	0.08	1.6	1.75	0.8
a_(μ/μ+2σ)	1.6	0.8	2	0.16	0.08	2.2	0.8	2.75	0.22	0.08	1.6	1.9	0.8
r_(μ/μ-σ)	1.6	0.8	2	0.16	0.08	1.6	0.65	2.46	0.16	0.07	1.6	1.6	0.725
r_(μ /μ-2σ)	1.6	0.8	2	0.16	0.08	1.6	0.5	3.20	0.16	0.05	1.6	1.6	0.65
S_(μ-σ)	1.6	0.8	2	0.16	0.08	1.6	0.8	2.00	0.16	0.08	1.3	1.6	0.8
S_(μ-2σ)	1.6	0.8	2	0.16	0.08	1.6	0.8	2.00	0.16	0.08	1	1.6	0.8
S_(μ+2σ)	1.6	0.8	2	0.16	0.08	1.6	0.8	2.00	0.16	0.08	2.245	1.6	0.8

Table 0.2: Different symbolic representations of the reference geometry

Reference geometry	
a_(μ/μ)	r_(μ/μ)
	S_μ
	LR_0.1
	Stress_290

Appendix B

Different tests performed and the associated loading conditions

Table 0.3: Loading conditions for each test, stress is in MPa

Sample #	Applied stress	LR
a_(μ-2σ/μ-2σ) a_(μ/μ) a_(μ/μ-2σ) a_(μ/μ-σ) a_(μ/μ+σ) a_(μ/μ+2σ) r_(μ/μ-σ) r_(μ /μ-2σ) S_(μ-σ) S_(μ-2σ) S_(μ+2σ)	290	0.1
a_(μ/μ)	290	0.05
a_(μ/μ)	290	0.2
a_(μ/μ)	280	0.1
a_(μ/μ)	270	0.1

Appendix C

An example of the experimental data elicited from the fractography analysis performed

Table 0.4: A data sample from the experimental work, reference geometry a_(μ/μ)

Date:		13-May	
Geometry:		different depth a _ 1.6/1.9	
Stress:		290 Mpa	
Frequency:		2 Hz	
File Name:		different_a _ 1.6/1.9 (date05_13)	
Test Start time:	10:31	13-May	
Coalescence time:	17:40	13-May	24 hr system
Failure time:	20:52	13-May	

Coalescence	
Seconds	25740
hrs	7.15
cycles	51480
Failure	
Seconds	37260
hrs	10.35
cycles	74520

Before coalescence (Right crack) BIGGER CRACK

Time	time difference	hours	mins	# of cycles	Pixcels 1	Pixcels 2	Pixcels avarage	c (mm)	c (m)	dc/dn	Pixcels for a	pixcels 1	pixcels 2	pixcels avarage	a (mm)	a (m)	da/dn
10:31	0:00	0	0	0	0	0	0	0.0000	0.0E+00	/	0.0	94.0	90.0	92.0	1.90	1.9E-03	/
12:51	2:20	2	20	16800	61	61	61	0.1310	1.3E-04	7.8E-09	6.3	97.0	95.0	96.0	2.0	2.0E-03	4.9E-09
13:09	2:38	2	38	18960	81	86	83.5	0.1793	1.8E-04	2.2E-08	8.7	100.0	101.0	100.5	2.1	2.1E-03	4.3E-08
13:51	3:20	3	20	24000	108	106	107	0.2298	2.3E-04	1.0E-08	11.1	103.0	105.0	104.0	2.1	2.1E-03	1.4E-08
14:33	4:02	4	2	29040	152	152	152	0.3264	3.3E-04	1.9E-08	15.8	107.0	108.0	107.5	2.2	2.2E-03	1.4E-08
14:53	4:22	4	22	31440	164	166	165	0.3544	3.5E-04	1.2E-08	17.2	111.0	110.0	110.5	2.3	2.3E-03	2.6E-08
15:31	5:00	5	0	36000	200	200	200	0.4295	4.3E-04	1.6E-08	20.8	115.0	114.0	114.5	2.4	2.4E-03	1.8E-08
15:49	5:18	5	18	38160	253	237	245	0.5262	5.3E-04	4.5E-08	25.5	119.0	117.0	118.0	2.4	2.4E-03	3.3E-08
16:08	5:37	5	37	40440	262	264	263	0.5648	5.6E-04	1.7E-08	27.3	123.0	120.0	121.5	2.5	2.5E-03	3.2E-08
16:27	5:56	5	56	42720	286	280	283	0.6078	6.1E-04	1.9E-08	29.4	127.0	129.0	128.0	2.6	2.6E-03	5.9E-08
16:42	6:11	6	11	44520	310	309	309.5	0.6647	6.6E-04	3.2E-08	32.2	131.0	132.0	131.5	2.7	2.7E-03	4.0E-08
16:47	6:16	6	16	45120	324	326	325	0.6980	7.0E-04	5.5E-08	33.8	136.0	138.0	137.0	2.8	2.8E-03	1.9E-07
17:00	6:29	6	29	46680	400	409	404.5	0.8687	8.7E-04	1.1E-07	42.1	141.0	145.0	143.0	3.0	3.0E-03	7.9E-08
17:23	6:52	6	52	49440	412	414	413	0.8870	8.9E-04	6.6E-09	42.9	146.0	148.0	147.0	3.0	3.0E-03	3.0E-08
17:40	7:09	7	9	51480	413	415	414	0.8891	8.9E-04	1.1E-09	43.1	150.0	151.0	150.5	3.1	3.1E-03	3.5E-08

Before coalescence (Left crack) SMALLER CRACK

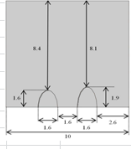| # of cycles	Pixcels 1	Pixcels 2	Pixcels average	c (mm)	c (m)	dc/dn	Pixcels for a	pixcels 1	pixcels 2	pixcels avarage	a (mm)	a (m)	da/dn
0	48	46	47	0.1009	1.01E-04	/	4.9	77.0	79.0	78.0	1.61	1.6E-03	/
16800	70	72	71	0.1525	1.52E-04	3.1E-09	7.4	79.0	78.0	78.5	1.6	1.6E-03	6.1E-10
18960	76	78	77	0.1654	1.65E-04	6.0E-09	8.0	81.0	82.0	81.5	1.7	1.7E-03	2.9E-08
24000	94	88	91	0.1954	1.95E-04	6.0E-09	9.5	83.0	84.0	83.5	1.7	1.7E-03	8.2E-09
29040	126	129	127.5	0.2738	2.74E-04	1.6E-08	13.3	85.0	86.0	85.5	1.8	1.8E-03	8.2E-09
31440	130	136	133	0.2856	2.86E-04	4.9E-09	13.8	87.0	88.0	87.5	1.8	1.8E-03	1.7E-08
36000	146	149	147.5	0.3168	3.17E-04	6.8E-09	15.3	90.0	91.0	90.5	1.9	1.9E-03	1.4E-08
38160	189	192	190.5	0.4091	4.09E-04	4.3E-08	19.8	93.0	94.0	93.5	1.9	1.9E-03	2.9E-08
40440	209	212	210.5	0.4521	4.52E-04	1.9E-08	21.9	96.0	95.0	95.5	2.0	2.0E-03	1.8E-08
42720	229	228	228.5	0.4907	4.91E-04	1.7E-08	23.8	99.0	100.0	99.5	2.1	2.1E-03	3.6E-08
44520	273	272	272.5	0.5852	5.85E-04	5.2E-08	28.3	102.0	103.0	102.5	2.1	2.1E-03	3.4E-08
45120	286	292	289	0.6207	6.21E-04	5.9E-08	30.1	105.0	106.0	105.5	2.2	2.2E-03	1.0E-07
46680	321	325	323	0.6937	6.94E-04	4.7E-08	33.6	108.0	109.0	108.5	2.2	2.2E-03	4.0E-08
49440	324	321	322.5	0.6926	6.93E-04	-3.9E-10	33.5	111.0	112.0	111.5	2.3	2.3E-03	2.2E-08
51480	325	323	324	0.6958	6.96E-04	1.6E-09	33.7	116.0	115.0	115.5	2.4	2.4E-03	4.0E-08

After coalescence (Left crack)

Time	time difference	hours	mins	# of cycles	Pixcels 1	Pixcels 2	Pixcels avarage	c (mm)	c (m)	dc/dn	Pixcels for a	pixcels 1	pixcels 2	pixcels avarage	a (mm)	a (m)	da/dn
18:08	7:37	7	37	54840	385	381	383.00	0.78	7.78E-04	/	37.7	152.0	153.0	152.5	3.1	3.1E-03	/
18:36	8:05	8	5	58200	424	426	425.00	0.86	8.63E-04	2.53906E-08	41.8	156.0	157.0	156.5	3.2	3.2E-03	2.5E-08
19:00	8:29	8	29	61080	465	462	463.50	0.94	9.41E-04	2.71539E-08	45.6	160.0	162.0	161.0	3.3	3.3E-03	3.2E-08
19:14	8:43	8	43	62760	584	586	585.00	1.19	1.19E-03	1.46903E-07	57.5	164.0	164.0	164.0	3.4	3.4E-03	3.7E-08
19:27	8:56	8	56	64320	598	597	597.50	1.21	1.21E-03	1.6276E-08	58.8	168.0	169.0	168.5	3.5	3.5E-03	6.0E-08
19:35	9:04	9	4	65280	676	652	664.00	1.35	1.35E-03	1.40706E-07	65.3	172.0	173.0	172.5	3.6	3.6E-03	8.6E-08
19:43	9:12	9	12	66240	721	698	709.50	1.44	1.44E-03	9.62728E-08	69.8	176.0	173.0	174.5	3.6	3.6E-03	4.3E-08
19:54	9:23	9	23	67560	809	813	811.00	1.65	1.65E-03	1.56191E-07	79.8	181.0	180.0	180.5	3.7	3.7E-03	9.4E-08
20:03	9:32	9	32	68640	902	886	894.00	1.82	1.82E-03	1.56105E-07	87.9	186.0	186.0	186.0	3.8	3.8E-03	1.1E-07
20:11	9:40	9	40	69600	984	976	980.00	1.99	1.99E-03	1.81966E-07	96.4	191.0	190.0	190.5	3.9	3.9E-03	9.7E-08
20:32	10:01	10	1	72120	1001	1010	1005.50	2.04	2.04E-03	2.05543E-08	98.9	196.0	195.0	195.5	4.0	4.0E-03	4.1E-08
20:40	10:09	10	9	73080	1030	1018	1024.00	2.08	2.08E-03	3.91439E-08	100.7	201.0	202.0	201.5	4.2	4.2E-03	1.3E-07
20:49	10:18	10	18	74160	1228	1222	1225.00	2.49	2.49E-03	3.78038E-07	120.5	206.0	205.0	205.5	4.2	4.2E-03	7.6E-08
20:52	10:21	10	21	74520	1278	1280	1279.00	2.60	2.60E-03	3.04688E-07	125.8	213.0	215.0	214.0	4.4	4.4E-03	4.9E-07

Appendix D

Crack front SIF simulation MATLAB code

For aspect ratios greater than 1:

```matlab
clear all
WW=xlsread('file name','sheet name')
format long

a=WW(row number : row number, column number)
c2= WW(row number : row number, column number)
deltaf= 261*ones(size(a));      %stress
t= input*ones(size(a));           %Sample thickness
b= input*ones(size(a));            %Half of the total width
theta90=pi/2*ones(size(a));     %Crack growth angle
P=(c2./a);

        M1=(P.^0.5).*(1+0.04.*P);
%Boundary correction factor
        M2=0.2.*(P.^4);
%Boundary correction factor
        M3=-0.11*(P.^4);
%Boundary correction factor
        fw=(sec((pi*c2./(2.*b)).*(a./t).^0.5)).^0.5;
%Finite width correction factor
        Q=1+1.464*(P.^1.65);
%Shape factor for an ellipse
        g90=1;
%Used to fine tune the equation, theta=90
        ftheta90=(P.^2).^0.25;
%Angular function derived from the solution for an elliptical crack in
infinite solid, theta=90
        Fs90=((M1+M2.*(a./t).^2+M3.*(a./t).^4)).*g90.*ftheta90.*fw;
%Boundary correction factor, theta=90
        K90f=deltaf.*((pi*a./Q).^0.5).*Fs90
%Stress intensity factor, Fatigue cycles
```

For aspect ratios less than or equal to 1:

```matlab
clear all
WW= xlsread('file name','sheet name')
format long

a= WW(row number : row number, column number)
c2= WW(row number : row number, column number)
deltaf= input*ones(size(a));  %Range of stress, Fatigue cycles
t= input*ones(size(a));        %Sample thickness
b= input*ones(size(a));         %Half of the total width
theta90=pi/2*ones(size(a));   %Angle of crack growth in the depth direction
P=(a./c2);


        M1=1.13-(0.09.*P);
%Boundary correction factor
        M2=-0.54+(0.89./(0.2+P));
%Boundary correction factor
        M3=0.5-(1./(0.65+P))+(14.*(1-P).^24);
%Boundary correction factor
        fw=(sec((pi*c2./(2.*b)).*(a./t).^0.5)).^0.5;
%Finite width correction factor
        Q=1+1.464.*(P.^1.65);
%Shape factor for an ellipse
        g90=1;
%Used to fine tune the equation, theta=90
        ftheta90=1;
%Angular function derived from the solution for an elliptical crack in
infinite solid, theta=90
        Fs90=((M1+M2.*(a./t).^2+M3.*(a./t).^4)).*g90.*ftheta90.*fw;
%Boundary correction factor, theta=90
        K90f=deltaf.*((pi.*a./Q).^0.5).*Fs90
%Stress intensity factor, Fatigue cycles
```

Appendix E

An example of the simulation data and the associated CIF analysis

Table 0.5: SIF and the associated cracks interaction correction factor calculations, reference geometry a_(μ/μ)

da/dn	a (m)	r (m)	s (m)	s/r	s/a	s/r × s/a	ΔK_SC	CIF	ΔK _MC	Ligament failure
2.19E-09	0.001649	0.000893	0.001415	1.59	0.86	1.36	8.43	1	8.43	
2.35E-08	0.001709	0.00091	0.00138	1.52	0.81	1.23	8.48	1.1	9.33	
1.69E-08	0.001788	0.000972	0.001256	1.29	0.70	0.91	8.81	1.1	9.69	
8.98E-09	0.001847	0.001035	0.00113	1.09	0.61	0.67	9.16	1.1	10.08	
1.33E-08	0.001906	0.001122	0.000956	0.85	0.50	0.43	9.66	1.2	11.59	
8.82E-09	0.001965	0.001143	0.000914	0.80	0.47	0.37	9.72	1.2	11.67	
2.47E-08	0.002025	0.001246	0.000707	0.57	0.35	0.20	10.29	1.2	12.35	
2.74E-08	0.002084	0.001287	0.000627	0.49	0.30	0.15	10.47	1.2	12.57	
1.03E-07	0.002183	0.001316	0.000568	0.43	0.26	0.11	10.55	1.3	13.71	
5.49E-08	0.002242	0.001347	0.000505	0.37	0.23	0.08	10.68	1.3	13.88	
3.23E-08	0.002351	0.001406	0.000387	0.28	0.16	0.05	10.91	1.4	15.28	
2.99E-08	0.00239	0.001462	0.000276	0.19	0.12	0.02	11.19	1.5	16.79	
4.94E-08	0.002449	0.001595	1.09E-05	0.01	0.00	0.00	11.87	2	18.40	LF[2]
5.35E-08	0.002598	0.00303	-	-	-	-	18.40	-	18.40	
3.15E-08	0.002775	0.003121	-	-	-	-	18.83	-	18.83	
6.4E-08	0.002914	0.003246	-	-	-	-	19.42	-	19.42	
9.33E-08	0.003081	0.003456	-	-	-	-	20.44	-	20.44	
1.28E-07	0.00322	0.00347	-	-	-	-	20.56	-	20.56	
1.17E-07	0.003388	0.003525	-	-	-	-	20.89	-	20.89	
2.4E-08	0.003526	0.003763	-	-	-	-	22.18	-	22.18	
1.44E-07	0.003664	0.003923	-	-	-	-	23.15	-	23.15	
9.41E-08	0.003743	0.004002	-	-	-	-	23.66	-	23.66	
1.12E-07	0.003891	0.004214	-	-	-	-	25.09	-	25.09	
1.37E-07	0.00404	0.0044	-	-	-	-	26.51	-	26.51	
9.73E-08	0.004168	0.004617	-	-	-	-	28.30	-	28.30	
2.47E-07	0.004375	0.004829	-	-	-	-	30.49	-	30.49	
6.93E-08	0.004533	0.004992	-	-	-	-	32.45	-	32.45	

---

[2] Ligament failure

Appendix F

Sample of the data used for the models development

Table 0.6: A sample of the data used for the models development, a_(μ/μ), σ=290MPa

da/dn	ΔK	LR
2.19E-09	8.43	0.1
2.35E-08	9.33	0.1
1.69E-08	9.69	0.1
8.98E-09	10.08	0.1
1.33E-08	11.59	0.1
8.82E-09	11.67	0.1
2.47E-08	12.35	0.1
2.74E-08	12.57	0.1
1.03E-07	13.71	0.1
5.49E-08	13.88	0.1
3.23E-08	15.28	0.1
2.99E-08	16.79	0.1
4.94E-08	18.40	0.1
5.35E-08	18.40	0.1
3.15E-08	18.83	0.1
6.40E-08	19.42	0.1
9.33E-08	20.44	0.1
1.28E-07	20.56	0.1
1.17E-07	20.89	0.1
2.40E-08	22.18	0.1
1.44E-07	23.15	0.1
9.41E-08	23.66	0.1
1.12E-07	25.09	0.1
1.37E-07	26.51	0.1
9.73E-08	28.30	0.1
2.47E-07	30.49	0.1
6.93E-08	32.45	0.1

Appendix G

WinBUGS program to find the posterior distributions of the developed PPoF models uncertain

parameters

```
model {


      c~dnorm(2.33E-10,1.72E19)
      n~dnorm(3.10,0.71)
      m~dunif(-3,3)
      s~dunif(0,5)

       C <- 1000

       for( i in 1 : N ) {
                   zeros[i] <- 0
                   L[i] <-(1/(s*pow(2*3.141592654,0.5)))*exp(-0.5*pow(x[i,1]-
((c*pow(x[i,2],n)*pow(x[i,3]/0.1167,m))),2)/pow(s,2))

              ghr[i] <- ( -1) * log(L[i]) + C
      zeros[i] ~ dpois(ghr[i])
  }
tau<-1/pow(s,2)
e~dnorm(0,tau)
```

Appendix H

An example of the data set used in the uncertainty quantification

Table 0.7: A sample of the data used for the modified Paris law model uncertainty quantification and validation

da/dn (Model prediction)	da/dn (Experimental measurement)
1.46943E-08	1.18383E-08
1.99872E-08	1.48667E-08
2.85257E-08	3.47902E-08
3.94695E-08	1.19119E-08
3.98715E-08	4.56621E-08
4.99E-08	2.60926E-08
5.1945E-08	9.13242E-08
5.30728E-08	2.88392E-08
5.39786E-08	2.38237E-08
5.67434E-08	5.37201E-08
6.11847E-08	6.44641E-08
6.26986E-08	5.93607E-08
6.92956E-08	7.17547E-08
9.26112E-08	9.13242E-08
1.00915E-07	5.1618E-08
1.16793E-07	7.69046E-08
1.45847E-08	1.43418E-08
1.89751E-08	1.43418E-08
1.93862E-08	2.58152E-08
2.08105E-08	1.81159E-08
2.62542E-08	3.34642E-08
2.69773E-08	3.17029E-08
3.14324E-08	5.88768E-08
3.71062E-08	4.0157E-08

Appendix I

WinBUGS program to quantify the developed models uncertainty

```
+model;
{

        bm~dunif(-10,10)
        sm~ dunif(0,10)
        taum<-1/pow(sm,2)
        #Exp uncertainty
        pe<-0.175

        be<-(log(1+pe)+log(1-pe))/2
        se<-(log(1+pe)-log(1-pe))/(2*1.95996398454005)

        bt<-bm-be
        st<-sqrt(pow(sm,2)+pow(se,2))

        C <- 1000

          for( i in 1 : N ) {
                        zeros[i] <- 0
                        L[i] <- pow(exp(-0.5*pow((log(x[i,2]/x[i,1])-
bt)/st,2))/(sqrt(2*3.141592654)*st)/(x[i,2]/x[i,1]),x[i,3])
                    ghr[i] <- ( -1) * log(L[i]) + C
          zeros[i] ~ dpois(ghr[i])
                                                                }
        fm~dlnorm(bm,taum)

        logfm<-log(fm)
                    for( j in 1 : 7 ){

yy[j]<-xx[j]*fm


}

}
```

Bibliography

Abdallah Al Tamimi is a mechanical engineer and a PhD graduate of the reliability engineering program, University of Maryland, College Park, USA. He earned his mechanical engineering degree from the Petroleum Institute, Abu Dhabi, United Arab Emirates. Also, he earned both his Master's and PhD in Reliability engineering from the University of Maryland, College Park, United States. Over the last four years, he has worked in a variety of professional organizations in both academia and the oil and gas industry. He worked in Abu Dhabi Marine Operating Company (ADMA-OPCO) as a mechanical supervisor. Afterwards, he made his transition to academia by working as a teaching assistant at the Petroleum Institute. During his last year of PhD, he was the Mechanics and Reliability laboratory manager. He started his PhD studies in reliability engineering in 2011 after he was granted a fellowship by Abu Dhabi National Oil Company (ADNOC) and was able to complete both his Masters and PhD degrees requirements in three years.

References

[1] C. Bayley, Parametric Investigation on the Coalescence of Coplanar Fatigue Cracks, Masters' thesis, Ottawa: Carelton University , 1997.

[2] T. Leek and I. Howard, "An Examination of Methods of Assessing Interacting Surface Cracks by Comparison with Experimental Data," *International Journal of Pressure Vessels and Piping,* vol. 68, pp. 181-201, 1996.

[3] T. Leek and I. Howard, "Estimating the Elastic Interaction Factors of Two Coplanar Surface Cracks Under Mode I load," *International Journal of Pressure Vessels and Pipeing ,* vol. 60, pp. 307-321, 1994.

[4] Y. Murakami and S. Nemat-Nasser, "Interacting Dissimilar Semi-elliptical Surface Flaws Under Tension and Bending," *Engineering Fracture Mechanics,* vol. 16, pp. 373-386, 1982.

[5] Y. Murakami and H. Nisitani, "Stress Intensity Factors for Interacting Two Equal Semi-elliptical Surface Cracks in Tension," *Trans. Japan Soc. Mech. Engrs SerA,* vol. 47, pp. 295-303, 1981.

[6] M. C. Alseyabi, Structuring a Probabilistic Model for Reliability Evaluation of Piping Subject to Corrosion-fatigue Degradation, PhD dissertation, College Park: University of Maryland, 2009.

[7] Z. Ahmad, "Corrosion Fatigue," in *Principles of Corrosion Engineering and Corrosion Control ,* Elsevier, 2007, pp. 221-241.

[8] R. Stephens, A. Fatemi, R. Stephens and H. Fuchs, Metal fatigue in engineering, John Wiley & Sons , 2000.

[9] H. Zhang, Fatigue Crack Growth and Coalescence Study, Ontario: Carleton University, 1993.

[10] P. Paris and F. Erdogan, "A critical analysis of crack propagation laws," *Journal of Basic Engineering ,* pp. 528-534, 1963.

[11] X. Lin and R. Smith, "Numerical Prediction of Fatigue Crack Growth of a Surface Defect," *Fatigue and Fracture of Engineering Materials and Structures,* vol. 18, no. 2, pp. 247-256, 1995.

[12] P. Roberge, "Corrosion Pit Shapes," Corrosion Doctors , 2012 . [Online]. Available: http://corrosion-doctors.org/Forms-pitting/shapes.htm. [Accessed Tuseday, the 26th June 2012].

[13] M. Nuhi, T. Abu Seer, A. Al Tamimi, M. Modarres and A. Seibi, "Reliability Analysis for Degredation Effects of Pitting Corrosion in Carbon Steel Pipes," in *ICM11*, Como , 2011.

[14] G. Irwin, "Crack Extension Force for a Part Through Crack in a Plate," *Journal of Applied Mechanics ,* vol. 29, pp. 651-654, 1962.

[15] T. Leek, "The Interaction and Growth of Two Surface Cracks Under Fatigue Loading, PhD dissertation," University of Sheffield, UK, 1990.

[16] J. Newman and I. Raju, "An Emperical Stress Intensity Factor Equation for the Surface Crack," *Engineering Fracture Mechanics,* vol. 15, 1981.

[17] J. Newman and I. Raju, "Stress intensity Factors for a Wide Range of Semi-Elliptical Suface Cracks in Finite Width Plates," *Engineering Fracture Mechanics,* vol. 11, 1979.

[18] J. Newman, "A Review and Assessment of the Stress Intensity Factors for Surface Cracks," ASTM STP 687, 1979, pp. 16-37.

[19] J. Newman and I. Raju, "Stress Intensity Factor Equations for Cracks in Three Dimensional Finite Bodies Subjected to Tension and Bending Loads," NASA, Hampton, Virginia, 1984.

[20] S. Pitt and R. Jones, "Multiple-Site and Widespread Fatigue Damage in Aging Aircrafts," *Engineering Failure Analysis ,* vol. 4, pp. 237-257, 1997.

[21] E. DeBartolo and B. Hillberry, "Effects of Constituent Particle Clusters on Fatigue Behavior of 2024-T3 Aluminum Alloy," *Int. J. Fatigue,* vol. 20, pp. 727-735, 1998.

[22] D. Harrington, Fatigue Crack Coalescence and Shape Development and Experimental Invistigation, Masters Thesis, Carleton University, Department of Mechanical and Aerospace Engineering , 1995.

[23] T. Leek and I. Howard, "Rules for the Assessment of Interacting Suface Cracks Under Mode I Load," *Internationl Journal of Pressure Vessels and Piping ,* vol. 60, pp. 323-339, 1994.

[24] W. Soboyejo and J. Knott, "Fatigue Crack Propagation of Copalanr Semi-elliptical Cracks in Pure Bending," *Engineering Fracture Mechanics,* vol. 37, no. 2, pp. 323-340, 1990.

[25] K. Kishimoto, W. Soboyejo, R. Smith and J. Knott, "A Numerical Invistigation of the Interaction and Coalescence of Twin Coplanar Semi Elliptical Fatigue Cracks," *International Journal of Fatigue ,* vol. 11, no. 2, pp. 91-96, 1989.

[26] J. Twaddle and B. Hancock, "The Development of Cracks by Defect Coalescence," *Engineering Materials Advisory Service,* pp. 185-198, 1988.

[27] T. O'Donoghure, P. Nishioka and N. Atluris, "Multiple Surface Cracks in Pressure Vessels," *Engineering Fracture Mechanics,* vol. 20, no. 3, pp. 545-560, 1984.

[28] P. Forsyth, "A unified Description of Micro and Macro-scopic Fatigue Crack Behaviour," *International Journal of Fatigue,* vol. 5, pp. 3-14, 1983.

[29] R. Chang, "On Crack-Crack Interaction and Coalescence in Fatigue," *Engineering Fracture Mechanics,* vol. 16, pp. 683-693, 1982.

[30] M. Chaussumier, M. Shahzad, C. Mabru, R. Chieragatti and F. Rezai-Aria, "A Fatigue Multi-Site Cracks Model Using Coalescence, Short and Long Crack Growth Laws, for Anodized Aluminum Alloys," 2010.

[31] S. Melin, "Why do Cracks Avoid Each Other," *International Journal of Fracture,* vol. 23, pp. 37-45, 1983.

[32] T. Swift, "The influence of slow stable crack growth and net section yeilding on the residual strenght of stiffened structure," in *13th International Committee on Aeronautical Fatigue ,* Pisa, 1985.

[33] E. Moukawsher, M. Heinimann and A. Grandt, "Residual strenght of panels with multiple site damage," *Journal of Aircrafts,* vol. 5, pp. 1014-1021, 1996.

[34] D. Jeong and J. Brewer, "On the linkup of multiple cracks," *Engineering Fracture Mechanics ,* vol. 51, pp. 233-238, 1995.

[35] J. Kuang and C. Chen, "The failrue of ligaments due to multiple-site damage using interactions of dugdale-type cracks," *Fatigue and Fracture of Engineering Materials & Structures,* vol. 21, pp. 1147-1156, 1998.

[36] ASME, "Rules for inservice inspection of nuclear power plant components," in *Boiler and Pressure Vessel Code*, ASME, 1992, pp. Appendix A, Section XI.

[37] BSI, Guidance on methods for assessing the acceptability of flaws in fusion welded joints,

British Standard Institute, 1991.

[38] K. Iida, "Shapes and Coalescence of Suface Fatigue Cracks," in *I.C.F. International Symposium on Fracture Mechanics*, Beijing, 1983.

[39] F. Erdogan, "On the stress distribuion in plates with collinear cuts under arbitary loads," in *4th US Nat. Cong. Appl. Mech.*, PP. 547-553, 1962.

[40] T. Yokobori, M. Ohashi and M. Ichikawa, "The interaction of two collinear asymmetrical elastic cracks," Tohoku University , Vol. 1, PP. 33-39, 1965.

[41] G. N. Savin, Stress concentration around holes, Oxford: Pergamon Press, 1981.

[42] S. Suresh, "Fatigue of Materials," Cambridge University Press, 1991.

[43] C. Li, Probabilistic Modeling for Corrosion-Fatigue Crack Growth, PhD Dissertation, Lehigh University , 1996.

[44] M. Modarres, "Accelerated Life Testing, ENRE64, Class Presentation Slides," University of Maryland, College Park, 2012.

[45] Materials Evaluation and Engineering Inc, "Energy Dispersive X-ray Spectroscopy," Materials Evaluation and Engineering, Inc., 2009. [Online]. Available: http://mee-inc.com/eds.html. [Accessed 02 December 2013].

[46] R. Carlton, c. Lyman and J. Roberts, "Accuracy and Precision of Quantitative Energy Dispersive X-ray Spectrometry in the Environmental Scanning Electron Microscope," *Scanning 26,* pp. 167-174, 2004.

[47] Alabama Specialty Products, Metal Samples , 2014. [Online]. Available: http://www.alspi.com/MS-machining.htm.

[48] K. Ho and S. Newman, "State of the Art Electrical Discharge Machining (EDM)," *International Journal of Mchine Tools and Manufacture,* vol. 43, no. 13, pp. 1287-1300, 2003.

[49] S. A. Willard, "Use of of Marker Bands for Determination of Fatigue Crack Growth Rates and Crack Front Shapes in Pre-Corroded Coupons," NASA, Hampton, Virginia , 1997.

[50] J. Terrell, "Effect of Cyclic Frequency on the Fatigue Life of ASME SA-106-B Piping Steel in BWR Environments," *Journal of Material Engineering ,* vol. 10, pp. 193-203, 1988.

[51] J. Newman and I. Raju, "An empirical stress intensity factor equation for the surface crack," *Engineering Fracture Mechanics,* vol. 15, pp. 185-192, 1981.

[52] M. Modarres, Accelerated Testing, ENRE 641, College Park : Center of Risk and Reliability, UMD, College Park, USA, 2008.

[53] M. Neves Beltrao, E. Castrodeza and F. Bastian, "Fatigue crack propagation in API 5L X-70 pipeline steel longitudinal welded joints under constant and variable amplitude," *Fatigue and Fracture of Engineering Materials and Structures,* vol. 34, pp. 321-328, 2010.

[54] Y. Shi, B. Chen and J. Zhang, "Effects of welding residual stresses on fatigue crack growth behaviour in butt welds of a pipline steel," *Engineering Fracture Mechanics,* vol. 36, pp. 893-902, 1999.

[55] J. Fernandes, Uma metodologia para a analise e modelagem, PhD dissertation, Rio de Jeneiro, Brasil: PUC, 2002.

[56] M. Cortie and G. Garrett, "On the correlation between the C and m in the Paris equation for fatigue crack propagation," *Engineering Fracture Mechanics,* vol. 30, no. 1, pp. 49-58, 1988.

[57] R. Hamam, S. Pommier and F. Bumbieler, "Variable amplitude fatigue crack growth, experimental results and modeling," vol. 29, no. 1634-1646, 2007.

[58] S. Beretta, M. Carboni, S. Cantini and A. Ghidini, "Application of fatigue crack growth algorithms to railway axles and comparison of two steel grades," *Journal of Rail and Rapid Transit,* vol. 218, no. 4, pp. 317-326, 2004.

[59] K. Krishnaprasad and V. Prakash, "Fatigue crack growth behavior in dissimilar metal weldment of staniless steel and carbon steel," *World Academy of Science, Engineering and Technology,* vol. 3 , pp. 8-22, 2009.

[60] N. Dowling, C. Calhoun and A. Arcari, "Mean stress effects in stress-life fatigue and the Walker equation," *Fatigue and Fracture of Engineering Materials and Structures,* vol. 32, pp. 163-179, 2008.

[61] D. Spiegelhalter, A. Thomas, N. Best and D. Lunn, "WinBUGS 1.4 manual," 2003.

[62] M. Azarkhail and M. Modarres, "A Novel Bayesian Framework for Uncertainity Management in Physics-Based Reliability Models," in *ASME International Mechanical Engineering Congress and Expositon* , Seattle, Washignton, USA, 2007.

[63] M. Azarhkail and M. Modarres, "Markov chain Monte Carlo simulation for estimating accelerated life model parameters," in *Annual Reliability and Mainitainability Symposium (RAMS) Proceedings*, Orlando, 2007.

[64] UNCERT project, in *Manual of codes of practice for the determination of uncertainties in mechanical tests on metallic materials*, European Commission's Standards, 2000, pp. ISBN 0-946754-41-1.

[65] P. Georgsson, "The determinatino of uncertainties in fatigue crack growth measurements," Volvo Aero Corporation , Trollhattan, Sweden , 2000.

[66] ISO TAG4, in *Guide to the expression of uncertainty in measurement*, Geneva, Switzerland, International Organization for Standardisation, 1993, pp. ISBN 92-67-10188-9.

[67] M. Modarres, M. Kaminskiy and V. Krivtsov, Reliability engineering and risk analysis, CRC Press, 2010.

[68] V. Ontiveros, A. Cartillier and M. Modarres, "An Integrated Methodology for Assessing Fire Simulation Code Uncertainity," *Nuclear Science Engineering ,* vol. 166, pp. 179-201, 2010.

[69] M. Azarkhail, V. Ontiveros and M. Modarres, "A Bayesian Framework for Model Uncertainity Consideration in Fire Simulation Codes," in *17th International Conference on Nuclear Engineering* , Brussels, 2009.

[70] J. Cavanaugh, "Lecture V: The Bayesian Information Criterion," University of Iowa, 25 September 2012. [Online]. Available: http://myweb.uiowa.edu/cavaaugh/ms_lec_5_ho.pdf. [Accessed 29 August 2014].

[71] National Research Council, "Effects of Diluted Bitumen on Crude Oil Transmission Pipeline, Special Report 311," National Research Council, 2013.